DISTRIBUTION AGREEMENT

In presenting this dissertation as a partial fulfillment of the requirements for an advanced degree from Emory University, I hereby grant to Emory University and its agents the non-exclusive license to archive, make accessible, and display my dissertation in whole or in part in all forms of media, now or hereafter known, including display on the world wide web. I understand that I may select some access restrictions as part of the online submission of this dissertation. I retain all ownership rights to the copyright of the dissertation. I also retain the right to use in future works (such as articles or books) all or part of this dissertation.

Signature:

Sean P. Doyle	Date

Characterization and therapeutic targeting of SPOP missense mutation-mediated oncogenesis

By

Sean Patrick Doyle
Doctor of Philosophy

Graduate Division of Biological and Biomedical Sciences
Molecular and Systems Pharmacology

Haian Fu, Ph.D.
Advisor

Ray Dingledine, Ph.D.
Committee Member

Nael McCarty, Ph.D.
Committee Member

David Yu, M.D., Ph.D.
Committee Member

Accepted:

Lisa A. Tedesco, Ph.D.
Dean of the James T. Laney School of Graduate Studies

Date

Characterization and therapeutic targeting of SPOP missense mutation-mediated oncogenesis

By

Sean Patrick Doyle
B.S., University of North Carolina at Chapel Hill, 2010

Advisor: Haian Fu, Ph.D.

An abstract of
a dissertation submitted to the Faculty of the
James T. Laney School of Graduate Studies of Emory University
in partial fulfillment of the requirements for the degree of
Doctor of Philosophy
in the Graduate Division of Biological and Biomedical Sciences,
Molecular and Systems Pharmacology
2021

ABSTRACT

Characterization and therapeutic targeting of SPOP missense mutation-mediated oncogenesis
By Sean Patrick Doyle

SPOP is an adaptor subunit of Cullin3-RING E3 ubiquitin ligase complexes that plays a key role in maintenance of cellular homeostasis through its interactions with other proteins. Missense mutations in SPOP's substrate binding cleft alter SPOP's ability to bind to other proteins and frequently drive prostate cancer development. However, our knowledge of the SPOP interactome and our understanding of how SPOP mutations influence SPOP function remain limited. In this dissertation, the characterized SPOP interactome is expanded through SPOP-focused, high-throughput protein-protein interaction (PPI) screens to generate new hypotheses for SPOP-mediated biology. We further evaluate how recurrent, prostate adenocarcinoma-associated missense mutations in SPOP alter SPOP PPIs. Recurrent SPOP missense mutations reduce interaction with several cancer-associated proteins, but recurrent SPOP F133L and F133V mutations are also observed to enhance or induce interaction with another set of proteins, including oncogenic transcription factor c-Jun. This dissertation further characterizes SPOP F133L- and F133V-mutation-induced interactions with c-Jun. Mechanistically, SPOP F133L and F133V mutants bind to c-Jun through the mutated SPOP MATH domain and serve to enhance c-Jun protein stability and transcriptional activity. Overall, these data reveal new differential protein-protein interaction connectivity for SPOP point variants, and suggest unique mechanisms of oncogenesis for recurrent SPOP F133L/V mutants through mutation-induced gain-of-interaction with oncogenic transcription factor c-Jun.

Therapeutic approaches that selectively target SPOP mutation-driven oncogenesis are currently limited. Because recurrent, prostate cancer-associated SPOP missense mutations have been characterized to promote prostate tumorigenesis in part through loss of SPOP interaction with chromatin reader BRD4, restoration of mutant SPOP interactions with BRD4 may represent a therapeutic strategy to reverse SPOP missense mutation-driven tumorigenesis. This dissertation describes the development and pilot implementation of a time-resolved, fluorescence resonance energy transfer (TR-FRET)-based high-throughput screening assay to identify small molecule inducers of SPOP missense mutant F133V interaction with BRD4.

Overall, this dissertation explores novel mechanisms of SPOP mutation-mediated oncogenesis that occur through SPOP PPI dysregulation and describes a strategy to rescue mutant SPOP function through restoration of SPOP PPIs. These studies suggest several novel cellular signaling axes mediated by SPOP and nominate potential therapeutic strategies that may be developed to treat patients with SPOP mutation-driven prostate tumors.

Characterization and therapeutic targeting of SPOP missense mutation-mediated oncogenesis

By

Sean Patrick Doyle
B.S., University of North Carolina at Chapel Hill, 2010

Advisor: Haian Fu, Ph.D.

A dissertation submitted to the Faculty of the
James T. Laney School of Graduate Studies of Emory University
in partial fulfillment of the requirements for the degree of
Doctor of Philosophy
in the Graduate Division of Biological and Biomedical Sciences,
Molecular and Systems Pharmacology
2021

ACKNOWLEDGEMENTS

I thank several individuals whose support has made this dissertation work possible. First, I thank my dissertation research advisor Dr. Haian Fu for his mentorship, his unwavering support, and for providing outstanding research opportunities that have collectively enabled me to develop into an independent scientist. I also thank my dissertation committee members, members of the Emory Cancer Target Discovery and Development (CTD^2) center, and my fellow lab members for their support and advice that have made this research work possible. Last, I thank my family for their constant encouragement throughout my PhD training experience.

TABLE OF CONTENTS

FIGURES

TABLES

ABBREVIATIONS

Abbreviation	Full Term
3’ UTR	3’ untranslated region (mRNA)
ADT	Androgen deprivation therapy
APC	Adenomatous polyposis coli
AR	Androgen receptor
BRD4	Bromodomain-containing protein 4
BRET	Bioluminescence resonance energy transfer
BTB	Bric à brac, tramtrack, broad complex
ccRCC	Clear cell renal cell carcinoma
CRPC	Castration-resistant prostate cancer
mCRPC	Metastatic, castration-resistant prostate cancer
CSPC	Castration-sensitive prostate cancer
CUL3	Cullin3
DSB	DNA double strand break
E3	E3 ubiquitin ligase
EBRT	External beam radiation therapy
EGLN2	Prolyl hydroxylase EGLN2
ER	Estrogen receptor
ETS	Erythroblast transformation-specific
FP	Fluorescence polarization
FRET	Fluorescence resonance energy transfer
TR-FRET	Time-resolved fluorescence resonance energy transfer

H2AX	Histone H2AX
γH2AX	Phosphorylated (serine 139) histone H2AX
HDR	Homology-directed repair
HIF	Hypoxia inducible factor
HTS	High-throughput screening
IR	Ionizing radiation
MATH	Meprin and TRAF-C homology
Mdm2/Hdm2	Mouse/human double minute 2
MFS	Metastasis-free survival
miR	MicroRNA
MRN	MRE11-RAD50-NBS1 protein complex
NHEJ	Non-homologous end joining
PARP	Poly (ADP-ribose) polymerase
PFS	Progression-free survival
PPI	Protein-protein interaction
PTEN	Phosphatase and tensin homolog
RBX1	RING-box protein 1
SCNA	Somatic copy number alteration
SMAD	Mothers against decapentaplegic homolog 2
SPOP	Speckle-type POZ protein
SPOPL	Speckle-type POz protein-like
SRC-3	Steroid receptor coactivator protein 3
TDP2	Tyrosyl-DNA phosphodiesterase 2

TP53	Tumor protein p53
TRIM24	Tripartite motif-containing 24
uHTS	Ultra-high-throughput screening
WT	Wild-type

CHAPTER 1:

INTRODUCTION

1.1 Overview

Interactions between proteins, or protein-protein interactions, tightly regulate fundamental cellular signaling pathways that influence overall cellular behavior. Dysregulation of protein-protein interactions results in aberrant cell signaling patterns that frequently contribute to pathology such as cancer. This dissertation explores protein-protein interaction dysregulation in prostate cancer caused by recurrent missense mutations in the E3 ubiquitin ligase protein SPOP. This introductory chapter will introduce fundamental concepts related to cancer, protein-protein interactions, and E3 ubiquitin ligases, summarize our current understanding of SPOP-mediated biology and tumorigenesis, and highlight current gaps in knowledge that have motivated the dissertation research work described in chapters 2 and 3 of this dissertation.

1.2 Cancer

Cancer, the second leading cause of mortality in the United States (1), is a heterogenous group of diseases that arises from single cellular clones in higher-order multicellular organisms. Despite their heterogenous nature, cancers broadly contribute to host morbidity and mortality through common features such as uncontrolled cellular growth, cellular invasion of surrounding host tissue, and cellular metastasis to distant sites within the host (2). Cancer-initiating and -promoting cellular states result from cumulative cellular genetic dysregulation that promotes cancer 'hallmarks', or particular biological capabilities that confer a cellular survival advantage, including 1) sustained proliferative signaling, 2) evasion of growth suppression, 3) resistance to cell death, 4) replicative immortality, 5) angiogenesis, 6) activation of invasion and metastasis, 7) reprogramming of energy metabolism, and 8) evasion of immune destruction (3; 4). This cumulative dysregulation of gene expression frequently occurs through inherited and/or acquired

genetic insults, such as gene mutations, deletions, or amplifications, that result in altered levels and/or activities of genes' biological products (2). Because many genes encode proteins, genetic dysregulation frequently mediates cancer initiation and progression through protein dysregulation (5). Consequently, proteins represent a critical class of molecular targets for approaches that seek to reverse or inhibit cancer-promoting cellular states.

1.3 Protein-protein interaction network mapping to identify therapeutic opportunities for cancer

Proteins are a major macromolecular class of executors and regulators of cellular function. Virtually all proteins carry out biological functions through intermolecular interactions, and many proteins specifically regulate diverse cellular processes through transient, selective physical interactions with other proteins (i.e., through protein-protein interactions [PPIs]) (5). Through PPIs, proteins relay extracellular and intracellular stimuli into biological signals that are further communicated within and between cells. These PPI-propagated biological signals ultimately effect changes in cellular behaviors such as growth, replication, differentiation, migration, and death, and frequently result in long-lasting changes in cell behavior through modulation of gene transcription. As such, PPIs serve as essential mediators of cellular responses to environmental cues and are critical regulators of cellular behavior.

Because PPIs play crucial roles in mediating fundamental cellular processes, dysregulation of PPIs can contribute to pathological cellular behavior and cancer-promoting cellular states (6). PPI dysregulation often stems from aberrances in PPI-component proteins' 1) expression levels (i.e., abnormal elevation or depression), 2) structure and function (e.g., through genetic alteration, such as a truncating deletion or a missense mutation in the encoding gene),

and/or 3) subcellular localization. For example, deletions or mutations in the gene *APC* (*adenomatous polyposis coli*) lead to diminished expression or an inactivated form of the APC protein that the gene encodes (7). Under normal physiological conditions in intestinal crypt cells, APC protein forms a protein complex that physically binds to the protein β-catenin in the cytosol to inhibit β-catenin's promotion of cellular proliferation. Upon APC deletion or mutation, however, APC complex interaction with β-catenin is lost, and APC regulation of β-catenin is consequently abrogated. This loss of the APC complex-β-catenin PPIs leads to unchecked β-catenin activity, which promotes the hyperproliferation of intestinal crypt cells that, with the acquisition of further genetic mutations, may become invasive colorectal cancer cells (8).

Highlighting the broad importance of PPIs in human diseases such as cancer, several recent studies have observed that pathology-associated proteins tend to participate in more protein-protein interactions on average than non-pathology-associated proteins (9-11). Other studies have also suggested that proteins implicated in the same pathological processes have a high tendency to interact with one another (12; 13). Given this prevalence of PPIs in mediating pathological cellular processes, strategies that identify and target critical PPIs in disease-defining PPI networks may represent a promising therapeutic approach to inhibit or reverse pathological cellular states (6; 14). To enable therapeutic targeting of disease-relevant PPIs (including cancer-driving PPIs), significant effort has been made in recent decades to generate comprehensive maps of the human protein-protein interactome to identify PPIs that mediate essential biological and/or disease-driving functions (15-20). Though meaningful progress has been made in characterizing human protein-protein interactomes, our depth of knowledge of the human protein-protein interactome in both normal physiological and pathophysiological cellular states remains limited. Future efforts toward comprehensive elucidation of the human protein-protein

interactome, and particularly toward characterization of PPI networks centered around disease-associated proteins, thus continue to hold significant promise for identification of disease-driving PPIs that may be modulated for therapeutic purposes.

1.4 E3 ubiquitin ligases are essential mediators of cell biology that function through selective protein-protein interactions

E3 ubiquitin ligases (E3s) are one example of a class of proteins that mediate essential biological functions through PPIs. E3s selectively interact with specific substrate proteins to coordinate the covalent conjugation of ubiquitin, a 9 kDa protein, to one or more substrate protein lysine residues (21-24) (Figure 1.1). This ubiquitin conjugation to a substrate protein, or ubiquitination, modifies the substrate's activity by altering the substrate's intermolecular interactions, resulting in diverse functional consequences that can include changes in substrate abundance, catalytic activity, subcellular localization, and binding to other proteins.

The myriad effects of protein ubiquitination are attributable to the distinct patterns of ubiquitin conjugation catalyzed by E3s. Ubiquitin may be conjugated as monomers (monoubiquitination) or as polymeric ubiquitin chains (polyubiquitination) to one or more lysine residues on a substrate protein. Topologically diverse polymeric ubiquitin chains are generated on substrates through successive linkage of ubiquitin molecules via one of seven ubiquitin lysine residues (K6, K11, K27, K29, K33, K48, and K63) or via the N-terminal methionine of ubiquitin (25; 26). These distinct patterns of monoubiquitination and polyubiquitination result in unique functional consequences for a given substrate. For example, homo-K48-linked polyubiquitination, the most extensively characterized type of homo-linkage polyubiquitination to date, generates branched ubiquitin chains on substrates that typically target substrates for

proteasomal degradation (27-30). Homo-K63-linked polyubiquitination, in contrast, forms linear ubiquitin chains that usually promote substrate protein-protein interactions (31-36) and protein-DNA interactions (37).

E3s must physically interact with protein substrates to catalyze substrate ubiquitination, and E3 interactions with other proteins must be specific to confer selective ubiquitination of substrates (38). Exquisite specificity of substrate ubiquitination is enabled by extensive E3 structural diversity, which is currently characterized to span three major structural classes (RING, HECT, RBR) that encompass more than 600 known E3s (39). Each E3's individual architecture and protein binding selectivity are defined primarily by each E3's singular combination of protein domains that mediate unique protein-protein interactions. Overall, E3s selectively interact with thousands of unique substrate proteins to regulate their activity through post-translational, covalent attachment of diverse ubiquitin moieties. This E3 modulation of substrate proteins is then propagated further through the substrates' interactions with other biological macromolecules, including with other proteins through PPIs, to influence overall cellular behavior. In this manner under normal physiological conditions, E3s collectively function to maintain cellular homeostasis and control cellular growth through their interactions with substrate proteins.

1.4.1 Dysregulation of E3 ligase-protein interactions promotes oncogenesis

Virtually all cell signaling pathways essential for control of cell growth, differentiation, and death are regulated by E3-protein interactions, including cancer-associated, PPI-mediated pathways such as the MAPK/Erk pathway, the PI3K/Akt pathway, the TGF-β pathway, the Hippo/YAP pathway, and the WNT/β-catenin pathway (40). Through their ubiquitin-mediated

modulation of proteins within these and other signaling pathways, individual E3s can play a cellular growth- and survival-*promoting* role (i.e., proto-oncogenic function) or a growth- and survival-*suppressing* role (i.e., tumor suppressive function). However, E3 dysregulation (i.e., change in expression level, gene deletion/mutation/amplification, altered subcellular localization) alters E3 control of these essential cell signaling pathways, and tumor cells often exploit such E3 aberrancies as mechanisms to promote their own survival and proliferation. Examples of E3s whose dysregulation is associated with tumor initiation and development include the following:
1) VHL (von Hippel-Lindau) is an E3 that binds to HIFs (hypoxia-inducible factors), mediates degradative ubiquitination of HIFs, and modulates HIF-promoted cellular response to hypoxic conditions (41-43). Inherited mutations in *VHL* cause autosomal-dominant von-Hippel Lindau disease, a neoplastic disease characterized by the development of hemangioblastomas, renal cell carcinoma, pheochromocytoma, and pancreatic neuroendocrine tumors (44; 45). Acquired somatic mutations/deletions in *VHL* also drive the development of non-hereditary clear cell renal cell carcinoma (ccRCC) (46-50). Mechanistically, these *VHL* deletions and mutations are inactivating genetic lesions that lead to loss of VHL interaction with HIFs and loss of VHL-mediated HIF destruction, which results in abnormally high cellular levels of HIFs (51-53). High cellular levels of proto-oncogenic HIFs, particularly HIF-2α, promote uncontrolled cell growth and angiogenesis that contribute to tumor development (54-57). Under normal physiological conditions, VHL thus acts as an E3 tumor suppressor in its modulation of the HIF pathway.
2) Mdm2/Hdm2 (mouse/human double minute 2) is an E3 that binds to the protein TP53 (tumor protein P53), facilitates degradative ubiquitination of TP53, and regulates TP53-mediated cellular response to stress or DNA damage (58-62). *MDM2/HDM2* gene amplification leading to Mdm2/Hdm2 overexpression promotes oncogenesis in multiple tissue types by enhancing

Mdm2/Hdm2 interaction with TP53, which increases Mdm2/Hdm2-mediated ubiquitination and degradation of TP53 (63; 64). Mdm2/Hdm2 overexpression thus results in abnormally low cellular levels of TP53, which inhibit TP53's ability to induce cellular growth arrest when a cell experiences catastrophic stress or DNA damage. Without the brakes on cell growth imposed by normal TP53 function, catastrophically stressed or damaged cells, which would normally undergo TP53-mediated programmed cell death (apoptosis), may continue to replicate uncontrollably and acquire further, permanent genetic damage that cumulatively causes cells to become tumor cells. In this manner, Mdm2/Hdm2 acts as an E3 proto-oncogene in its modulation of TP53 activity.

E3s may act as either tumor suppressors or proto-oncogenes in a tissue- and cell context-specific manner. One such example of an E3 protein that regulates several critical, cancer-associated cellular pathways as a tumor suppressor or a proto-oncogene in a tissue-specific manner is SPOP. SPOP is an E3 protein subunit that is emerging as a conserved and ubiquitously expressed regulator of cellular homeostasis that functions through PPIs. SPOP operates as an adaptor subunit of trimeric SPOP-CUL3-RING E3 ubiquitin ligase complexes that catalyze the ubiquitination of specific substrate proteins. Dozens of SPOP protein substrates involved in diverse cell signaling pathways have been characterized since SPOP's initial discovery in 1997 (65) (Table 1.1), and the list of characterized SPOP substrates continues to grow each year. Like for other E3s, SPOP dysregulation, which occurs through changes in SPOP expression, genetic mutation/deletion, or altered subcellular localization, is increasingly recognized to promote pathology, particularly cancer, across a wide variety of tissues through alteration of SPOP-protein interactions. The remainder of this introduction chapter will provide a detailed overview

of our biological and clinical understanding of SPOP, whose PPIs in prostate cancer are the focus of this dissertation research work.

1.5 SPOP: An E3 ubiquitin ligase subunit frequently altered in cancer

1.5.1 SPOP discovery and initial characterization

First identified through an immunoscreening approach for human nuclear autoantibodies using serum from a scleroderma patient in 1997, SPOP (speckle-type POZ protein) was named for its characteristic speckled nuclear immunostaining appearance and its inclusion of a C-terminal POZ (poxvirus and zinc finger; also known as BTB [bric à brac, tramtrack, broad complex,]) structural domain (65). Further structural analysis demonstrated that SPOP also contains an N-terminal MATH (meprin and TRAF-C homology) domain. The N-terminal MATH domain and C-terminal BTB domain are the only major structural domains that the SPOP protein features, with the two domains connected by a short series of amino acids that act as a flexible linker (Figure 1.2). At the time of SPOP's initial discovery, nothing was known about its biological roles (including its role as an E3 ubiquitin ligase) or the functions of its component MATH and POZ/BTB structural domains. In 2003, however, a yeast two-hybrid screen for Cullin3 (CUL3) protein interaction partners identified for the first time that CUL3 selectively binds to proteins containing BTB domains, and specifically identified SPOP as a protein that binds to CUL3 through the SPOP BTB domain (66). This same study further suggested that BTB domain-containing proteins may serve as adaptor subunits of CUL3-RING (CRL3) ubiquitin ligase complexes that function to recruit specific substrates for CRL3-mediated ubiquitination, though this study did not specifically demonstrate that SPOP-CUL3-RING E3 complexes ($CRL3^{SPOP}$) mediate ubiquitination of any SPOP-binding proteins. In 2005, MacroH2A, a histone

variant that functions in X chromosome inactivation, was the first protein reported to be ubiquitinated by $CRL3^{SPOP}$ complexes in human cell line models (67), and several other proteins across a variety of species were subsequently characterized to be ubiquitinated by SPOP (or SPOP homolog)-CUL3 complexes in 2006 and 2007 (e.g., human DAXX (68), *Drosophila* Ci (69; 70) and Puc (71)).

1.5.2 SPOP structure and determinants of SPOP-protein interactions

A structural basis for SPOP E3 ligase functionality was provided through the first extensive crystallographic characterization of SPOP and SPOP-substrate-CUL3 complexes in 2009 (72). The SPOP MATH domain forms an antiparallel β sandwich that features a central shallow groove, through which SPOP binds to specific substrate proteins (Figure 1.2). This central shallow groove, referred to as the SPOP substrate binding cleft, is lined by aromatic SPOP residues Y87, F102, Y123, F125, W131, and F133 that are characterized as essential for enabling SPOP binding to substrates. SPOP recognizes substrate proteins, such as MacroH2A, DAXX, Ci and Puc, via conserved five-residue SPOP-binding consensus (SBC) motifs on substrates: φ-π-S-S/T-S/T (φ, nonpolar residue; π, polar residue). Importantly, these five-residue SPOP SBCs in substrates feature phosphorylatable serine and threonine (S and T) residues. Phosphorylation of these S/T residues was later demonstrated to be a mechanism by which SPOP binding to Pdx1 and NANOG, both SPOP substrates, is inhibited (73; 74), suggesting a general mechanism by which SPOP binding to substrates may be downregulated through phosphorylation. The SPOP BTB domain, in contrast to the SPOP MATH domain, features a series of hydrophobic alpha helices that enable both SPOP binding to the CUL3 N-terminal domain (75) and SPOP-SPOP multimerization (72; 76) (homo-multimerization with SPOP as

well as hetero-multimerization with SPOPL (75)) to promote formation of oligomeric SPOP-CUL3 complexes. Thus, SPOP's two major protein domains, its N-terminal MATH domain and its C-terminal BTB domain, each enable SPOP function by mediating specific PPIs: the SPOP MATH domain selectively binds to substrates that contain an SPOP SBC motif, while the SPOP BTB domain recruits CUL3-RING complexes that facilitate ubiquitination of an SPOP-MATH-domain-bound substrate.

Higher-order SPOP-CUL3 multimerization through the SPOP BTB domain was subsequently characterized to enhance $CRL3^{SPOP}$ E3 ligase activity. SPOP BTB domain-mediated oligomerization increases SPOP avidity for substrates with multiple SBCs, thereby increasing overall SPOP-substrate interaction affinity through multivalent interactions, to enhance SPOP-mediated ubiquitination of substrates (77). SPOP homo-multimerization has also been demonstrated to promote SPOP-driven formation of 'membrane-less' organelles (liquid-liquid phase separation) that results in SPOP's characteristic speckled subcellular distribution pattern (78). These membrane-less organelles formed by SPOP multimers are hypothesized to serve as hubs for SPOP-mediated ubiquitination, as disruption of SPOP multimer liquid-liquid phase separation impairs substrate ubiquitination by SPOP (78; 79).

1.5.3 SPOP mechanistic function and biological roles

As a substrate-recognition subunit of multi-subunit $CRL3^{SPOP}$ E3 ubiquitin ligase complexes, SPOP is thought to facilitate ubiquitination via mechanisms common among multi-subunit CRL complexes as follows (23; 38): In $CRL3^{SPOP}$ complexes, CUL3 scaffolds RBX1, a RING E3 ligase that recruits an E2 ubiquitin-conjugating enzyme (E2), to SPOP, which recruits specific substrates (Figure 1.2a). RBX1 binds to an E2-ubiquitin thioester complex in a manner

that positions the E2's covalently linked ubiquitin into a high energy conformation, such that it is poised for nucleophilic attack by a substrate protein lysine. Substrate-SPOP-CUL3 binding to RBX1 subsequently facilitates close proximity of a substrate lysine residue to the RBX1-E2-ubiquitin, allowing for direct covalent transfer of the ubiquitin from the E2 to the substrate's lysine. As such, SPOP does not catalyze conjugation of ubiquitin to a substrate protein in the traditional sense of directly lowering the chemical activation energy of the conjugation reaction. Rather, SPOP acts as a bridge within substrate-SPOP-CUL3-RBX1-E2~Ub PPI complexes to facilitate direct transfer of ubiquitin from an E2 ubiquitin-conjugating enzyme to a substrate protein.

Over the past twenty-five years, SPOP has emerged as a critical regulator of a diverse array of cellular processes across tissue types through its regulation of a wide range of proteins (examples given in Table 1.1). SPOP's best understood role is in proteostasis, in which SPOP has largely been characterized to facilitate the ubiquitin-mediated degradation of protein substrates. In this proteostatic capacity, SPOP function overall has been characterized to be tumor suppressive across cell lineages (with some notable exceptions, discussed below). Nevertheless, SPOP has also been observed to perform nondegradative functions, in some cases by facilitating nondegradative ubiquitination of substrates, such as for MacroH2A (67), MyD88 (80), and INF2 (81). The cellular consequences of SPOP biological function largely derive from the functions of the substrates that SPOP binds to and differentially modulates in distinct tissues, as SPOP substrates include proteins that are tumor suppressors and proto-oncogenes. Thus, SPOP negative modulation of tumor suppressors (typically through ubiquitin-mediated degradation), such as the anti-cellular growth PTEN kinase in renal cells, promotes cell growth and survival, while SPOP negative modulation of proto-oncogenes, such as the pro-cellular

growth c-Myc transcription factor in prostate cells, inhibits cell growth and survival (82; 83). The number of characterized SPOP protein binding partners has increased substantially in recent years (Table 1.1), and our understanding of SPOP's biological roles in different cellular contexts will continue to be enhanced by further identification of SPOP protein binding partners. Contributing to this identification of SPOP binding partners to nominate new mechanisms of SPOP-mediated biology, our lab has conducted parallel high-throughput PPI screens to detect new SPOP protein binding partners from among more than 600 cancer associated-proteins, which will be discussed in chapter 2 of this dissertation.

1.5.4 Mechanisms of SPOP regulation

It is currently unclear exactly how SPOP interactions with different protein substrates are regulated, particularly in situations where SPOP substrates are ubiquitously expressed across tissue types, but SPOP has only been characterized to regulate a given substrate within a specific tissue lineage. For example, SPOP has been characterized to bind to and degrade the protein PTEN in renal cells (82), but not in prostate cells where PTEN and SPOP are also expressed (84; 85). To address this question, several research groups have begun to examine mechanisms of SPOP regulation at the transcriptional, posttranscriptional, and posttranslational levels:

SPOP transcriptional regulation: In 2014, HIFs (hypoxia inducible factors) were found to positively regulate SPOP transcription in kidney lineage cells under hypoxic conditions (82). In a later study on epigenetic silencing phenomena in colorectal cancer development and progression, *SPOP* transcription was also found to be positively regulated by binding of the RXRA (retinoid X receptor alpha) nuclear receptor to the *SPOP* promoter, while hypermethylation of the RXRA consensus sequence in the *SPOP* promoter effectively silenced *SPOP* gene expression (86).

SPOP transcription has been found to be downregulated by binding of SMADs to SMAD-binding elements in the SPOP promoter. However, outside of HIF-, RXRA-, and SMAD-mediated regulation of *SPOP* gene expression, relatively little is known about specific transcription factors or cell signaling pathways that strongly influence *SPOP* gene expression, although the endogenous *SPOP* gene promoter features numerous transcription factor consensus motifs suggesting extensive regulation in different cellular contexts(87).

SPOP post-transcriptional regulation: Several microRNAs (miRs) have been characterized to regulate *SPOP* mRNA levels. MiR-145 (88), miR-543 (89), miR-372 (90), and miR373 (90) have all been found to bind to the 3' untranslated region (UTR) of *SPOP* transcripts, leading to inhibition of *SPOP* mRNA translation into protein. Various cancers have been observed to exploit miR-downregulation of *SPOP* mRNA translation to promote oncogenesis.

SPOP post-translational regulation: Several posttranslational mechanisms regulating SPOP activity have recently been described. In one study, SPOP was found to be phosphorylated at S6 (within a serine-proline motif) by cyclin D1-CDK4, which both promoted binding to 14-3-3γ and inhibited ubiquitin-mediated degradation by FZR1-E3 ligase complexes (91). Another group used chemical-genetic approaches (92) to identify two kinases, AURKA (aurora kinase A) and LIMK2 (LIM domain kinase 2), that bind to and phosphorylate SPOP. AURKA was reported to phosphorylate SPOP at residues S33, T56, and S105 (93), while LIMK2 was reported to phosphorylate SPOP at residues S59, S171, and S226 (94). SPOP phosphorylation by both kinases was also characterized to induce ubiquitin-mediated degradation of SPOP. Collectively, these studies suggest mechanisms by which SPOP expression may be regulated through phosphorylation by kinases. These studies did not characterize how these phosphorylation events influence SPOP binding to substrates, though AUKRA- and LIMK2-mediated phosphorylation

of SPOP was found to promote nuclear subcellular localization of SPOP. Further characterization of the functional consequences of these phosphorylation events will be necessary to determine how these posttranslational modifications enhance SPOP degradation, and how they may influence SPOP-substrate and SPOP-CUL3 interactions to impact overall SPOP function.

1.5.5 Mechanisms of SPOP dysregulation

Because SPOP regulates critical, wide-ranging biological processes, dysregulation of SPOP activity frequently results in pathology, particularly cancer. SPOP dysregulation that promotes cancer development commonly occurs through several mechanisms:

Aberrant expression*:* Aberrant downregulation of SPOP expression, through repression of gene transcription, posttranscriptional downregulation, or posttranslational modification leading to higher SPOP turnover, is associated with tumorigenesis in prostate cancer (95; 96), colorectal cancer (86; 97-99), gastric cancer (99), glioma (100), liver cancer (101-103), ovarian cancer (104), and lung cancer (105). Mechanistically, SPOP downregulation in these tissue lineages reduces SPOP-mediated ubiquitination and proteasomal turnover of SPOP's oncogenic substrates. In kidney cells, however, SPOP overexpression has been associated with promotion of characteristics of clear cell renal cell carcinoma (ccRCC) (71; 106).

Deletion*:* Estrogen-sensitive breast and ovarian tissues feature SPOP deletion or loss of heterozygosity as a contributing factor to tumorigenesis. *SPOP* deletion in breast tissue promotes oncogenesis partly through loss of SPOP degradation of SRC-3 (steroid receptor coactivator protein 3; also *NCOA3*), a transcriptional co-activator of ER (estrogen receptor) (107; 108).

Missense mutation*:* Recurrent missense mutations in the SPOP MATH domain at residues lining the SPOP substrate binding cleft are drivers of tumorigenesis in sex hormone-responsive prostate and endometrial tissues (109; 110) (Figure 1.2b). These recurrent missense mutations function to inhibit SPOP interaction with oncogenic substrates, leading to their reduced SPOP-mediated degradation and their aberrant accumulation. Of note, prostate cancers feature a set of recurrent missense mutations in the MATH domain that is unique from the set observed in endometrial cancers (serous endometrial and clear-cell endometrial subtypes).

Alteration of subcellular localization*:* Under hypoxic conditions and in the setting of clear cell renal cell carcinoma (ccRCC), hypoxia-inducible factors (HIFs) upregulate transcription of *SPOP*. Tissue hypoxia also promotes redistribution of SPOP protein to the cytoplasm from the nucleus, where SPOP predominantly localizes under normoxic conditions (82). In contrast to the tumor suppressive function of nuclear SPOP, cytoplasmic SPOP has been characterized to act as an oncogene by targeting tumor suppressors PTEN and DUSP7, which respectively downregulate pro-cellular growth PI3K/Akt and MAPK/ERK pathway activation, for ubiquitin-mediated degradation. The exact mechanism by which SPOP translocates to the cytoplasm from the nucleus under hypoxic conditions remains unclear, but it has been hypothesized that posttranslational modifications of SPOP protein may be responsible. AURKA and LIMK2, two kinases recently identified to phosphorylate SPOP on distinct residues, have been described to promote nuclear localization of SPOP through both phosphorylation and protein-protein interactions, and knockdown of AURKA and LIMK2 has been characterized to result in redistribution of SPOP from the nucleus to the cytoplasm (93; 94). Further work will be required to identify the detailed mechanisms by which SPOP subcellular localization is altered, however.

1.5.6 SPOP is the most frequently mutated gene in primary prostate adenocarcinoma

In the early 2010s, large-scale efforts to sequence the exomes of patient prostate tumors revealed that SPOP is the most frequently mutated gene in primary prostate adenocarcinoma (110-113), suggesting a critical biological function for SPOP in prostate lineage cells. Recurrent missense mutations in SPOP are mutually exclusive of other frequent genetic alterations that drive prostate tumorigenesis, such as ETS (erythroblast transformation-specific) gene rearrangements, PTEN deletions, and TP53 deletions/mutations. SPOP mutant tumors furthermore feature distinct somatic copy number alteration (SCNA) profiles (including co-occurring CHD1 deletion in roughly 50% of tumors), DNA methylation patterns, and gene expression patterns (110). Collectively, these genetic features nominate SPOP mutant tumors as a distinct molecular subclass of primary prostate adenocarcinomas.

Subsequent mechanistic studies into SPOP's role in prostate lineage cells have described an overall tumor suppressive function for SPOP, in which SPOP targets oncoproteins in androgen-responsive cell signaling pathways (e.g., AR, SRC-3, TRIM24, BRD4) for ubiquitin-mediated degradation (107; 114-121). Missense mutations recur in the SPOP MATH domain at residues that line the SPOP substrate binding cleft (Figure 1.2c). These recurrent mutations serve to inhibit SPOP interaction with oncogenic substrate proteins, leading to a reduction in their SPOP-mediated ubiquitination/degradation and their aberrant accumulation. This aberrant accumulation of oncogenic substrates then upregulates the activity of pro-cellular growth AR and PI3K/Akt cell signaling pathways, which subsequently promotes the uncontrolled growth of prostate cells into tumors (85).

Despite progress in characterizing SPOP mutation-mediated oncogenesis in prostate lineage cells, several questions related to the role of SPOP mutations in driving prostate

tumorigenesis remain outstanding. All prostate cancer-associated missense mutations in the SPOP MATH domain are currently characterized to uniformly induce loss of SPOP interaction with substrates, but are there any functional differences between these prostate cancer-associated SPOP missense mutations? Do prostate cancer-associated missense mutations in SPOP have any function in cancer beyond inducing loss-of-interaction with oncogenic SPOP substrates? SPOP mutant tumors also feature defects in DNA double strand break repair and transcriptome profiles akin to *BRCA1*-deficient tumors (98). By what specific mechanisms might recurrent SPOP mutations impair DNA repair and contribute to genomic instability? Do co-occurring CHD1 deletions, which are present in ~50% of SPOP-mutant primary prostate adenocarcinomas, have a synergistic effect with SPOP mutation in promoting tumorigenesis?

To begin to address these questions, I and others in our lab have characterized SPOP PPIs that are altered by recurrent, prostate cancer-associated missense mutations in SPOP to nominate PPI-mediated mechanisms of SPOP mutant-mediated oncogenesis. The results of this work and the characterization of a newly discovered SPOP missense mutation-induced PPI with implications for cancer development, the SPOP-c-Jun PPI, will be discussed in Chapter 2 of this dissertation.

1.5.7 Current therapeutic strategies targeting SPOP-driven tumorigenesis

To better understand patient risks and medical treatment responses associated with SPOP-mutant prostate cancer, several recent studies have sought to define unique clinicopathologic characteristics of SPOP-mutant prostate tumors. In these studies, SPOP-mutant prostate tumors have been characterized to have relatively benign features compared with other prostate tumor subtypes, with lower frequency of invasive tumor margins, extraprostatic

extension, and seminal vesicle invasion (122) that is independent of PSA levels, patient age, and tumor Gleason score (123). SPOP mutant tumors have also been found to be uniquely associated with high AR pathway activity (110), high patient blood prostate specific antigen (PSA) levels, and favorable patient prognoses for progression-free survival (PFS) and metastasis-free survival (MFS) (122). *SPOP* mutations have furthermore been found at lower frequency in prostate cancer metastases than in primary tumors. Collectively, these studies suggest that recurrent SPOP mutations drive a clinically localized and readily detectable prostate tumor phenotype rather than an invasive, metastatic, and occult tumor phenotype (112; 113; 124; 125). For the type of localized prostate cancer most often driven by recurrent SPOP mutations, radical prostatectomy, external beam radiation therapy (EBRT), and brachytherapy are mainstays for first-line treatment (126). Androgen deprivation therapy (ADT) is used as a therapeutic adjuvant for EBRT in the treatment of primary prostate tumors, and in situations of disease recurrence or metastasis. For the treatment of metastatic prostate cancer resistant to androgen deprivation therapy (i.e., castration-resistant prostate cancer, or CRPC), additional chemotherapeutics, such as docetaxel, cabazitaxel, olaparib, and mitoxantrone, are generally employed.

Several clinical and basic science studies have also begun to examine whether SPOP mutant prostate tumors feature unique therapeutic vulnerabilities. Given the aforementioned association of SPOP mutation with high AR pathway activity in prostate tumors, three recent clinical studies have specifically examined the outcomes of patients with SPOP-mutant prostate tumors treated with chemical ADT (127-129). In one study, castration-resistant prostate tumors with recurrent SPOP mutations and co-occurring CHD1 deletions were particularly sensitive to ADT with systemic abiraterone, a CYP17A1 inhibitor that blocks androgen synthesis (127). In a second study, it was observed that castration-sensitive prostate tumors (CSPC) with recurrent

SPOP mutations are sensitive to a wide variety of ADT therapies, including systemic abiraterone and enzalutamide (an androgen receptor antagonist), though it is unclear whether CHD1 deletion status influenced the observed clinical response (128). A third study observed that for prostate tumors in patients that progressed post-cancer treatment, there was also a lower prevalence of SPOP mutations among progressing ADT-treated prostate tumors than among IR- and/or surgery-treated prostate tumors, which further indicated that ADT strategies may be particularly effective in treating SPOP mutant tumors (129). Outside ADT approaches, results from a fourth (basic science) study suggested that SPOP-mutant tumors may also be more resistant to therapy with docetaxel, a microtubule-inhibiting taxane commonly used in mCRPC treatment (130). In a fifth study, expression of prostate cancer-associated SPOP mutants and endometrial cancer-associated SPOP mutants in cancer cell line models altered sensitivity to BET inhibitors, compounds that reversibly bind to BET proteins (BRD2, BRD3, and BRD4, which are all SPOP substrates) to inhibit their interactions with acetylated histones and transcription factors. Expression of prostate cancer-associated SPOP mutants, which lose interaction with BET proteins relative to SPOP wild-type (WT), results in an elevation of BET protein levels that dampens sensitivity to BET inhibitors. In contrast, expression of endometrial cancer-associated SPOP mutants, which exhibit enhanced interaction with BET proteins, lowers BET protein levels in a manner that increases cellular sensitivity to BET inhibitors. Last, defects in DNA damage repair pathways induced by recurrent SPOP mutations have also been demonstrated to enhance SPOP mutant tumor sensitivity to ionizing radiation (131) and inhibition of PARP (Poly (ADP-ribose) polymerase; functions to recognize and initiate repair of DNA single strand breaks) (98). Altogether, these studies suggest that SPOP mutation status in primary and metastatic prostate tumors may strongly influence tumor response to systemic chemotherapies.

Because SPOP executes its biological functions through PPIs, direct small molecule modulation of SPOP-protein interactions has recently been explored as a potential therapeutic strategy to reverse SPOP-driven pathology. To date, these studies have focused exclusively on inhibition of SPOP WT PPIs in ccRCC cancers driven by SPOP WT overexpression and cytoplasmic SPOP subcellular localization. In the first study reporting discovery of small molecule inhibitors of SPOP-protein interactions, a virtual screening approach was employed to nominate compounds which could bind to the SPOP substrate binding cleft *in silico* (132). A fluorescence polarization assay with SPOP as the receptor and Puc_SBC1 as the fluorophore-tracer was then developed to validate compounds that could inhibit the SPOP-Puc_SBC1 interaction, and subsequent surface plasmon resonance (SPR), nuclear magnetic resonance (NMR), and cellular thermal shift assay (CETSA) approaches confirmed direct binding of compounds to the SPOP MATH domain. Further functional evaluation of validated compounds demonstrated that the compounds were able to inhibit oncogenic SPOP-PTEN and SPOP-DUSP7 interactions, and that compound treatment of SPOP-driven ccRCC cell lines and tumor xenografts resulted in an antiproliferative effect. A subsequent study by the same research group further optimized this identified SPOP inhibitor's chemical scaffold through structure-activity relationship (SAR) analysis to further improve potency for inhibition of SPOP-PTEN and SPOP-DUSP7 interactions and ccRCC cell line colony formation and cellular proliferation assays (133).

While small molecule inhibition of SPOP WT has been explored, no studies to date have examined whether selective small molecule modulation of SPOP missense mutants might also be possible. One strategy to restore mutant SPOP function may be to use small molecules as molecular glues to re-induce SPOP-protein interactions that are lost through SPOP missense

mutations in prostate cancer, thereby restoring SPOP E3 ubiquitin ligase functionality in SPOP-mutant prostate tumors. The feasibility of utilizing small molecules to induce and stabilize PPIs for therapeutic purposes has been demonstrated through prior clinical implementation of both synthetic and natural-product PPI inducers, including the immunosuppressants cyclosporin and rapamycin and the microtubule stabilizers docetaxel and paclitaxel (134-139). Several other studies have nominated additional compounds with PPI inducer activity that may have therapeutic potential, including recent work by our lab that describes the first small molecule PPI inducer of mutated tumor suppressor $SMAD4^{R361H}$ with SMAD3 to restore tumor-suppressive TGF-β signaling (140). Toward this goal of identifying small molecule restorers (i.e., re-inducers) of SPOP PPIs for SPOP missense mutants, we have developed an ultra-high-throughput, time-resolved fluorescence resonance energy transfer (uHTS TR-FRET) assay and conducted a pilot screen to identify small molecule inducers of SPOP F133V interactions with oncogenic chromatin reader protein BRD4. While SPOP WT normally downregulates BRD4 protein levels through degradative ubiquitination of BRD4 in prostate lineage cells, recurrent prostate cancer-associated SPOP missense mutants (the most frequent of which is F133V) lose interaction with BRD4 and produce aberrantly high intracellular levels of BRD4 protein that promote prostate tumorigenesis. Restoration of SPOP F133V interaction with BRD4 in SPOP F133V prostate tumors through direct small molecule modulators may thus represent a promising therapeutic strategy to reverse SPOP F133V-mediated tumorigenesis. I summarize this research work in chapter 3 of this dissertation.

1.6 Dissertation scope

Overall, this dissertation describes research work 1) to identify and characterize SPOP PPIs relevant to prostate cancer and 2) to discover small molecule modulators of SPOP PPIs. In chapter 2, I will summarize work that 1) expands our understanding of the SPOP protein-protein interactome and 2) characterizes the interaction interface and function of a novel SPOP PPI, the SPOP-c-Jun PPI, that is induced by recurrent, prostate cancer-associated SPOP F133L/V missense mutations. In chapter 3, I will summarize work to develop an ultra-high-throughput screening (uHTS) assay to identify small molecules inducers of SPOP F133V-BRD4 interactions. Finally, in chapter 4 I will discuss the overall implications of this research work within the conceptual frameworks established by this introductory chapter. Collectively, this dissertation work aims to contribute to our understanding of how recurrent SPOP missense mutations drive prostate tumorigenesis and to nominate novel therapeutic approaches to reverse SPOP mutation-driven oncogenesis.

Figure 1.1. Overview of ubiquitin conjugation and its functional consequences.

Ubiquitin is conjugated to a substrate protein through a sequence of three enzymatic reactions. First, an ubiquitin-activating enzyme (E1) harnesses the energy of ATP hydrolysis to form a covalent thioester bond with the carboxy terminus of a ubiquitin monomer. Second, the E1 covalently transfers the attached ubiquitin to an ubiquitin-conjugating enzyme (E2). Third, an ubiquitin ligase (E3) then binds to the E2-ubiquitin and to a substrate protein, bringing the E2-ubiquitin and substrate into proximity. The E3 facilitates bond formation between the C-terminal carboxyl group of the ubiquitin and an ε-amino group on a substrate lysine (i.e., substrate ubiquitination). Consecutive cycles of ubiquitination on a substrate protein can be promoted by E3 ligases to generate polyubiquitin chains, which are linked through different ubiquitin lysine residues. Different topologies produced by protein monoubiquitination or polyubiquitination are recognized by distinct effector macromolecules with unique ubiquitin-binding domains, which then subsequently mediate unique functional consequences.

Figure 1.1

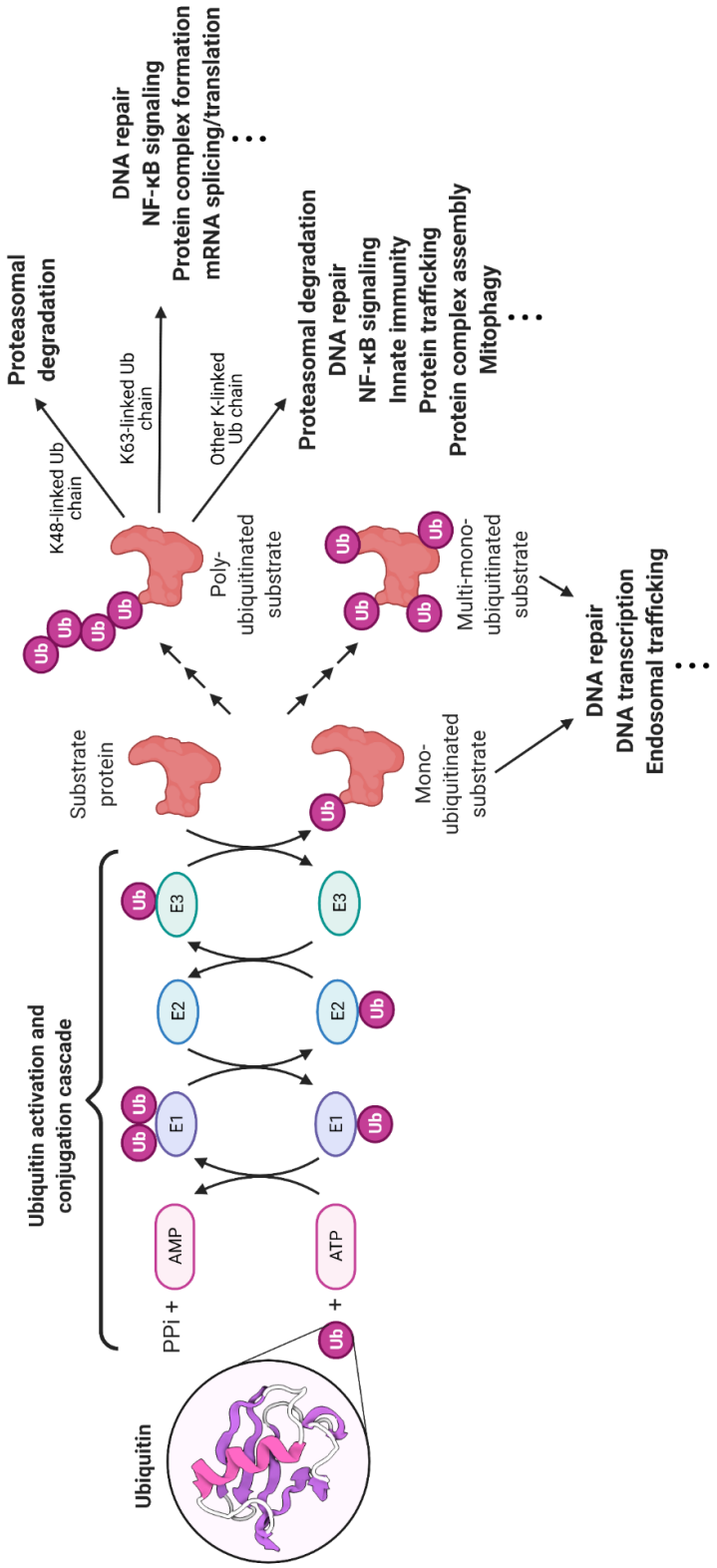
Ubiquitin activation and conjugation cascade
Ubiquitin
PPi +
AMP
ATP
+
E1
E2
E3
Substrate protein
Mono-ubiquitinated substrate
Poly-ubiquitinated substrate
Multi-mono-ubiquitinated substrate
K48-linked Ub chain
K63-linked Ub chain
Other K-linked Ub chain
Proteasomal degradation
DNA repair
NF-κB signaling
Protein complex formation
mRNA splicing/translation
...
Proteasomal degradation
DNA repair
NF-κB signaling
Innate immunity
Protein trafficking
Protein complex assembly
Mitophagy
...
DNA repair
DNA transcription
Endosomal trafficking
...

Figure 1.2. Overview of SPOP function and structure.

a) Illustration of SPOP-CUL3-RBX1 E3 ubiquitin ligase complex-mediated ubiquitination of SPOP substrates.

b) Diagram of SPOP protein domains (141; 142). The frequency of mutations at particular amino acid residues in patient prostate adenocarcinomas are indicated. Residue mutation frequencies determined from combination of TCGA and MSKCC datasets representing a total of 2,977 patient prostate tumors (110; 113; 143).

c) Crystal structure of SPOP dimer (PDB: 3hqi) (72). Individual SPOP monomers shaded in dark grey and light grey. The sites of amino acid mutations indicated in (b) are highlighted in dark green (141; 142).

Figure 1.2

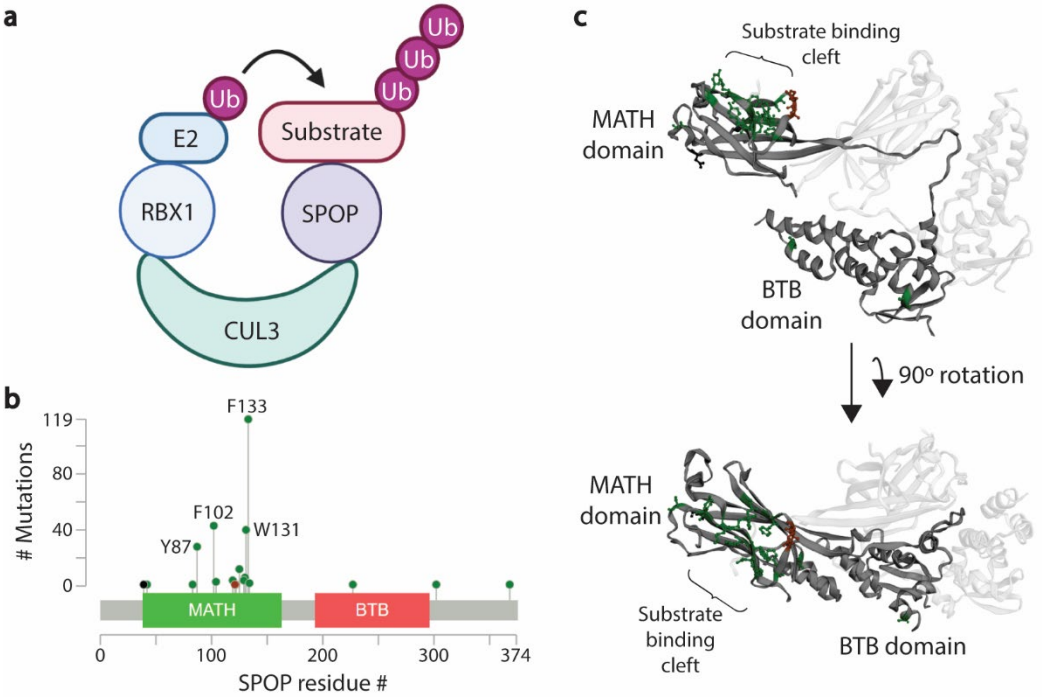
a
Ub
Ub
Ub
Ub
E2
Substrate
RBX1
SPOP
CUL3
b
Mutations
119
80
40
0
F133
F102
W131
Y87
MATH
BTB
0
100
200
300
374
SPOP residue #
c
Substrate binding cleft
MATH domain
BTB domain
90° rotation
MATH domain
Substrate binding cleft
BTB domain

Table 1.1 Examples of reported SPOP substrates

SPOP substrate	Associated cellular process/pathway	Cell lineage observed	Reference(s)
AR	Androgen receptor signaling	Prostate	(114; 115)
ATF2	Gene transcription and DNA damage response	Prostate	(144)
AURKA	Mitosis	Prostate	(93)
BRD2	Global gene transcription	Endometrial, prostate	(118-120)
BRD3	Global gene transcription	Endometrial, prostate	(118-120)
BRD4	Global gene transcription	Endometrial, prostate	(119; 120)
BRMS1	Metastasis	Breast	(145)
Caprin1	Stress granule assembly	Prostate	(130)
CDC20	Cell cycle	Prostate	(146)
Cyclin E1	Cell cycle	Prostate	(84)
DAXX	Apoptosis, global gene transcription	Endothelial, prostate, renal	(68; 147; 148)
DDIT3	Endoplasmic reticulum stress response	Prostate	(149)
DEK	Gene transcription	Prostate	(121)
DHX9	DNA replication, transcription, translation, DNA repair	Uterine	(150)
DUSP7	MEK/ERK signaling	Renal	(82)
EGLN2	HIF signaling	Prostate	(151)
ER	Estrogen receptor signaling	Endometrial	(152)
ERG	Transcription regulation	Prostate	(153; 154)
FADD	NF-κB signaling	Lung, pancreatic	(155; 156)
FASN	Lipid metabolism	Prostate	(157)
GLI2	Sonic hedgehog signaling	Colon, gastric, lung	(70; 158-165)
GLI3	Sonic hedgehog signaling	Lung	(70; 158-165)
GPER1	Extra-nuclear estrogen signaling	Breast	(166)
HDAC6	Chromatin accessibility	Colon	(167)
ILF3	Serine biosynthesis	Colon	(168)
INF2	Mitochondrial fission	Prostate	(81)
LATS1	Hippo signaling	Renal	(169)
LIMK2		Prostate	(94)
MacroH2A	X-chromosome inactivation		(67; 170)
MBI1	X-chromosome inactivation		(67)
MYC	Gene transcription	Prostate	(83)
MYD88	Innate inflammation, NF-κB signaling	Hematopoietic cells	(80; 171-173)

NANOG	AMPK signaling, BRAF signaling	Pancreatic, prostate	(74; 174; 175)
PD-L1	Adaptive immunity	Prostate	(91)
PDX1	Endocrine pancreas differentiation	Pancreatic	(176)
PR	Progesterone receptor signaling	Breast	(177)
PTEN	PI3K/mTOR signaling	Renal	(82)
SENP7	Sumolyation regulation	Hepatic	(103)
SIRT2	Chromatin accessibility	Lung	(178)
SLC7A1	Arginine metabolism	Hepatic	(179)
SRC3	Androgen receptor signaling, estrogen receptor signaling, PI3K/mTOR signaling	Breast, prostate	(85; 107; 116)
TRIM24	Androgen receptor signaling	Prostate	(117; 121)
XBP1	Endoplasmic reticulum stress response	Pancreatic	(180)
ZBTB3	Sonic hedgehog pathway	Endometrial	(181)
ZMYND11	Androgen receptor signaling	Prostate	(129)

CHAPTER 2:

ANALYSIS OF DIFFERENTIAL WILD-TYPE AND MUTANT SPOP PROTEIN-PROTEIN INTERACTIONS REVEALS SPOP F133L/V MUTATION-INDUCED GAIN OF INTERACTION THAT PROMOTES C-JUN PROTEIN STABILITY AND TRANSCRIPTIONAL ACTIVITY

This chapter is under review for publication as:

Doyle SP, Gu L, Mo X, Niu Q, Du Y, Fu H. “Analysis of differential wild-type and mutant SPOP protein-protein interactions reveals SPOP F133L/V mutation-induced gain of interaction that promotes c-Jun protein stability and transcriptional activity”.

2.1 Introduction

Speckle-type POZ protein (SPOP) is a conserved and ubiquitously expressed protein that functions to regulate essential cellular signaling pathways through its interactions with other proteins. SPOP's primary cellular function has been ascribed to its role in proteostasis as a substrate-recognition adaptor subunit of Cullin3 (CUL3)-RING E3 ubiquitin ligase complexes (182). In this role, SPOP bridges CUL3-RING E3 ubiquitin ligase complexes to specific substrate proteins to facilitate substrate ubiquitination and modulate substrate expression level and function (72; 183). Dysregulation of SPOP activity, which occurs through alterations in SPOP expression (71; 99), mutation (109; 111; 184), and changes in subcellular localization (82), has been characterized to promote pathology, particularly oncogenesis. SPOP's emerging roles in developmental biology, normal cellular homeostasis, and pathology remain incompletely understood, however, because the number of identified protein binding partners for SPOP remains limited.

In prostate lineage cells specifically, SPOP has been characterized to function primarily as a tumor suppressor by targeting oncogenic proteins in androgen-sensitive cell regulatory pathways, including AR (114; 115), SRC3 (85; 107; 116), BRD4 (118-120), and TRIM24 (117; 121), for ubiquitin-mediated degradation. Missense mutations recur in SPOP's substrate recognition MATH domain in up to 15% of primary prostate adenocarcinomas (110; 111) and are characterized to drive cellular transformation by impairing SPOP's ability to bind to its substrates, leading to a decrease in SPOP-mediated degradation and aberrant accumulation of substrates (185). Despite SPOP's characterization as a tumor suppressor in prostate lineage cells, *SPOP* genetic alterations in prostate adenocarcinoma occur almost exclusively as heterozygous missense mutations (110; 111), rather than homozygous deletions or homozygous missense

mutations, in a pattern suggestive of potential oncogenic gain-of-function (186). According to patient adenocarcinoma exome sequencing data from The Cancer Genome Atlas (110), the most frequently mutated SPOP MATH domain residues are Y87 (mutation frequency of ~10.7% among all SPOP mutant tumors), F102 (~18.3%), W131 (~12.4%), and F133 (~46.7%). SPOP F133L and F133V mutations furthermore represent ~45.6% and 39.2% of all F133 missense mutations reported for prostate adenocarcinomas, respectively, though less frequent F133C (~3.80%), F133I (~5.06%) and F133S (~6.33%) mutations have also been reported. All identified recurrent, prostate cancer-associated missense mutations in the SPOP MATH domain are currently characterized to induce loss of interaction with SPOP substrate proteins (85; 107; 114-120). It is currently unclear whether there are functional differences among distinct, prostate adenocarcinoma-associated *SPOP* missense mutations, however. Because SPOP exerts its effects through protein-protein interactions, it has been hypothesized that recurrent missense mutations in *SPOP* may promote *de novo* gain-of-function interactions with novel partner proteins to promote prostate tumorigenesis (111; 119), though no studies to date have systematically examined this possibility.

Here, we expand the characterized SPOP interactome through focused, SPOP-centric high throughput protein-protein interaction screens to propose novel mechanisms of SPOP biology. We then examine how recurrent, prostate adenocarcinoma-associated mutations in SPOP alter SPOP's binding affinity with the identified protein binding partners. SPOP mutations induce loss-of-interaction with several cancer-associated proteins as previously reported, but F133L and F133V mutations also enable gain-of-interaction with other cancer-associated proteins, suggesting a potential gain of oncogenic function for SPOP F133L/V mutations beyond loss of SPOP tumor suppressor activity. We conclude by characterizing how SPOP variants

interact with and influence the activity of oncogenic transcription factor c-Jun, one of the highest-confidence gain-of-interaction partners detected through our PPI screens for SPOP F133L/V point mutants.

2.2 Experimental procedures

Cell lines

All cell lines were incubated at 37°C in humidified conditions with 5% CO_2. Human embryonic kidney 293T cells (HEK293T; ATCC #CRL-3216) were maintained in Dulbecco's Modified Eagle Medium (DMEM; Corning #10-0103-CV). C4-2 (ATCC #CRL-3314) and 22Rv1 (ATCC #CRL-2505) were maintained in RPMI-1640 with L-glutamine (Corning #10-040-CV). All cell culture medium was supplemented with 10% fetal bovine serum (Atlanta Biologicals #S11550) and 100 units/mL of penicillin/streptomycin (Cell Gro, #30-002-CI).

Antibodies for western blot

The following primary antibodies were used at a 1:1000 dilution in TBST (20 mM Tris-base, 150 mM NaCl, 0.05% Tween-20) with 5% (w/v) non-fat milk for western blot: GST (#2624), FLAG (#14793), GFP (#2956), V5 (#13202), HA (#3724), BRD4 (#13440), SRC3 (#2126), and c-Jun (#9165) antibodies were purchased from Cell Signaling Technology; SPOP (#16750-1-AP) and TRIM24 (#14208-1-AP) antibodies were purchased from Proteintech; CUL3 (A301-109A-T-1) antibody was purchased from Bethyl Laboratories; γ-tubulin (T6557) was purchased from Sigma. The following secondary antibodies were used at a 1:5000 dilution in TBST with 5% non-fat milk for chemiluminescent western blot detection: goat anti-rabbit IgG (111-035-003) and goat anti-mouse IgG (115-035-003) from Jackson Immunoresearch Laboratories.

Plasmids, molecular cloning, and mutagenesis

Plasmids for mammalian expression of fusion proteins were generated using the Gateway cloning system (Invitrogen) according to the manufacturer's instructions. The following vector backbones were used as Gateway destination vectors: GST (pDEST27; Invitrogen #11812013), Venus-FLAG (VF; pSCM167), and V5 (pHAGE). Genes in the OncoPPi library were provided by Dr. Kenneth Scott and purchased from the DNASU Plasmid Repository as previously described (17). SPOP (#HsCD00081806), JUN (#HsCD00520171), JUNB (#HsCD00719007) and JUND (#HsCD00820950) cDNA plasmids were purchased from DNASU. SPOP mutations were introduced with the QuikChange Lightning Site-Directed Mutagenesis kit (Agilent #210518) using the SPOP cDNA plasmid from DNASU as a template, and with the following primers:

Y87C forward primer (5'- GAT TAC CTG TCA CTT TGC CTG TTA CTG GTC AGC),

F102C forward primer (5'- GAA GTT CGG GCA AAA TGC AAA TTC TCC ATC CTG),

W131C forward primer (5'-TTT GTG CAA GGC AAA GGG GGA TTC AAG AAA TTC ATC),

W131G forward primer (5'-AGG TTT GTG CAA GAC TGT GGA TTC AAG AAA TTC ATC CGT),

F133C forward primer (5'-CAA GGC AAA GAC TGG GGA TGC AAG AAA TTC ATC CGT AGA),

F133I forward primer (5'-CAA GGC AAA GAC TGG GGA ATC AAG AAA TTC ATC CGT AGA),

F133 forward primer (5'- CAA GGC AAA GAC TGG GGA CTC AAG AAA TTC ATC CGT AGA),

F133S forward primer (5'-CAA GGC AAA GAC TGG GGA TCC AAG AAA TTC ATC CGT AGA),

F133V forward primer (5'-CAA GGC AAA GAC TGG GGA GTC AAG AAA TTC ATC CGT AGA)

and corresponding reverse complement primers.

Transfection and lentivirus infection

HEK293T cells were transiently transfected using XtremeGene HP (Sigma #06366546001) according to the manufacturer's instructions. Lentivirus was generated by transfecting VSV-G, pCMVΔ8.91 and pHAGE transgene expression plasmids into HEK293T cells. Supernatant containing lentivirus was collected 72 hours after transfection and filtered through 0.22 μm PES membrane (Corning 431229). C4-2 and 22Rv1 cells were infected with filtered viral supernatant in the presence of 8 ug/mL polybrene (Sigma #TR-1003-G) and selected in growth medium containing 1 ug/mL puromycin (Acros Organics #227420100).

RNA interference and stable gene knockdown cell line generation

Mammalian non-target (#SHC016) and CUL3-specific (TRC295899, TRC307983) shRNA vectors were purchased from the Sigma MISSION human shRNA library. Stable gene knockdown cell lines were generated by transducing HEK293T cells with shRNA lentivirus and performing cell selection with DMEM containing 2 ug/mL puromycin (Acros Organics #227420100).

Quantitative reverse transcription polymerase chain reaction (RT-qPCR)

Total mRNA was purified using the E.Z.N.A Total RNA Kit (Omega Bio-tek #R6834), followed by DNase I (Invitrogen #18068-015) treatment and DNase heat inactivation at 65 °C for 10 minutes in the presence of 2 mM EDTA. cDNA was synthesized using 250 ng of total RNA and

the SuperScript III First-Strand cDNA Synthesis System (Invitrogen #18080-051). qPCR was performed using SsoAdvanced Universal SYBR Green Supermix reagent (BioRad #172-5271) with an Eppendorf Mastercycler Realplex system (Eppendorf) in 45 cycles of the following: 95 °C for 15 second, 55 °C for 15 seconds, and 72 °C for 20 seconds. Normalized target gene expression (ΔCt, delta cycle threshold) was calculated as ΔCt = Ct(GAPDH) – Ct(JUN). SPOP expression-associated changes in JUN gene expression were calculated as ΔΔCt = ΔCt(+SPOP) – ΔCt(EV negative control). Relative mRNA expression levels are expressed as $2^{-\Delta\Delta Ct}$.

Western blot

Proteins in 2x Laemmli sample buffer were resolved by 10% polyacrylamide gel electrophoresis (SDS-PAGE) and transferred to nitrocellulose membranes at 100 V for 2.5 hours at 4 °C. Membranes were blocked in 5% (w/v) nonfat dry milk prepared in 1x TBST (20 mM Tris-base, 150 mM NaCl, 0.05% Tween-20) for 1 hour at 25 °C, then incubated with primary antibodies overnight at 4 °C with gentle shaking. Membranes were washed using 1x TBST, 3x10 minutes, then incubated with secondary antibodies at 25 °C for 1 hour with gentle shaking. Membranes were developed using SuperSignal West Pico PLUS Chemiluminescent Substrate (ThermoFisher #34580). Chemiluminescent images were captured using the ChemiDoc Touching Imaging System (Bio-Rad).

Time-resolved fluorescence resonance energy transfer (TR-FRET) assay

TR-FRET assays were performed using cell lysate from HEK293T cells co-expressing a pair of GST-tagged and Venus-FLAG-tagged proteins. TR-FRET high throughput PPI screen (HTS) conditions were used as previously described (17).

For non-HTS TR-FRET assays, HEK293T cells were grown in 6-well plates (Corning #3506) and transiently transfected with 1 μg GST-tagged expression plasmid and 1 μg Venus-FLAG-

tagged expression plasmid using XtremeGene HP (Sigma #06366546001) as a transfection reagent, at a ratio of (3μL XtremeGene HP):(1μg plasmid DNA). Forty-eight hours after transfection, cell lysates were prepared in 200 μL lysis buffer containing 150 mM NaCl, 10 mM HEPES pH 7.5, 1% nonidet P-40 (IGEPAL CA-630, Sigma), 5 mM sodium pyrophosphate, 5 mM NaF, 2 mM sodium orthovanadate, 10 mg/L aprotinin, 10 mg/L leupeptin and 1 mM PMSF. 15 μL of cell lysate was mixed with 15 μL of GST-terbium antibody (Cisbio Bioassays #61GSTTLB; prepared in FRET buffer (20 mM Tris-HCl pH 7.0, 50 mM NaCl, 0.01% nonidet P-40)) to a total volume of 30 μL and final antibody dilution of 1:1000 per well in black 384-well plates (Corning #3573). Plates were centrifuged at 1000 rpm for 5 min and incubated at 25 °C for 30 min. TR-FRET signals were measured using a BMG Labtech PHERAstar *FSX* reader with the HTRF optic module (λ_{ex}: 337 nm, $\lambda_{em,\,1}$: 486 nm, $\lambda_{em,\,2}$: 520; mirror: D400/D505; time delay: 50 us). TR-FRET signals are expressed as the ratio ($F520/F486 \cdot 10^4$). Non-HTS TR-FRET assay data reflect subtraction of assay background signal, defined as TR-FRET background signal detected in non-interaction PPI control consisting of GST-c-Jun plus Venus-FLAG (equivalent to background signal from control wells with no GST-/Venus-protein expression).

Glutathione-S-transferase (GST) pull-down and FLAG co-immunoprecipitation

HEK293T cells were seeded in 6-well plates (Corning #3506) to reach a well confluence of 70-90% by 24 hours. Twenty-four hours after seeding, cells were transfected with 1 μg GST-tagged expression plasmid and 1 μg Venus-FLAG or FLAG-expression plasmid. Forty-eight hours after transfection, cells were lysed in 0.25% Triton X-100 lysis buffer (25 mM HEPES, 150 mM NaCl, 5 mM EDTA, 5 mM NaF, 0.25% Triton X-100) and lysates were incubated with glutathione-conjugated beads (GE #17527901) or FLAG agarose beads (Sigma #F2426) for 2

hours with rotation at 4 °C. Beads were washed 3x5 minutes with 0.25% Triton X-100 lysis buffer, eluted by boiling in 2x Laemmli sample buffer (Bio-Rad #1610737), and processed via western blot.

Cycloheximide Chase Assay

HEK293T cells were seeded in 6-well plates and grown to a plate density of 10-20% by 24 hours, then transfected with 1 μg SPOP plasmid or control plasmid per well using XtremeGene HP (Sigma #06366546001) as described. Twenty-four hours after transfection, cells were treated with 100 μg/mL cycloheximide (Tocris Bioscience #9701) to inhibit ribosome protein synthesis, collected at 0, 6, 12, and 24 hour timepoints post-treatment, and lysed in 0.25% Triton X-100 lysis buffer (25 mM HEPES, 150 mM NaCl, 5 mM EDTA, 5 mM NaF, 0.25% Triton X-100). Sample lysate protein concentrations were measured using the Pierce BCA Protein Assay Kit (ThermoFisher #23225). 4x Laemmli sample buffer (Bio-Rad #1610747) was added to sample lysates at a 3:1 (v/v) ratio and boiled for 5 min, then samples were stored at -30 °C. After all lysates were collected, 30 μg total sample protein was loaded onto lanes of 10% SDS-PAGE gels and analyzed by western blotting. Protein expression was quantified using Bio-Rad Image 6.0 Lab software, and c-Jun protein levels were normalized to γ-tubulin loading control band densities.

AP-1 Luciferase Reporter Assay

AP-1 complex (c-Jun) transcriptional activity was measured using the Cignal AP-1 Reporter Assay Kit (Qiagen #CCS-011L), which features a TRE (tetradecanoylphorbol-13-acetate response element)-luciferase reporter system. HEK293T cells were plated in 12-well plates (Corning #3512) and 24 hours later were co-transfected with Cignal AP-1 reporter plasmid (200 ng) and GST-SPOP or GST-control plasmid (800 ng) per well using XtremeGene HP (Sigma

#06366546001). Forty-eight hours after transfection, Renilla and Firefly luciferase activities were measured using an Envision Multilabel plate reader (PerkinElmer) using the Dual-Glo luciferase kit (Promega #2920) according to the manufacturer's instructions. Normalized luminescence was calculated as the ratio of Firefly luciferase luminescence to Renilla luciferase luminescence.

2.3 Results

Parallel high throughput protein-protein interaction screens expand the SPOP protein-protein interactome and identify SPOP missense mutation-enhanced protein-protein interactions

Mutation- and protein expression-level perturbations in SPOP are characterized to promote pathology by altering SPOP's interactions with other proteins. To nominate new potential mechanisms of SPOP-mediated biology, we sought to expand the characterized SPOP protein-protein interactome using two parallel high throughput screening platforms developed for PPI detection. In the first high throughput screen, SPOP WT was screened against the OncoPPi library (17) of cancer-associated genes using a cell lysate-based, time resolved-fluorescence resonance energy transfer (TR-FRET) approach to identify SPOP WT protein binding partners. This OncoPPi screen identified 19 cancer-associated proteins which bind to SPOP WT with TR-FRET fold over control (FOC) > 2 (Figure 2.1a) and which could be validated by orthogonal GST pulldown protein-protein interaction assays (Figure 2.1b). Four of these SPOP-protein interactions have been previously reported: MyD88 (80; 171-173), SPOP (72), CUL3 (66; 72) and BRD4 (118-120). The remaining fifteen validated SPOP WT interactors have not been previously described: BRAF, E2F6, MAGEA6, SDHA, MRE11, ELOC (*TCEB1*), OLIG2, E2F2, AXL, prostasin (*PRSS8*), ASCL1, ZNF483, FAM46C (*TENT5C*), VHL, FOXP1. In prostate

adenocarcinoma, recurrent missense mutations in SPOP's substrate-recognition MATH domain have been characterized to promote oncogenesis by inhibiting SPOP's interaction with oncogenic protein substrates, leading to their reduced ubiquitin-mediated degradation and aberrant accumulation (85; 107; 111; 114-120). We thus examined how four of the most frequently recurring, prostate adenocarcinoma-associated missense mutations in SPOP (Y87C, F102C, F133L and F133V) (110) alter SPOP's interaction with the protein partners identified through the TR-FRET SPOP OncoPPi screen. This approach confirmed previously characterized SPOP mutation-induced loss of interaction with BRD4, and further nominated several additional proteins which exhibit loss of interaction with one or more SPOP prostate cancer-associated point mutants (Figure 2.1c, Supplementary Figure 2.1). A second group of proteins demonstrated no strong differences in interaction with SPOP missense mutants relative to SPOP WT (Figure 2.1d, Supplementary Figure 2.1). Recurrent SPOP point mutants, particularly SPOP F133L and F133V, also appeared to exhibit enhanced interaction with a third set of proteins (Figure 2.1e, Supplementary Figure 2.1), a phenomenon that has not been previously described for prostate adenocarcinoma-associated SPOP point mutants.

An orthogonal, *in vivo*, bioluminescence resonance energy transfer (BRET)-based high throughput protein-protein interaction screen was carried out in parallel to validate the SPOP WT PPIs detected by the first OncoPPi TR-FRET screen and to evaluate the ability of recurrent, prostate adenocarcinoma-associated SPOP missense variants (Y87C, F102C, F133L, F133V) to differentially interact with proteins represented in the OncoPPi library. This BRET screen confirmed SPOP variant interactions with cancer-associated proteins identified from the OncoPPi TR-FRET screen (E2F6, MAGEA6, SDHA, MRE11, ELOC, E2F2, AXL, prostasin (*PRSS8*), ASCL1, FAM46C, VHL with FOC > 1.5). This BRET-based screen also detected

previously characterized SPOP missense mutation-induced loss of interaction with BRD4 and SRC-3 (*NCOA3*) and further suggested new missense mutation-induced loss of interaction with CBFA2T1 (*RUNX1T1*) and synphilin-1 (*SNCAIP*), which could be validated by orthogonal TR-FRET and GST-pull down protein-protein interaction assays (Supplementary Figure 2.2). This BRET screen additionally suggested that prostate cancer-associated SPOP point mutants, particularly point mutants F133L and F133V, do indeed gain interaction with several cancer-associated proteins, which could also further be validated through orthogonal protein-protein interactions assays (Figures 2.1f). Of these missense-mutation induced interactions identified in the BRET screen, SPOP F133L/V neomorph interactions with c-Jun were identified as the highest confidence interactions.

Structural determinants of SPOP variant interactions with c-Jun

Prostate adenocarcinoma-associated missense mutations in SPOP recur in its N-terminal substrate-recognition meprin and TRAF homology (MATH) domain at residues that line SPOP's substrate binding cleft (111). To determine whether SPOP F133L/V mutation-enhanced interactions with c-Jun represent a general feature of all patient-reported SPOP F133 missense mutations and whether the two most common missense mutations of adjacent site W131 may also induce interaction with c-Jun, we expanded our original SPOP mutation panel (Y87C, F102C, F133L, F133V) to test the ability of SPOP mutants F133C, F133I, F133S, W131C and W131G to bind to c-Jun (Figure 2.2c, 2.2d) in GST-pull down and TR-FRET PPI assays. Relative to SPOP WT, SPOP mutants Y87C, F102C, W131C and W131G demonstrated reduced interaction with c-Jun. In contrast, SPOP mutations F133C, F133I, F133L and F133V, but not F133S, strongly enhanced SPOP interaction with c-Jun. These results suggest that SPOP

mutation-induced interaction with c-Jun is a feature specific to a subset of SPOP F133 mutations, though different F133 mutations exhibit distinct c-Jun binding affinities.

We next sought to define minimal protein structural elements that enable SPOP-c-Jun interactions. SPOP is 374 residues in length and contains two major structural domains (72) (Figure 2.2a): 1) an N-terminal MATH domain (residues 28-166) that mediates binding to target substrate proteins, and 2) a C-terminal bric-a-brac, tramtrack and broad complex (BTB)/POZ domain (residues 190-297) that enables SPOP homo-multimerization and recruitment of CUL3. In GST-pull down and TR-FRET PPI assays, the SPOP MATH domain alone (designed as SPOP residue region 1-165) demonstrated interaction with c-Jun, while the SPOP BTB domain alone (designed as SPOP residue region 175-374) did not interact with c-Jun, suggesting that SPOP interaction with c-Jun is mediated through the mutation-containing SPOP MATH domain (Figure 2.2d, 2.2e). To further determine a minimal SPOP residue region that mediates binding to c-Jun, smaller fragments of the SPOP MATH domain that included the mutated F133 residue were developed (Figure 2.2a). Surprisingly, an SPOP fragment consisting of residues 93-138 was detected in TR-FRET assays to bind to c-Jun with equal affinity regardless of SPOP F133 mutation status (WT vs F133L), although the smallest SPOP fragment tested (residues 113-138) could not bind to c-Jun (Figure 2.2f, 2.2g). Taken together, these results suggest that SPOP residue region 93-138 is sufficient to enable interaction with c-Jun regardless of F133 mutation status.

C-Jun is 331 residues in length and contains two major structural domains (187) (Figure 3a): 1) a JUN homology domain (residues 5-241) that consists of a N-terminal transactivation domain (TAD; residues 5-164) and high intrinsic disorder region (HID; residues 165-243), and 2) a C-terminal basic leucine zipper (bZIP) domain (DBD; residues 250-313) that mediates DNA

binding and dimerization with leucine zipper transcriptions factors in the JUN, FOS and ATF families to form AP-1 transcription complexes. Of these domains, the c-Jun transactivation domain in isolation (residues 1-164) was sufficient to enable interaction with SPOP F133L in GST-pull down and TR-FRET PPI assays (Figure 2.3b, 2.3c). Further c-Jun sub-TAD domain fragments were developed to identify minimal c-Jun protein elements that are sufficient to enable interaction with SPOP F133L, and subsequent GST-pull down and TR-FRET PPI assays identified a minimal protein region consisting of c-Jun residues 1-84 that retains interaction with SPOP F133L (Figure 2.3d, 2.3e). Because c-Jun residue region 1-84 shares partial sequence homology with paralogs JunB and JunD(188) (Figure 2.3f), we also tested whether SPOP F133 missense mutations similarly induce interaction with JunB and JunD. SPOP WT was observed to interact with c-Jun and JunD, but not JunB, in both GST-pull down and TR-FRET assays (Figure 2.3g, 2.3h). Furthermore, in contrast to the strong induction of interaction observed for SPOP F133L/V mutants with c-Jun relative to SPOP WT, SPOP F133 mutations did not alter interaction with JunD. These data suggest that SPOP F133L/V mutation-induced interaction is a phenomenon specific to c-Jun and does not extend to JUN protein family members JunB and JunD, and furthermore that SPOP-JunD interactions, which are not influenced by SPOP mutation, may occur through a distinct mode.

SPOP variants differentially enhance endogenous c-Jun protein levels and AP-1 transcriptional activity

SPOP is an adaptor subunit of CUL3-RING E3 ubiquitin ligase complexes that has been characterized to promote the ubiquitin-mediated degradation of its protein substrates. We thus next examined how expression of SPOP missense variants influences c-Jun protein levels. Stable overexpression of SPOP WT in prostate adenocarcinoma cell lines C4-2 and 22Rv1 resulted in a

decrease in the protein levels of previously characterized substrates BRD4 (118-120), SRC3 (107; 116) and TRIM24 (117; 121), while overexpression of loss-of-interaction SPOP missense variants Y87C, F102C, F133L and F133V resulted in an elevation of these substrates' protein levels through a previously characterized dominant negative effect (Figure 2.4a, 2.4c), consistent with previous reports (116-118). Surprisingly, however, overexpression of SPOP WT or missense mutant variants resulted in an increase in c-Jun protein levels in a manner directly correlating with SPOP variant-c-Jun binding affinities. RT-qPCR analysis suggested that these elevations in c-Jun protein level were not caused by an increase in *JUN* gene transcription (Figure 2.4b, 2.4d). Cycloheximide (CHX) chase assays were utilized to assess c-Jun protein stability in the presence of ectopic SPOP expression, and revealed that SPOP expressed enhanced c-Jun protein half-life (Figure 2.4e). SPOP variant binding to c-Jun and stabilization of c-Jun protein levels furthermore correlated proportionally with increases in c-Jun (AP-1) transcriptional activity as measured through AP-1 luciferase reporter assays (Figure 2.4f).

We next sought to further characterize how SPOP variants stabilize c-Jun protein levels. SPOP's primary characterized function is substrate recruitment for CUL3-RING E3 ligase complex-mediated ubiquitination, in which SPOP recruits substrates through its N-terminal SPOP MATH domain and recruits CUL3 through its C-terminal SPOP BTB domain (72). We thus examined whether SPOP expression influences ubiquitination of c-Jun. We confirmed the ability of SPOP WT to ubiquitinate previously characterized SPOP WT substrate SRC3 (Supplementary Figure 2.4b), and were able to detect SPOP F133L-enhanced ubiquitination of c-Jun (Supplementary Figure 2.4a, 2.4b) that was both SPOP BTB domain- and CUL3-dependent (Supplementary Figure 2.4c, 2.4d). Our data further suggested that c-Jun ubiquitination may occur through ubiquitin lysine 63 (K63)-linkage (Supplementary Figure 2.4e, 2.4f), a type of

polyubiquitination linkage which has been characterized to mediate non-degradative functions (31; 35; 37). In CHX protein stability and AP-1 transcriptional reporter assays, expression of the SPOP MATH domain alone, which mediates binding of SPOP variants to c-Jun, was unable to promote c-Jun protein stabilization and transcriptional activity (Figures 2.4h, 2.4i), which indicates that the SPOP BTB domain is necessary for SPOP promotion of c-Jun protein stability and transcriptional activity. Interestingly, CUL3 knockdown also reversed SPOP-mediated stabilization of c-Jun and partly reversed SPOP enhancement of c-Jun transcriptional activity (Figures 2.4i, 2.4j). These data suggest that SPOP variants may promote c-Jun protein stability and transcriptional activity in a manner that requires SPOP-CUL3 complexes, potentially through SPOP-CUL3-mediated ubiquitination of c-Jun.

2.4 Discussion

SPOP is emerging as a conserved regulator of fundamental biological processes across species through its role as an adaptor subunit of CUL3-RING E3 ubiquitin ligase complexes. Recurrent missense mutations in SPOP, as occur in primary prostate adenocarcinoma, have typically been characterized to induce SPOP loss of interaction with protein binding partners. There are currently few studies that examine how recurrent cancer-associated SPOP mutations may functionally differ from one another (119; 189), nor whether these missense mutations may have functions beyond simply promoting SPOP loss of function.

Our study reports the results of the first systematic approaches to expand the characterized SPOP interactome and explore differential protein-protein interactions among SPOP WT and prostate adenocarcinoma-associated SPOP missense variants through SPOP-focused, high throughput binary protein-protein interaction screens. Through our approaches, we have identified several novel SPOP binding partners that collectively suggest new hypotheses for

SPOP biology mediated by protein-protein interactions which may be perturbed by changes in SPOP protein levels, mutation, or subcellular localization. Our data suggest that SPOP-interacting proteins generally fall into three groups based on their ability to differentially interact with prostate cancer-associated SPOP missense variants relative to SPOP WT: 1) proteins that bind with equivalent affinity to SPOP WT and prostate cancer-associated missense mutants, 2) proteins that exhibit reduced interaction affinity with SPOP missense mutants, and 3) proteins that exhibit enhanced or induced interaction with SPOP missense mutants. Proteins that fall into the equivalent-interaction-affinity category include SPOP, CUL3, E2F6 and ASCL1. Of these, SPOP-SPOP and SPOP-CUL3 interactions have been previously reported to be mediated through the SPOP BTB domain, a C-terminal SPOP domain that is structurally unperturbed by missense mutations in the N-terminal SPOP MATH domain (72). In the context of this previous work related to SPOP BTB domain-mediated protein-protein interactions, newly detected equivalent interaction-affinity proteins through our PPI assays, such as E2F6, ASCL1 and JunD, may similarly interact with SPOP through the SPOP BTB domain rather than the SPOP MATH domain. Alternatively, equivalent-affinity-interaction proteins may interact with SPOP through a region of the SPOP MATH domain that is not influenced by missense mutations in SPOP's characterized substrate binding cleft, a cavity defined by SPOP residues Y87C, F102, F125, W131, F133 (111), though this would represent a mode of binding to the SPOP MATH domain that has not to our knowledge been previously described. Further work will be required to determine how these proteins bind to SPOP and why their interaction affinities are unperturbed by recurrent, prostate adenocarcinoma-associated SPOP missense mutations.

Of particular importance for cancers driven by recurrent SPOP mutations are proteins that demonstrate differential interaction with SPOP missense variants, which provide further

hypotheses for how recurrent SPOP missense mutations may promote oncogenesis. Proteins which fall into the category of SPOP missense mutation-induced loss of interaction include BRD4, MyD88, BRAF, OLIG2, SRC-3 (*NCOA3*), CBFA2T1 (*RUNX1T1*) and synphilin-1 (*SNCAIP*), for which missense mutation-induced loss of interaction with BRD4 (118-120) and SRC3 (107; 116) has previously been reported. SPOP missense mutation-induced loss of interaction with BRD4 and SRC-3 has been characterized to have significant consequences for SPOP mutation-driven prostate tumorigenesis: Wild-type SPOP binds to and promotes the degradative ubiquitination of BRD4 and SRC-3 in prostate cells, but prostate cancer-associated SPOP missense mutants lose their ability to bind to and facilitate ubiquitination of these substrates. Reduced SPOP-mediated ubiquitination of BRD4 and SRC-3 subsequently leads to an aberrant elevation of these proteins that promotes prostate tumorigenesis.

This previous work on SPOP missense mutation-induced loss of interaction with BRD4, SRC-3, and other oncogenic substrates carries important implications for other proteins, such as MyD88, which we have detected to lose interaction with prostate cancer-associated SPOP missense mutants. MyD88 is a protein whose function has been characterized to be modulated by SPOP-mediated ubiquitination in hematopoietic lineage cells (80; 171; 173), but no studies to date have examined how recurrent, prostate cancer-associated missense mutations in SPOP influence interaction with MyD88 in prostate cells. However, previous work has characterized lymphoid malignancy-associated SPOP missense mutations in the SPOP MATH domain, including F102I, F102Y, M117I, S119R, D130H, D130N, and D140H, to induce loss of interaction with, and inhibit SPOP-mediated ubiquitination of, MyD88 (80). Our data similarly suggest that prostate cancer-associated SPOP missense mutations may also impair SPOP-mediated regulation of MyD88, though further experimental work will be required to specifically

examine the potential functional consequences of SPOP mutation-mediated loss of interaction with MyD88 in the setting of prostate tumorigenesis. The functional role of wild-type SPOP interactions with the other protein binding partners we have identified in this mutation-induced loss of interaction category, as well as the consequences of SPOP missense mutation-induced loss of interaction with these partners, will likewise need to be defined through future experimental work.

We also report the first validated SPOP F133L/V missense mutation-induced gain of interaction with several cancer-associated proteins, including AXL, MRE11, ELOC (*TCEB1*), FOXP1, cIAP-1 (*BIRC2*), Cbl-b, CUL4B, GATA1, c-Jun (*JUN*), c-Rel (*REL*), and ZBTB2. Our data additionally nominate several other proteins which may demonstrate enhanced interaction with SPOP F133L/V point mutants, but which did not reach our set threshold of 1.5x WT TR-FRET binding signal (eg, MAGEA6, SDHA, E2F2, PRSS8, ZNF483, FAM46C, VHL). This gain of interaction for SPOP F133L/V point mutants suggests unique mechanisms of oncogenesis that may be specifically mediated by SPOP F133L/V point mutants through physical intervention in various cell signaling pathways, and nominates SPOP F133L/V missense mutants as a distinct molecular subclass of SPOP mutants on the basis of their unique protein-protein interactomes. Of note, SPOP mutation-induced gain of interaction suggests several potential mechanisms by which SPOP F133L/V mutations may uniquely alter SPOP-CUL3-RING E3 ligase functionality (MAGEA6 (190)), influence DNA damage repair (MRE11 (191-193), CUL4B (194)), influence cellular response to hypoxia (VHL, ELOC (41-43)), directly modulate DNA transcription factor activity (FOXP1, GATA1, c-Jun, c-Rel, ZBTB2), and physically link SPOP to other E3 ubiquitin ligase-mediated pathways (cIAP-1, CUL4B, Cbl-b).

Because SPOP F133L/V-mutation induced interactions with c-Jun, a well-characterized oncogenic protein subunit of AP-1 transcription factor complexes (195), were the highest confidence neomorph interactions detected by our protein-protein interactions screens and validated through orthogonal methods, we chose to further characterize how these interactions occur. Through protein-protein interaction site mapping approaches, we have demonstrated that the SPOP MATH domain mediates interaction with c-Jun and that an SPOP MATH domain fragment comprised of SPOP residues 93-138 is sufficient to enable interaction with c-Jun. We further found that SPOP residue region 93-138 is sufficient to mediate interaction with c-Jun regardless of residue 133 mutation status (F133 vs F133L), yet full-length SPOP WT versus SPOP F133L, as well as the SPOP WT MATH domain versus SPOP F133L MATH domain, exhibit strong differences in c-Jun binding affinity. These results suggest that SPOP residue F133 may not mediate SPOP-c-Jun interactions directly, but rather that F133L/V mutations may induce a local conformational change in the MATH domain that enables enhanced c-Jun access to a sequence within SPOP residue region 93-138 (the SPOP substrate binding cleft region) common among all SPOP F133 variants tested. We have also determined that c-Jun N-terminal transactivation domain residue region 1-84 is sufficient to enable interaction with SPOP F133L. However, SPOP F133L/V mutations do not similarly induce binding with c-Jun paralogs JunB and JunD, despite shared partial N-terminal sequence homology among these JUN protein family members (188). Intriguingly, this region of c-Jun does not contain a canonical five-residue SPOP binding motif (φ-π-S-S/T-S/T, where φ represents a general non-polar residue and π indicates a general polar residue) (72), which suggests that SPOP variants may recognize and bind to c-Jun through a novel sequence motif.

SPOP function has largely been ascribed to SPOP's role as an adaptor subunit of CUL3-RING E3 ubiquitin ligase complexes, through which SPOP has been characterized to mediate the ubiquitination and subsequent proteasomal degradation of proteins that bind to the SPOP's substrate binding cleft (72). We confirmed previous reports of SPOP-induced degradation of SPOP WT substrates BRD4 (118-120), SRC3 (107; 116) and TRIM24 (117; 121), but SPOP variants demonstrated a surprising ability to stabilize c-Jun protein levels and increase AP-1 transcriptional activity in a manner proportionally correlating with SPOP variant-c-Jun interaction affinities (Figure 2.4a, 2.4c, 2.4f). Subsequent *in vivo* ubiquitination assays detected that SPOP F133L may facilitate K63-linked ubiquitination of c-Jun in a BTB domain- and CUL3-dependent manner. In contrast to K48-linked ubiquitination, the most prevalent type of ubiquitin modification that targets proteins to the 26S proteasome for degradation, K63-linked ubiquitination has been characterized to enhance protein binding to DNA (37) and to promote rapid and reversible formation of protein signaling complexes involved in a diverse array of processes, including NF-κB transcription pathway activation (31-33) and DNA repair (34; 35). Importantly, while SPOP-CUL3 complexes have been observed to facilitate degradative ubiquitination of most substrates described in prostate lineage cells thus far, SPOP-CUL3 complexes have also been characterized to facilitate nondegradative ubiquitination of a subset of substrates in specific contexts (67; 80; 81), though the ubiquitin linkage composition of these substrates' polyubiquitin chains have generally not been extensively explored. Because our results also indicate that SPOP-CUL3 complexes, and not SPOP alone, are necessary for SPOP to promote c-Jun protein stabilization and transcriptional activity, our data collectively suggest that SPOP-mediated K63-linked ubiquitination of c-Jun may be a mechanism by which SPOP variants stabilize c-Jun. Future experimental work will be required to further examine how

SPOP-CUL3 complexes may stabilize and regulate c-Jun. Nevertheless, SPOP F133L/V stabilization of c-Jun may represent a unique means by which SPOP F133L/V mutations promote oncogenesis, as overexpression of c-Jun and overactivation of AP-1 transcriptional activity have been reported to promote prostate adenocarcinoma progression and recurrence (196). Because SPOP WT also appears capable of stabilizing c-Jun and promoting AP-1 transcriptional activity, though to a lesser extent than SPOP F133L/V, it is also possible that cancers driven by SPOP WT overexpression, such as clear cell renal clear cell carcinoma (71; 82), may also feature SPOP-mediated stabilization of c-Jun and activation of AP-1 even in the absence of SPOP mutation.

In summary, our data expand the characterized SPOP interactome and reveal differential protein-protein interactomes among SPOP variants, including identification and validation of SPOP 133L/V mutation-induced gain of interaction. Currently, prostate adenocarcinoma-associated missense mutations in SPOP are considered to uniformly induce loss of interaction with characterized SPOP substrates. Our work, however, suggests that different missense mutations in SPOP may uniquely contribute to oncogenesis through the establishment of divergent protein-protein interactomes, and that different missense mutations in SPOP may thus represent distinct biomarkers for SPOP mutation-induced prostate adenocarcinoma behavior and treatment response. Future work will be necessary to define the specific mechanisms and pathways by which SPOP mutation-induced gain of interaction may promote oncogenesis.

Figure 2.1. Expansion of the SPOP interactome

(a) TR-FRET screen for binary SPOP WT-protein interactions (17). GST-tagged SPOP WT and a library of cancer-associated, Venus-FLAG (VF)-tagged genes were co-expressed in binary combinations in HEK293T cells for 48 hrs. Cell lysates with respective co-expressed proteins were prepared and incubated with Tb-conjugated anti-GST antibodies. TR-FRET was configured with Tb as FRET donor and Venus protein as FRET acceptor. Results are shown for SPOP WT PPIs with ≥2 fold-over-negative-control (FOC) FRET signal. Negative control was defined as TR-FRET background signal detected for non-interaction protein pair GST-SPOP WT plus Venus-FLAG (equivalent to background signal from wells with no GST-/Venus-protein expression). Screening data represent means ± SD from three independent experiments.

(b) GST-pull down validation of SPOP WT-protein interactions in (a). Binary combinations of GST-SPOP WT and VF-tagged genes were co-expressed in HEK293T cells. Cell lysates with respective co-expressed proteins were prepared, and GST-SPOP WT protein complexes were captured by glutathione resin to probe the presence of VF-protein. GST-SPOP WT and VF-protein were detected by blotting with anti-GST and anti-FLAG antibodies, respectively. Binary combinations of GST empty vector and VF-tagged genes were used as corresponding negative controls.

(c-e) TR-FRET assays evaluating ability of SPOP missense variants to bind to SPOP-binding proteins from (a-b) relative to SPOP WT. TR-FRET samples were prepared as described in (a). (c) Representative set of proteins that exhibit loss of interaction with mutant SPOP relative to SPOP WT. (d) Representative set of proteins that exhibit equivalent interaction affinity for mutant SPOP and SPOP WT. (e) Representative set of proteins that exhibit gain of interaction with mutant SPOP relative to SPOP WT.

(f) GST-pull down and TR-FRET validation of BRET-detected SPOP mutation-induced gain of interaction. Experimental conditions were the same as those described in (a-b).

For (c-f), all data represent means ± SD of a minimum of three independent experiments. TR-FRET signal is presented with the following transformation: $\log_2$[(SPOP mutant TR-FRET signal)/(SPOP WT TR-FRET signal)]. Corresponding raw data used for transformation are presented in Supplementary Figure 1. One-sample t test was used to determine whether SPOP mutant FRET signal means were significantly different from SPOP WT FRET signal means, defined as a surpassing a threshold of ±1.5x fold-change for mean SPOP mutant FRET signal relative to mean SPOP WT FRET signal. Statistical significance is denoted as follows: *: $p < 0.05$, **: $p < 0.01$, ***: $p < 0.001$, ****: $p < 0.0001$.

Figure 2.1

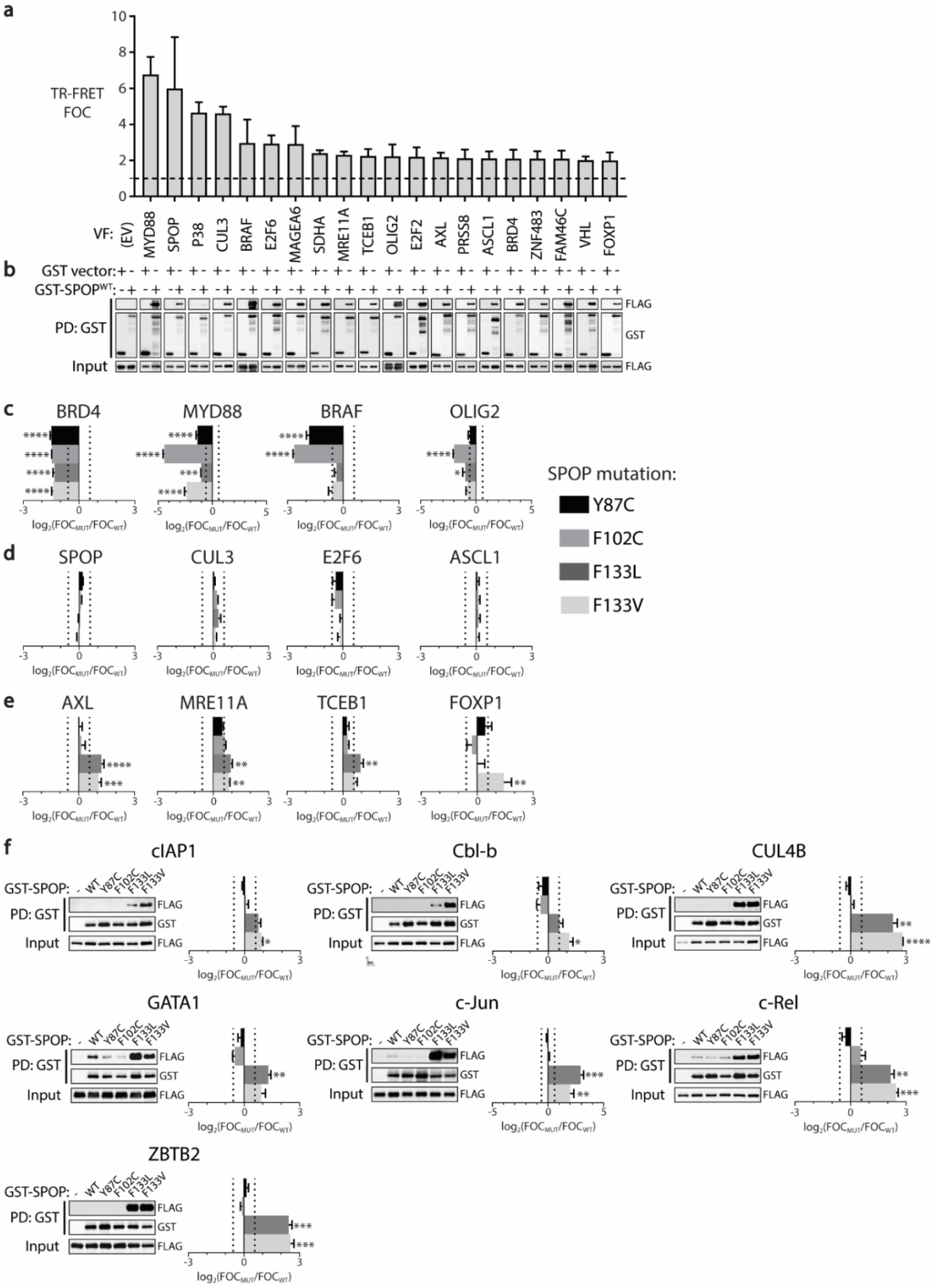
a
TR-FRET FOC
VF: (EV) MYD88 SPOP P38 CUL3 BRAF E2F6 MAGEA6 SDHA MRE11A TCEB1 OLIG2 E2F2 AXL PRSS8 ASCL1 BRD4 ZNF483 FAM46C VHL FOXP1
b
GST vector:
GST-SPOP^WT:
PD: GST
Input
FLAG
GST
c
BRD4
MYD88
BRAF
OLIG2
SPOP mutation:
Y87C
F102C
F133L
F133V
d
SPOP
CUL3
E2F6
ASCL1
e
AXL
MRE11A
TCEB1
FOXP1
f
cIAP1
Cbl-b
CUL4B
GATA1
c-Jun
c-Rel
ZBTB2
GST-SPOP: WT Y87C F102C F133L F133V
log2(FOC_MUT/FOC_WT)

Figure 2.2. SPOP F133L mutation induces interaction with c-Jun through the SPOP MATH domain.

(a) Diagram of SPOP protein domains indicating design of SPOP protein fragments used in the study.

(b) GST-pull down and (c) TR-FRET evaluation of SPOP mutation effects on SPOP interaction with c-Jun. One-way ANOVA with Dunnett's multiple comparisons test was used to determine statistical significance of differences between sample means and SPOP WT sample mean.

(d) GST-pull down and (e) TR-FRET evaluation of SPOP domains that enable interaction with c-Jun.

(f) GST-pull down and (g) TR-FRET evaluation of SPOP sub-MATH domain fragments that enable interaction with c-Jun. One-way ANOVA with Sidak's multiple comparisons test used to determine statistical significance of differences among indicated pairs of sample means. #, $, %, ^: no statistical difference among indicated sample mean pairs with identical symbols.

All TR-FRET data represent means ± SD of four independent experiments. Statistical significance is denoted as follows: *: $p < 0.05$, **: $p < 0.01$, ***: $p < 0.001$, ****: $p < 0.0001$.

Figure 2.2

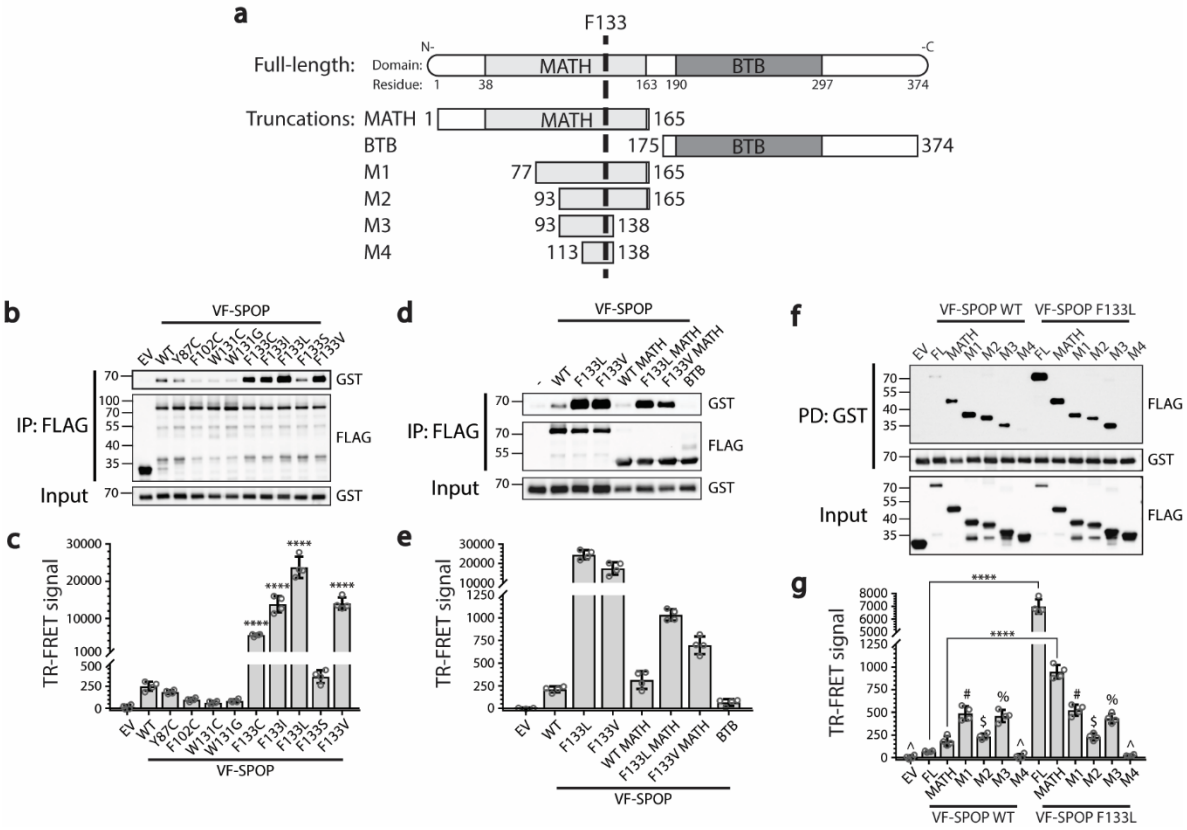
a
F133
Full-length:
Domain:
Residue:
MATH
BTB
Truncations:
M1
M2
M3
M4
b
VF-SPOP
IP: FLAG
Input
GST
FLAG
c
TR-FRET signal
VF-SPOP
d
e
f
VF-SPOP WT
VF-SPOP F133L
PD: GST
g

Figure 2.3. c-Jun interacts with SPOP through the JUN transactivation domain.

(a) Diagram of c-Jun protein domains indicating design of c-Jun protein fragments used in the study.

(b) GST-pull down and (c) TR-FRET evaluation of c-Jun protein domains that enable interaction with SPOP.

(d) GST-pull down and (e) TR-FRET evaluation of c-Jun sub-transactivation domain (sub-TAD) fragments that enable interaction with SPOP.

(f) Protein sequence alignment for N-terminal amino acid regions of JUN protein family members c-Jun, JunB, and JunD.

(g) GST-PD and (h) TR-FRET evaluation of SPOP mutation effects on interactions with c-Jun, JunB, and JunD. One-way ANOVA with Dunnett's multiple comparisons test was used to determine statistical significance of differences among indicated sample means.

All TR-FRET data represent means ± SD of three independent experiments. Statistical significance is denoted as follows: *: $p < 0.05$, **: $p < 0.01$, ***: $p < 0.001$, ****: $p < 0.0001$.

Figure 2.3

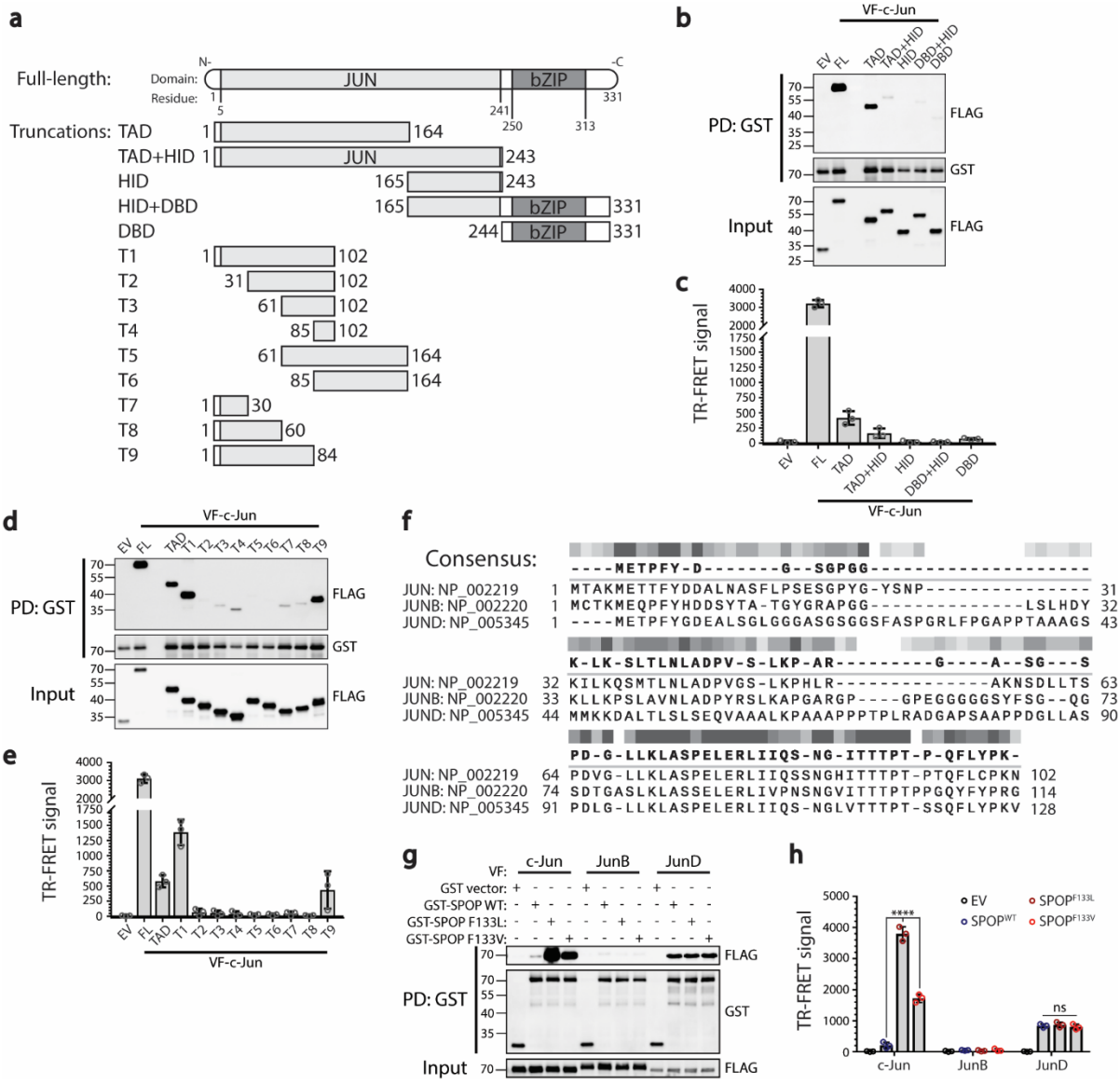
a
Full-length:
Domain:
Residue:
N-
-C
JUN
bZIP
Truncations: TAD
TAD+HID
HID
HID+DBD
DBD
T1
T2
T3
T4
T5
T6
T7
T8
T9
b
VF-c-Jun
EV
FL
TAD
TAD+HID
HID
DBD+HID
DBD
PD: GST
Input
FLAG
GST
c
TR-FRET signal
d
e
f
Consensus:
JUN: NP_002219
JUNB: NP_002220
JUND: NP_005345
g
VF:
c-Jun
JunB
JunD
GST vector:
GST-SPOP WT:
GST-SPOP F133L:
GST-SPOP F133V:
h
EV
SPOP^WT
SPOP^F133L
SPOP^F133V
****
ns

Figure 2.4. SPOP variant effects on c-Jun protein levels and AP-1 transcriptional activity.

(a, c) Western blot and densitometric quantification of endogenous protein levels for reported SPOP WT substrates (BRD4, SRC3, TRIM24) and c-Jun in prostate adenocarcinoma cell lines C4-2 (a) and 22Rv1 (c) with stable overexpression of SPOP variants. Stable overexpression of V5-tagged SPOP was introduced through lentiviral transgene delivery. For densitometry calculations, protein expression levels were normalized to protein level measured for corresponding empty vector control on the same membrane. Quantification represents densitometry means ± SD from (a) five and (c) four independent experiments. One-way ANOVA with Dunnett's multiple comparisons test was used to determine statistical significance of differences between sample means and empty vector sample mean.

(b, d) Relative JUN mRNA levels in (b) C4-2 and (d) 22Rv1 cell lines with stable overexpression of SPOP WT or SPOP F133L. Stable overexpression of V5-tagged SPOP was introduced through lentiviral transgene delivery. Data were normalized to average JUN mRNA levels for empty vector control. Quantification represents means ± SD from three independent experiments. One-way ANOVA with Dunnett's multiple comparisons test was used to determine statistical significance of differences among sample means.

(e, g, i) Cycloheximide chase assays evaluating FLAG-c-Jun protein stability in presence of ectopic overexpression of (e) empty vector, SPOP WT, or SPOP F133L; (g) SPOP WT, SPOP F133L, or SPOP F133L MATH domain; and (i) SPOP F133L in HEK293T cells with stable knockdown of CUL3. HEK293T cells were transfected at 20% confluence with SPOP gene constructs. 24 hrs after transfection, cell culture media were replaced with media containing 100 μg/mL cycloheximide (CHX) to fully inhibit ribosomal protein translation, and samples were collected for Western blot analysis at the indicated timepoints. Upper panel: representative

western blot; lower panel: densitometric quantification (means ± SD) of western blots from four independent experiments; middle panel (i only): western blot for CUL3 protein level in parental HEK293T cell line (P), HEK293T cell line with stable expression of non-target control shRNA (C), and HEK293T cell lines with stable knockdown of CUL3 using two different CUL3 shRNA constructs (#1, #2). One-way ANOVA with Dunnett's multiple comparisons test was used to determine statistical significance of differences among sample means at each timepoint.
(f, h, j) Effects of SPOP point variants on endogenous c-Jun-mediated transcriptional activity as measured by AP-1 luciferase reporter assays. Panels represent AP-1 transcriptional activity under conditions of (f) ectopic overexpression of SPOP point variants; (h) ectopic overexpression of SPOP point variant MATH domains or SPOP BTB domain; and (j) ectopic overexpression of SPOP WT and SPOP F133L in cells with stable CUL3 knockdown. HEK293T cells were co-transfected with GST-SPOP plasmid and TRE-Firefly luciferase/CMV-Renilla luciferase plasmids. After 48 hrs, cells were lysed and Firefly and Renilla luciferase activities were measured sequentially. Data represent AP-1-mediated TRE-Firefly luminescence signal normalized to constitutive CMV-Renilla luminescence signal for each sample, and means ± SD from three independent experiments. EV represents a GST-only negative control, and ASK1-KC represents a positive control with constitutive activation of JNK phosphorylation of endogenous c-Jun. For (f), one-way ANOVA with Dunnett's multiple comparisons test was used to determine statistical significance of differences between sample means and SPOP WT sample mean. For (g) and (j), one-way ANOVA with Sidak's multiple comparisons test was used to determine statistical significance of differences among indicated pairs of sample means. Statistical significance is denoted as follows: *: $p < 0.05$, **: $p < 0.01$, ***: $p < 0.001$, ****: $p < 0.0001$.

Figure 2.4

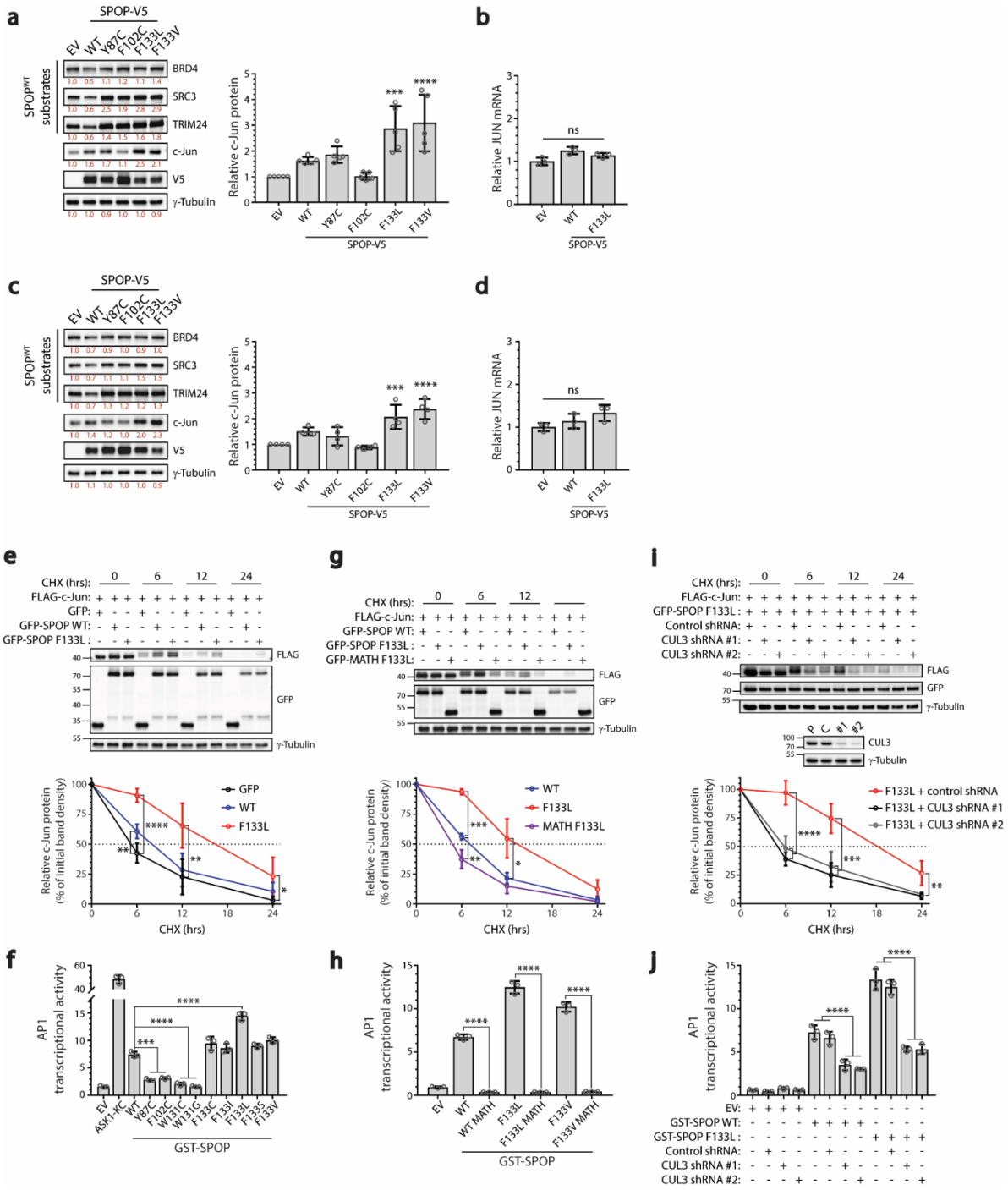
a
SPOP-V5
EV
WT
Y87C
F102C
F133L
F133V
SPOP^WT substrates
BRD4
SRC3
TRIM24
c-Jun
V5
γ-Tubulin
Relative c-Jun protein
SPOP-V5
b
Relative JUN mRNA
ns
c
d
e
CHX (hrs):
FLAG-c-Jun:
GFP:
GFP-SPOP WT:
GFP-SPOP F133L:
FLAG
GFP
Relative c-Jun protein (% of initial band density)
CHX (hrs)
g
GFP-MATH F133L:
MATH F133L
i
GFP-SPOP F133L:
Control shRNA:
CUL3 shRNA #1:
CUL3 shRNA #2:
CUL3
F133L + control shRNA
F133L + CUL3 shRNA #1
F133L + CUL3 shRNA #2
f
AP1 transcriptional activity
ASK1-KC
GST-SPOP
h
WT MATH
F133L MATH
F133V MATH
j
EV:
GST-SPOP WT:
GST-SPOP F133L:

Supplementary Figure 2.1. TR-FRET assays evaluating differential interactions of SPOP missense variants with SPOP-binding proteins.

GST-tagged SPOP WT and Venus-FLAG (VF)-tagged genes were co-expressed in binary combinations in HEK293T cells. Cell lysates with respective co-expressed proteins were prepared and incubated with Tb-conjugated anti-GST antibodies. TR-FRET was configured with Tb as FRET donor and Venus protein as FRET acceptor. Western blot was performed with the same lysates to confirm expression of GST- and Venus-FLAG-tagged proteins. Screening data represent means ± SD from three independent experiments. All data represent means ± SD of a minimum of three independent experiments.

Supplementary Figure 2.1

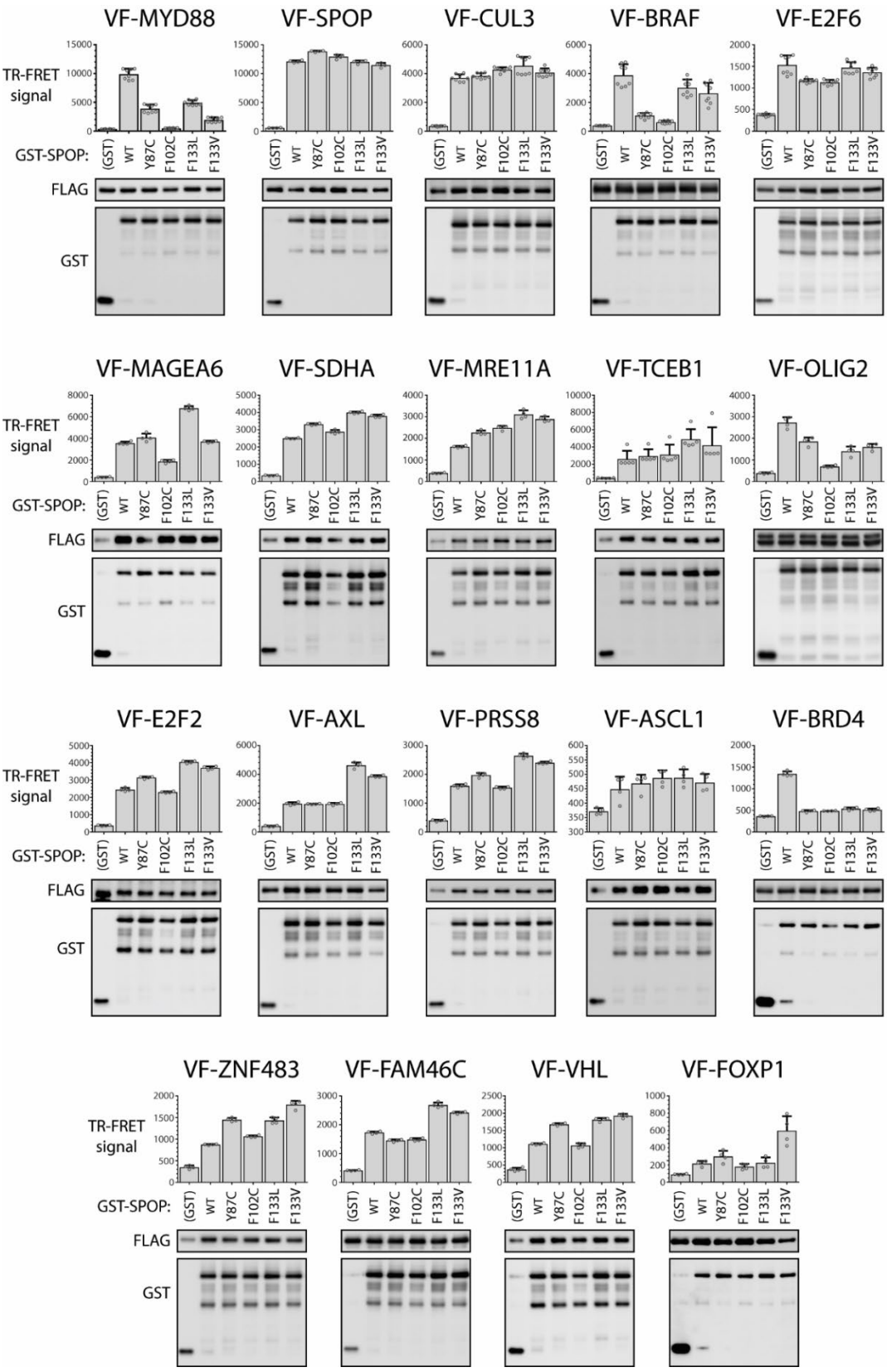

Supplementary Figure 2.2. Validation of BRET-detected differential SPOP protein-protein interactions through orthogonal protein-protein interaction assays.

(a) GST-pull down and TR-FRET validation of BRET-detected SPOP mutation-induced loss of interaction. Results obtained as described for Figure 2.1a, 2.1b. All data represent means ± SD of a minimum of three independent experiments. TR-FRET signal is presented with the following transformation: $\log_2$[(SPOP mutant TR-FRET signal)/(SPOP WT TR-FRET signal)]. One-sample t test was used to determine whether SPOP mutant FRET signal means were significantly different from SPOP WT FRET signal means, defined as a surpassing a minimum threshold of ±1.5x fold-change for SPOP mutant FRET signal relative to SPOP WT FRET signal. Statistical significance is denoted as follows: *: $p < 0.05$, **: $p < 0.01$, ***: $p < 0.001$, ****: $p < 0.0001$.

(b) Corresponding TR-FRET raw data used for TR-FRET transformations in Supplementary Figure 2.2a. Results obtained as described for Supplementary Figure 2.1.

(c) Corresponding TR-FRET raw data used for TR-FRET transformations in Figure 2.1f. Results obtained as described for Supplementary Figure 2.1.

Supplementary Figure 2.2

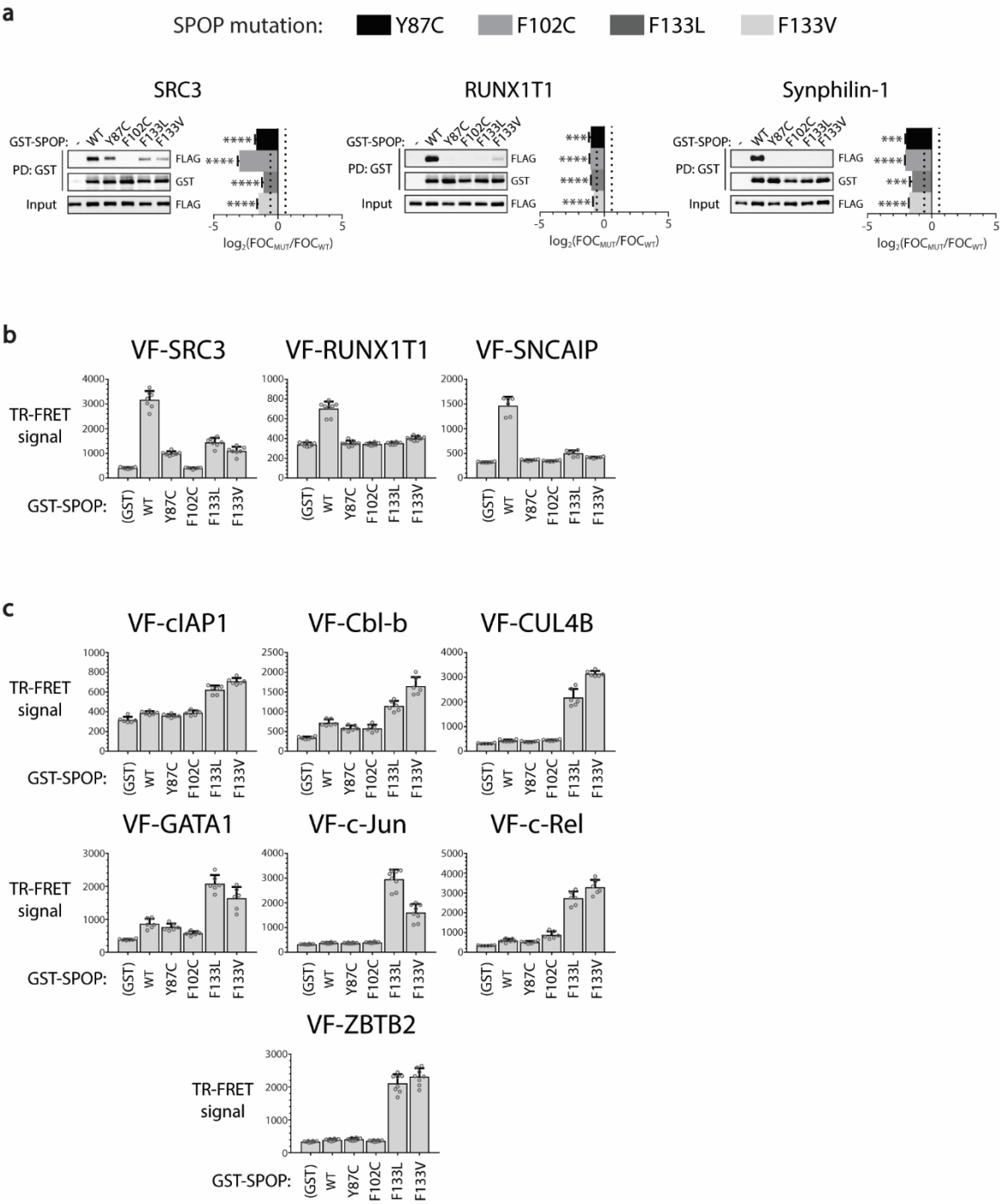

Supplementary Figure 2.3. Venus bimolecular fluorescence complementation (BiFC) assay to determine subcellular localization of SPOP-c-Jun protein-protein interactions in HEK293T and PC3M cells.

(a) HEK293T and (b) PC3M cells were singly transfected with individual Venus-tagged genes or co-transfected with a combination of N-terminal Venus-tagged (VN) gene and C-terminal Venus-tagged (VC) gene. Cells were fixed in 4% formaldehyde and incubated with WGA-lectin Alexa Fluor 633 (cell membrane stain; red) and Hoescht 33342 (nuclear stain; blue), and expression of Venus-tagged proteins was visualized (green). For comparison, full-length Venus-tagged c-Jun (i), SPOP WT (ii), and SPOP F133L (iii) were singly expressed to determine individual Venus fusion protein subcellular localization. The following were used as non-interaction negative controls: (iv) VN-c-Jun with VC empty vector, (v) VN empty vector with VC-SPOP WT, (vi) VN empty vector with VC-SPOP F133L. SPOP-c-Jun interaction PCA test conditions: (vii) VN-c-Jun with VC-SPOP WT, (viii) VN-c-Jun with VC-SPOP F133L. Corresponding bar graphs show integrated green pixel intensity per individual cells at 10x magnification. Bars represent means ± standard deviation.

SPOP has been characterized to localize predominantly to the nucleus and cytoplasm (65; 94), where SPOP further organizes into discrete puncta through liquid-liquid phase separation induced by SPOP homo-multimerization (78). C-Jun, in contrast, exhibits a diffuse nuclear subcellular localization pattern (197; 198). Using this Venus-based, bimolecular fluorescence complementation (BiFC) assay, we observed that SPOP-c-Jun interactions adopt an SPOP-like subcellular localization pattern in both HEK293T (kidney lineage; Supplementary Figure 2.3a) and PC3M (prostate lineage; Supplementary Figure 2.3b) cell lines, in which SPOP-c-Jun interactions occur in discrete nuclear and cytoplasmic puncta.

While the quantification of SPOP-c-Jun interactions here via integration of reconstituted Venus fluorescence intensity suggests that SPOP F133L interaction affinity with c-Jun is greater than SPOP WT with c-Jun, the difference in interaction affinity between the two PPI pairs detected by this PCA assay is less than the differences in interaction affinity detected by GST-PD, FRET and BRET assays. This is likely attributable to an artefact inherent to Venus (GFP)-based PCA assays: Venus fragment reconstitution is highly stable, and thus serves to stabilize PPIs between proteins the Venus fragments are conjugated to. This feature of Venus fragment reconstitution often enhances apparent interaction affinity for two proteins that may only weakly interact with one another. Thus, while Venus (GFP) PCA assays may be used to visualize subcellular localization of a PPI, they should be interpreted with caution regarding protein-protein interaction affinities. Greater differences in apparent interaction affinities between SPOP WT-c-Jun and SPOP F133L-c-Jun would likely be detected at different expression timepoints or expression levels of PCA-protein pairs.

Detailed method: HEK293T cells were seeded in 8-well chamber slides (Ibidi #80826) to reach a well confluence of 70-90% by 24 hours. Twenty-four hour after seeding, cells were transfected with plasmids containing SPOP and c-Jun conjugated, respectively, to the N-terminal and C-terminal fragments of Venus protein. Twenty-four hours post-transfection, cells were prefixed by addition of formaldehyde to culture medium to a final concentration of 2%. Culture media was then removed from chamber slide wells and replaced with 200 µL 4% formaldehyde for 15 minutes at 25 °C to completely fix cells. Cells were washed 3x 200 µL Hank's Balanced Salt solution (HBSS; Sigma #H8264), incubated with 200 µL HBSS containing (1) 5 µg/mL Hoescht 33342 nuclear stain and (2) 5 µg/mL wheat germ agglutinin (WGA) Alexa Fluor 633 conjugate (ThermoFisher #W21404) cell membrane stain for 30 minutes at 25 °C, washed 1x 200 uL

HBSS, then maintained in 200 uL fresh HBSS. Cells were imaged with a Nikon A1R HD25 for Hoescht 33342 (Ex 405 nm, Em 450 nm), WGA Alexa Fluor 633 conjugate (Ex 640, Em 7000) and Venus fluorescence (Ex 488 nm, Em 525 nm). ImageJ was used to determine integrated green pixel intensity per individual cell imaged at 10x.

Supplementary Figure 2.3

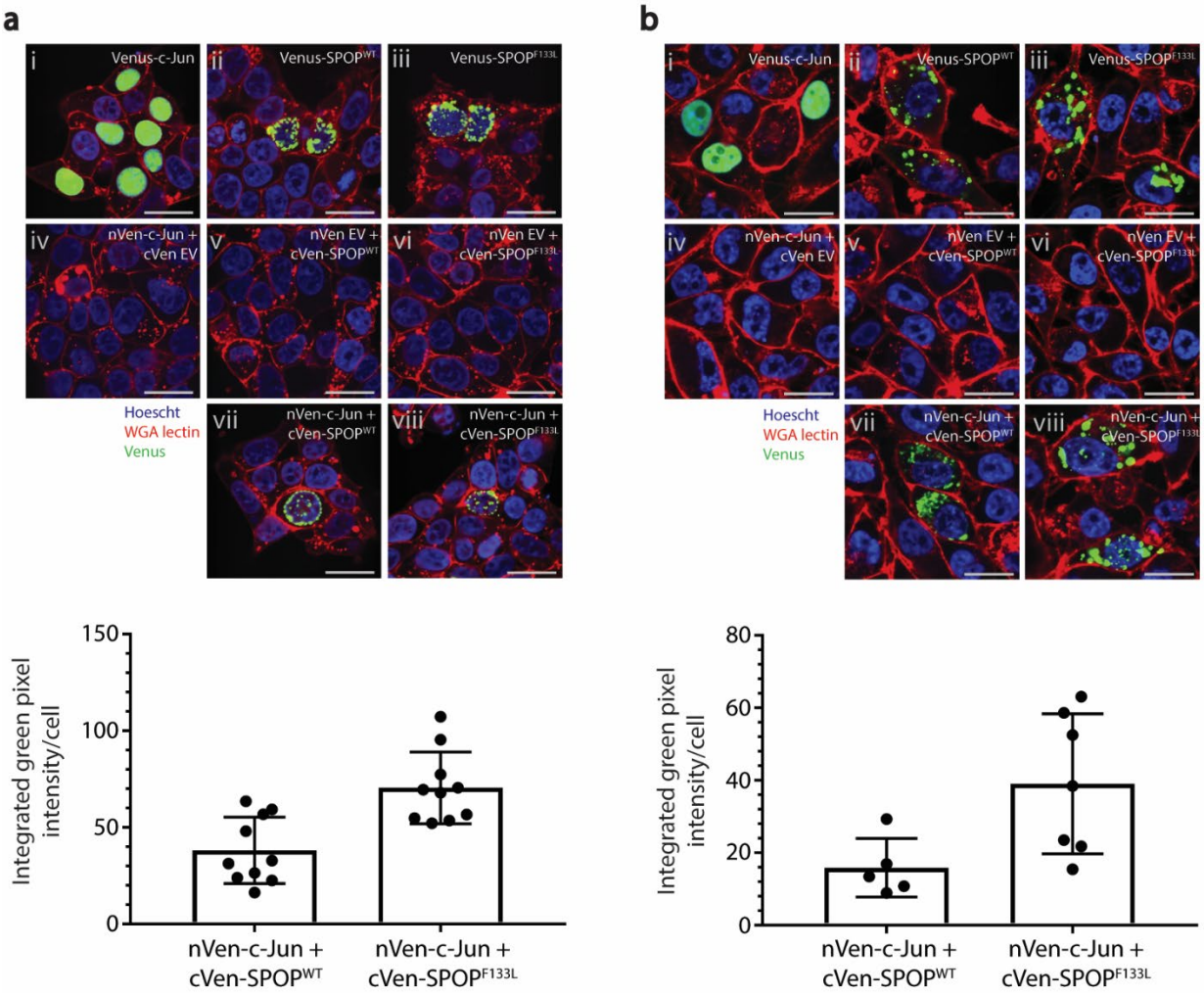

Supplementary Figure 2.4. SPOP F133L enhances ubiquitination of c-Jun.

(a) *In vivo* ubiquitination assay in HEK293T cells with overexpressed full-length SPOP (Venus-FLAG-tagged), overexpressed c-Jun (GST-tagged) and overexpressed ubiquitin (HA-tagged). HEK293T cells were seeded in 6-well plates (Corning #3506) to reach a well confluence of 70-90% by 24 hours. Twenty-four hours after seeding, cells were transfected with 1 μg GST-tagged expression plasmid, 1 μg Venus-FLAG or FLAG-expression plasmid, and 0.25 μg HA-Ubiquitin. Forty-eight hours after transfection, cells were lysed in 0.25% Triton X-100 lysis buffer (25 mM HEPES, 150 mM NaCl, 5 mM EDTA, 5 mM NaF, 0.25% Triton X-100) with 100 mM N-ethylmaleimide and lysates were incubated with glutathione-conjugated beads (GE #17527901), FLAG agarose beads (Sigma #F2426), or HA agarose beads (Sigma #E6779) for 2 hours with rotation at 4 °C. Beads were washed 3x5 minutes with 0.25% Triton X-100 lysis buffer, eluted by boiling in 2x Laemmli sample buffer (Bio-Rad #1610737), and processed via western blot.

(b) *In vivo* ubiquitination assay in HEK293T cells with overexpressed full-length SPOP (Venus-FLAG-tagged), overexpressed ubiquitin (HA-tagged), and endogenous c-Jun and SRC3. Assays performed as described in Supplementary Figure 2.4a.

(c) *In vivo* ubiquitination assay in HEK293T cells with SPOP MATH domain (Venus-FLAG-tagged), overexpressed c-Jun (GST-tagged), and overexpressed ubiquitin (HA-tagged). Assays performed as described in Supplementary Figure 2.4a.

(d) *In vivo* ubiquitination assay in HEK293T cells with overexpressed full-length SPOP (Venus-FLAG-tagged), overexpressed ubiquitin (HA-tagged) and stable CUL3 knockdown. Assays performed as described in Supplementary Figure 2.4a.

(e) *In vivo* ubiquitination assay in HEK293T cells with overexpressed full-length SPOP (GST-tagged), overexpressed c-Jun (Venus-FLAG-tagged), and overexpressed wild-type ubiquitin (HA-tagged) or ubiquitin with specific lysine-to-arginine mutations K48R or K63R. Assays performed as described in Supplementary Figure 2.4a.

(f) *In vivo* ubiquitination assay in HEK293T cells with overexpressed full-length SPOP (GST-tagged), overexpressed c-Jun (Venus-FLAG-tagged), and overexpressed wild-type ubiquitin (HA-tagged) or ubiquitin with all lysines mutated to arginines except K48 (K48-only: K48O) or K63 (K63-only: K63O). Assays performed as described in Supplementary Figure 2.4a.

Supplementary Figure 2.4

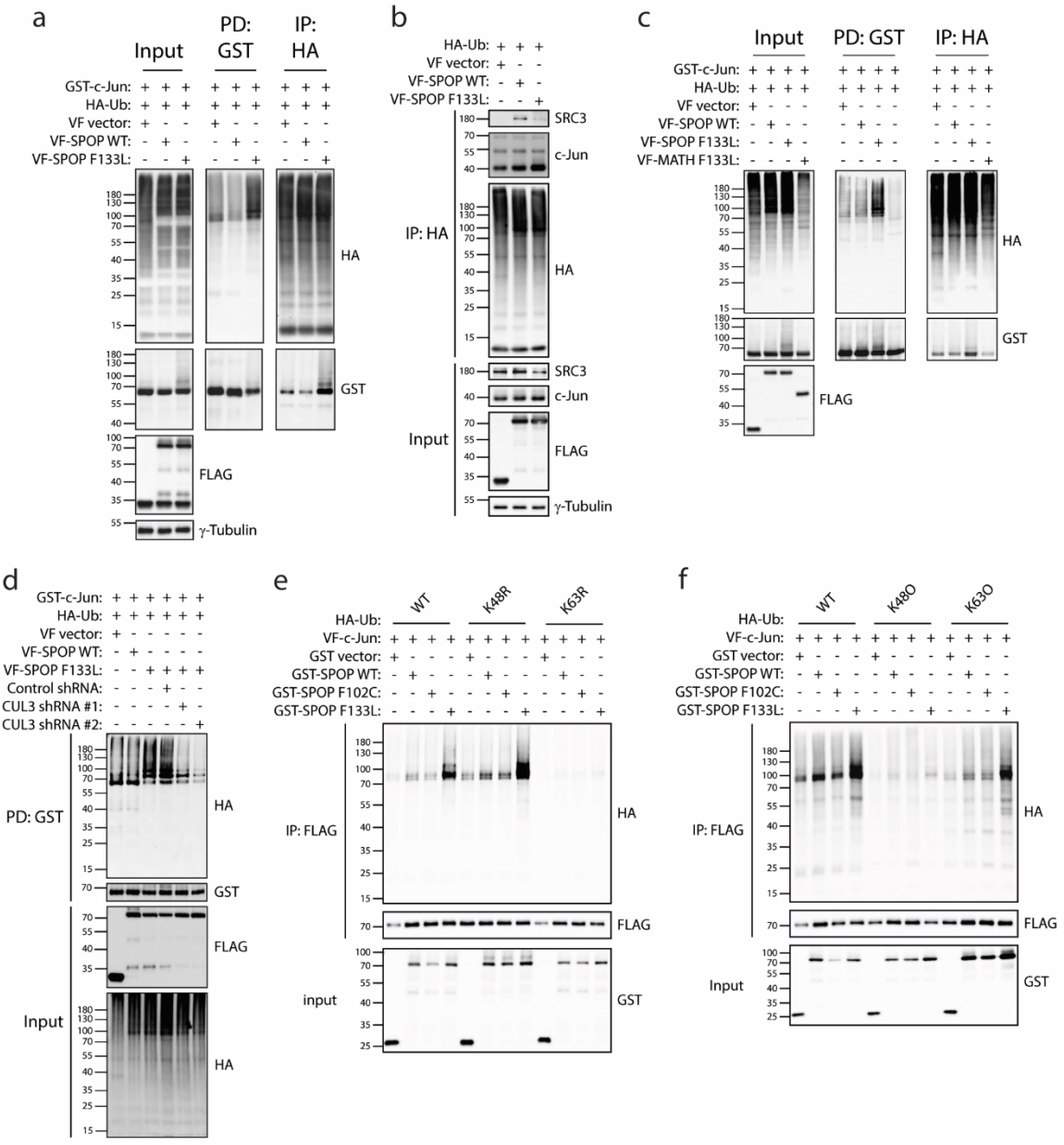

CHAPTER 3:

DEVELOPMENT OF AN ULTRA-HIGH-THROUGHPUT SCREENING ASSAY TO IDENTIFY SMALL MOLECULE INDUCERS OF SPOP F133V-BRD4 PROTEIN-PROTEIN INTERACTIONS

3.1 Introduction

SPOP is the most frequently mutated gene in primary prostate adenocarcinoma (110; 111). *SPOP* encodes a substrate recognition subunit of CUL3-RING E3 ubiquitin ligases that targets oncogenic substrates, such as BRD4 (118-120), SRC3 (107; 116), and TRIM24 (117; 121), for ubiquitin-mediated degradation. Missense mutations recur in SPOP's substrate-recognition MATH domain and serve to impair SPOP's ability to bind to substrate proteins, leading to a reduction in their SPOP-mediated ubiquitination and degradation (72). Previous studies have explored potential therapeutic vulnerabilities produced by the aberrant accumulation of SPOP substrates in tumors harboring SPOP mutations, and have collectively nominated several small molecule therapeutics, such as androgen receptor antagonists and PARP inhibitors, which may be particularly effective in inhibiting SPOP mutant tumor growth and metastasis by targeting SPOP substrate-modulated cellular pathways (98; 127; 128). Notably, however, these small molecule therapeutics exert their effects by binding to protein targets that are ubiquitously expressed and involved in cell signaling pathways critical to normal cellular function across multiple tissue types. Clinical use of these small molecule therapeutics that would target SPOP substrate-modulated cellular pathways thus frequently results in systemic tissue toxicity (i.e., patient side effects) through on-target effects in non-tumor tissues. No studies to date have explored direct therapeutic targeting of mutant SPOP itself, however, which represents a cancer-specific molecular target in tumors harboring recurrent SPOP missense mutations. Because SPOP mutants have been characterized to lose their tumor suppressor function primarily through loss of interaction with substrate proteins, chemical strategies that restore the ability of mutant SPOP to bind to its substrates may be able to therapeutically re-induce SPOP E3 ligase functionality and reverse SPOP mutant-mediated tumorigenesis.

Here, we present the development of an ultra-high-throughput, time-resolved fluorescence resonance energy transfer (uHTS TR-FRET) assay to enable identification of small molecules that restore SPOP missense mutant F133V interaction with SPOP substrate BRD4, an oncogenic chromatin reader protein that binds to acetylated lysine residues to facilitate gene transcription (199-202). We describe the results of a pilot screen that validates assay performance in a HTS format and identifies several small molecules which can induce SPOP interaction with BRD4.

3.2 Experimental Procedures

HEK293T cell culture

Human embryonic kidney 293T cells (HEK293T; ATCC #CRL-3216) were cultured in Dulbecco's Modified Eagle's Medium (DMEM; Corning #10-0103-CV). Cell culture medium was supplemented with 10% fetal bovine serum (Atlanta Biologicals #S11550) and 100 units/mL of penicillin/streptomycin (Cell Gro, #30-002-CI). Cells were maintained at 37°C in humidified conditions with 5% CO_2.

Plasmids, molecular cloning, and mutagenesis

Plasmids for mammalian expression of fusion proteins were generated using the Gateway cloning system (Invitrogen) according to the manufacturer's instructions. The following vector backbones were used as Gateway destination vectors: GST (pDEST27; Invitrogen #11812013), Venus-FLAG (VF; pSCM167). BRD4 cDNA plasmid (short isoform) was gifted by Dr. Kenneth Scott (Baylor). SPOP cDNA plasmid (#HsCD00081806) was purchased from DNASU. SPOP F133V mutation was introduced with the QuikChange Lightning Site-Directed Mutagenesis kit (Agilent #210518) using the SPOP cDNA plasmid from DNASU as a template, and with the

following primers: forward primer 5'-CAA GGC AAA GAC TGG GGA GTC AAG AAA TTC ATC CGT AGA; reverse primer 5'- TCT ACG GAT GAA TTT CTT GAC TCC CCA GTC TTT GCC TTG.

Transfection

HEK293T cells were transiently transfected using XtremeGene HP (Sigma #06366546001) according to the manufacturer's instructions at a ratio of (3μL XtremeGene):(1μg plasmid DNA). Transfection efficiency was monitored through visualization of Venus-FLAG-BRD4 fluorescence in live HEK293T cells prior to lysis.

Time-resolved fluorescence resonance energy transfer (TR-FRET) assays in 384-well microtiter plates

FRET buffer used throughout the TR-FRET assays consisted of 20 mM Tris-HCl pH 7.0, 50 mM NaCl, 0.01% nonidet P-40 (NP-40). HEK293T cells were grown in 6-well plates (Corning #3506) and transiently transfected with 1 μg GST-tagged expression plasmid and 1 μg Venus-FLAG-tagged expression plasmid using XtremeGene HP (Sigma #06366546001). Twenty-four hours after transfection, cell lysates were prepared in 200 μL lysis buffer containing 150 mM NaCl, 10 mM HEPES pH 7.5, 1% nonidet P-40 (IGEPAL CA-630, Sigma), 5 mM sodium pyrophosphate, 5 mM NaF, 2 mM sodium orthovanadate, 10 mg/L aprotinin, 10 mg/L leupeptin and 1 mM PMSF, pH 7.4. 15 μL of cell lysate was mixed with 15 μL of FRET antibody combinations (described below; prepared in FRET buffer) to a total volume of 30 μL per well in black 384-well plates (Corning #3573). Plates were centrifuged at 1000 rpm for 5 min and incubated at 25 °C for 2 hrs (unless otherwise indicated). TR-FRET signals were measured using a BMG Labtech PHERAstar *FSX* reader with the HTRF optic module (mirror: D400/D505; time

delay: 50 μs; total time window: 150 μs) using different TR-FRET donor and acceptor fluorophore pairs as follows:

Anti-GST-Tb cryptate donor to Venus acceptor configuration: 1:1000 anti-GST-Tb final concentration; λ_{ex}: 337 nm, $\lambda_{em,\,1}$: 486 nm, $\lambda_{em,\,2}$: 520; TR-FRET signal expressed as ratio ($F520/F486 \cdot 10^4$)

Anti-GST-Tb cryptate donor to anti-FLAG-d2 acceptor: 1:1000 anti-GST-Tb and 1:500 anti-FLAG-d2 final concentrations; λ_{ex}: 337 nm, $\lambda_{em,\,1}$: 615 nm, $\lambda_{em,\,2}$: 665; TR-FRET signal expressed as ratio ($F665/F615 \cdot 10^4$)

Anti-FLAG-Tb cryptate donor to anti-GST-d2 acceptor: 1:1000 anti-FLAG-Tb and 1:500 anti-GST-d2 final concentrations; ; λ_{ex}: 337 nm, $\lambda_{em,\,1}$: 615 nm, $\lambda_{em,\,2}$: 665; TR-FRET signal expressed as ratio ($F665/F615 \cdot 10^4$)

To determine an optimal cell lysate protein concentration for TR-FRET assays, two-fold serial dilutions of lysate in FRET buffer were prepared. Tb cryptate-conjugated anti-GST antibody (anti-GST-Tb, #61GSTTLF), Tb cryptate-conjugated anti-FLAG antibody (anti-FLAG-Tb, #61FG2TLF), d2-conjugated anti-GST antibody (anti-GST-d2, #61GSTDLF), and d2-conjugated anti-FLAG antibody (anti-FLAG-d2, #FG2DLF) were purchased from Cisbio.

Time-resolved fluorescence resonance energy transfer (TR-FRET) assay in 1536-well microtiter plates (uHTS format)

Cell lysates with co-expressed [GST-SPOP F133V and VF-BRD4] or [GST-SPOP WT and VF-BRD4] were prepared as described above for the 384-well plate format. 5 μL cell lysate (at the optimal protein concentration determined from serial dilution series in the 384-well plate format; Figure 3.2) with 1:1000 anti-GST-Tb antibody was added per well to black 1536-well plates using a multiple-drop Combi dispenser (ThermoFisher #5840320). Plates were centrifuged at

1000 rpm for 5 min and incubated at 25 °C. TR-FRET signals were measured for the anti-GST-Tb cryptate acceptor and Venus donor FRET pair using a BMG Labtech PHERAstar *FSX* reader with the HTRF optic module (λ_{ex}: 337 nm, $\lambda_{em,1}$: 486 nm, $\lambda_{em,2}$: 520; mirror: D400/D505; time delay: 50 us). TR-FRET signals are expressed as the ratio ($F520/F486 \cdot 10^4$). The stability of the assay in the 1536-well plate format was monitored by recording TR-FRET signals after incubation at 25°C for 10 min, 2 hrs, 4 hrs, and 24 hrs.

Evaluation of HTS assay performance

Cell lysates with co-expression of [GST-SPOP F133V and VF-BRD4] or [GST-SPOP WT and VF-BRD4] were used to measure TR-FRET signal for SPOP F133V-BRD4 interactions or SPOP WT-BRD4 interactions, respectively. TR-FRET signal for cell lysate with co-expression of GST with VF-BRD4 (non-interacting protein pair) was defined as negative control background signal. To evaluate assay performance for HTS, signal-to-background (S/B) ratios, signal windows (SW) between SPOP F133V-BRD4 and SPOP WT-BRD4 interactions, and Z-prime (Z') were calculated as follows:

$$\frac{S}{B} = \frac{\mu_{SPOP+BRD4}}{\mu_{background}}$$

$$SW = \frac{FRET_{WT}}{FRET_{F133V}}$$

$$Z' = 1 - \frac{3(\sigma_{WT} + \sigma_{F133V})}{|\mu_{WT} - \mu_{F133V}|}$$

Where $\mu_{SPOP+BRD4}$ equals TR-FRET signal for either 1) GST-SPOP WT with VF-BRD4 or 2) GST-SPOP F133V with VF-BRD4, and $\mu_{background}$ equals TR-FRET signal for GST with BRD4; $FRET_{WT}$ is TR-FRET signal for GST-SPOP WT with VF-BRD4, and $FRET_{F133V}$ is TR-FRET signal for GST-SPOP F133V with VF-BRD4; and μ_{WT} and σ_{WT} are the mean and standard deviation of TR-FRET signals from lysate with co-expressed GST-SPOP WT and VF-BRD4,

and μ_{F133V} and σ_{F133V} are the mean and standard deviation of TR-FRET signals from lysate with co-expressed GST-SPOP WT and VF-BRD4. All experiments were carried out with a minimum of three replicates per sample.

Small molecule pilot screen using uHTS TR-FRET

A pilot screen was performed using the LOPAC chemical library (Sigma #LO4200; 1280 total compounds) and the Emory Enriched Library (Emory Chemical Biology Discovery Center proprietary collection of small molecules; 2610 total small molecules). All small molecules were prepared in DMSO to a concentration of 1 mM prior to screening. 5 μL lysate with 1:1000 anti-GST-Tb was dispensed per well into 1536-well black plates, and 0.1 μL of 1 mM compound was added using a Beckman NX integrated pintool (Beckman Coulter, Brea, CA) to a final compound concentration of 20 μM and a final DMSO concentration of 2% (v/v) per well. Compounds were incubated for 4 hrs at 25°C, and TR-FRET signals were measured using a BMG Labtech PHERAstar *FSX* reader as described above for the 1536-well format. Compound effect on TR-FRET signal was expressed as percent change relative to GST-SPOP F133V/VF-BRD4 lysate with 2% DMSO addition only.

Glutathione-S-transferase (GST) pull down

HEK293T cells were seeded in 6-well plates (Corning #3506) to reach a well confluence of 70-90% by 24 hours. Twenty-four hours after seeding, cells were transfected with 1 μg GST-SPOP plasmid and 1 μg Venus-FLAG-BRD4 plasmid. Forty-eight hours after transfection, cells were lysed in 0.25% Triton X-100 lysis buffer (25 mM HEPES, 150 mM NaCl, 5 mM EDTA, 5 mM NaF, 0.25% Triton X-100) and lysates were incubated with compound for 1 hr with rotation at 4 °C, after which glutathione-conjugated beads (GE #17527901) were added and incubated for an additional 2 hours with rotation at 4 °C. Beads were 1x 2 min with 0.25% Triton X-100 lysis

buffer, proteins were eluted off beads by boiling in 2x Laemmli sample buffer (Bio-Rad #1610737), and samples were processed via western blot.

Western blot

Proteins in 2x Laemmli sample buffer were resolved by 10% polyacrylamide gel electrophoresis (SDS-PAGE) and transferred to nitrocellulose membranes at 100 V for 2.5 hours at 4 °C. Membranes were blocked in 5% nonfat dry milk prepared in 1x TBST (20 mM Tris-base, 150 mM NaCl, 0.05% Tween-20) for 1 hour at 25 °C, then incubated with primary antibodies overnight at 4 °C with gentle shaking. Membranes were washed using 1x TBST, 3x10 minutes, then incubated with secondary antibodies at 25 °C for 1 hour with gentle shaking. Membranes were again washed for 3x10 min in 1x TBST then developed using SuperSignal West Pico PLUS Chemiluminescent Substrate (ThermoFisher #34580). Chemiluminescent images were captured using the ChemiDoc Touching Imaging System (Bio-Rad). The following primary antibodies were used at a 1:1000 dilution in 5% (w/v) non-fat milk in TBST for western blot: GST (#2624) and FLAG (#14793) antibodies purchased from Cell Signaling Technology. The following secondary antibodies were used at a 1:5000 dilution in 5% (w/v) non-fat milk in TBST for chemiluminescent western blot detection: goat anti-rabbit IgG (111-035-003) and goat anti-mouse IgG (115-035-003) from Jackson Immunoresearch Laboratories.

3.3 Results

Development of an ultra-high-throughput, time-resolved fluorescence resonance energy transfer assay to monitor SPOP-BRD4 protein-protein interactions

To enable monitoring of SPOP-BRD4 protein-protein interactions in a homogenous, high-throughput format, a high-throughput screening platform was developed to monitor SPOP-

BRD4 interactions using time-resolved fluorescence resonance energy transfer (TR-FRET) technology (Figure 3.1). In our general assay format, cell lysates from HEK293T cells co-expressing glutathione-S-transferase (GST)-SPOP and Venus-FLAG (VF)-BRD4 are incubated with a pair of FRET donor and acceptor fluorophore-conjugated antibodies that bind to the GST and FLAG protein tags. Protein-protein interaction between GST-SPOP and VF-BRD4 in lysate brings the paired donor and acceptor fluorophores into proximity to enable fluorescence resonance energy transfer (FRET) from donor to acceptor that is detected as TR-FRET signal.

The TR-FRET assay was first optimized to detect TR-FRET signal for GST-SPOP WT and GST-SPOP F133V interactions with VF-BRD4 in 384-well microtiter plates. During our optimization, we evaluated several TR-FRET fluorophore donor-acceptor pairs and concentrations of lysate containing co-expressed GST-SPOP and VF-BRD4 to determine a combination that maximized 1) signal-to-background (S/B) ratios for SPOP WT-BRD4 and SPOP F133V-BRD4 interactions and 2) signal window between SPOP WT and SPOP F133V (Table 3.1). We also performed serial dilutions of cell lysates with co-expressed GST-SPOP and VF-BRD4 to determine an optimal lysate protein concentration for TR-FRET signal (Figure 3.1b, 3.2a). For GST-SPOP and VF-BRD4, an anti-GST-Tb antibody lanthanide conjugate and Venus fluorescent protein as FRET donor and acceptor, respectively, were observed to maximize S/B and signal window at a 125 μg/mL lysate protein concentration (Figure 3.2a): this configuration demonstrated a S/B ratio for SPOP WT-BRD4 interactions of 4.3 and a S/B ratio for SPOP F133V-BRD4 interactions of ~1.2 (Figure 3.2c), respectively, while signal window (ratio of SPOP WT-BRD4 signal to SPOP F133V-BRD4 signal) was determined to be 3.5. Because the assay was designed to screen for small molecules that can induce SPOP F133V-BRD4 interactions to a level matching SPOP WT-BRD4 interactions, a Z' parameter assessing

the suitability of assay for this screening purpose was calculated. Z' for a given HTS assay relates an assay's signal window to its signal variation; briefly, scores ≥ 0.5 suggest an assay is acceptable for HTS, while scores < 0.5 indicate that signal variation is too high for the assay to produce reliable results. Z' was calculated to be ~0.78 (Figure 3.2a, 3.2d) at the 125 μg/mL lysate protein concentration, indicating the assay signal window between SPOP WT and SPOP F133V in this configuration was suitable for small molecule screening purposes.

The TR-FRET assay was further optimized for use in a miniaturized 1536-well microtiter plate format to reduce reagent costs for small molecule screening campaigns. For the same 125 μg/mL lysate protein concentration, S/B ratios for SPOP WT-BRD4 interactions and SPOP F133V-BRD4 interactions were determined to be 6.35 and 1.3 (Figure 3.2c), respectively, with signal window and Z' calculated to be 4.9 and ~0.85 (Figure 3.2d). TR-FRET signals were also observed to remain stable over a 24-hour incubation period at 25 °C in this 1536-well plate configuration (Figure 3.2e). Because the 1536-well microtiter plate format demonstrated a higher signal assay window between SPOP WT and SPOP F133V, a higher Z' score, and suitable temporal stability over time, the 1536-well format was chosen to perform a pilot screen for small molecule inducers of SPOP F133V-BRD4 protein-protein interactions.

Pilot screen for small molecule inducers of SPOP F133V-BRD4 interactions

To validate assay performance for large-scale high-throughput small molecule screening using the ultra-high-throughput (uHTS) 1536-well plate format, a pilot screen for SPOP F133V-BRD4 PPI inducers was conducted using a collection of roughly 4000 small molecules sourced from the Library of Pharmacologically Active Compounds (LOPAC) and the Emory Enrichment Library (EEL). In the screen, cell lysates with co-expressed GST-SPOP F133V and VF-BRD4 were incubated with 20 μM compound for 4 hours at 25°C prior to plate reading. Using a cutoff

of ≥250% TR-FRET signal induction relative to control SPOP F133V-BRD4 PPI TR-FRET signal (DMSO-only control), 68 compounds were identified as primary hits (Figure 3.3a). Hits were further validated for SPOP F133V-BRD4 PPI induction activity in orthogonal, single dose (20 μM) GST-pull down (GST-PD) assays. Using a threshold of ≥2.5-fold GST-PD FLAG band densitometry relative to DMSO treatment control, three compounds were further confirmed in these secondary GST-PD assays to induce SPOP F133V-BRD4 protein-protein interactions (Figure 3.3b; #1: dasatinib, #16: mitoxantrone, #31: SGI-1027) at 20 μM compound concentration. New batches of these compounds were re-ordered from commercial sources, and dose-response GST-PD assays were used to further confirm small molecule inducer activity. Dose-response GST-PD assays with re-ordered compounds suggested that two compounds, mitoxantrone and SGI-1027, may be able to induce SPOP F133V-BRD4 interaction in a dose-dependent manner (Figure 3.3c, 3.3d). EC_{50} values for induction of SPOP F133V-BRD4 interaction were estimated to be 42.57 μM and 40.04 μM, respectively.

3.4 Discussion

Recurrent missense mutations in *SPOP* drive tumorigenesis in up to 15% of primary prostate carcinomas. These recurrent SPOP mutations induce loss of SPOP tumor suppressor activity by abolishing SPOP interaction with substrate proteins, though overall SPOP protein architecture has been characterized to remain preserved in the setting of SPOP mutation (72). While several chemical therapeutic strategies have been nominated to be more effective in treatment of SPOP mutation-driven prostate adenocarcinoma, these strategies often result in systemic toxicity in patients due to on-target effects in non-tumor tissue. Mutant SPOP itself, however, represents a tumor-specific therapeutic target because it is only expressed in tumor

tissue. Therapeutic strategies which selectively target mutant SPOP may thus provide a greater therapeutic index because mutant SPOP represents a tumor-specific marker and driver.

One strategy to restore mutant SPOP function may be to use small molecules to re-induce SPOP-protein interactions that are lost as a consequence of SPOP mutation, and thereby restore SPOP E3 ubiquitin ligase functionality. Feasibility of utilizing small molecules to induce and stabilize protein-protein interactions for therapeutic purposes has been demonstrated through prior clinical implementation of both synthetic and natural-product PPI inducers, including the immunosuppressants cyclosporin (134; 135) and rapamycin (136; 137) and the microtubule stabilizer paclitaxel (138; 139). Several other studies have nominated additional compounds with PPI inducer activity that may have therapeutic potential, including one recent notable study that described the first small molecule protein-protein interaction inducer of mutated tumor suppressor SMAD4^{R361H} with SMAD3 to restore tumor-suppressive TGF-β signaling (140). Small molecules specifically designed to induce interaction between a target protein and an E3 ubiquitin ligase to promote target protein ubiquitination and degradation have also been explored through proteolysis targeting chimera (PROTAC) approaches, and these approaches have successfully enabled selective degradation of specific proteins (203-205). Collectively, these previous studies demonstrate that it is feasible to identify small molecule inducers of protein-protein interactions with potential therapeutic and clinical applications.

Our work describes the first reported screen to identify small molecule inducers of SPOP-BRD4 protein-protein interactions. BRD4 is an oncogenic chromatin reader protein that is targeted by SPOP for ubiquitin-mediated degradation in prostate lineage cells (118-120). Recurrent SPOP missense mutations in prostate tumors, the most frequent of which is F133V (representing roughly 25% of all recurrent, prostate cancer-associated SPOP missense mutations)

(110), significantly reduce or abolish SPOP interaction with BRD4 and cause aberrant BRD4 accumulation in cells. BRD4 acetyl-lysine reader activity has been characterized to contribute to oncogenesis (206-208), partly by enabling transcriptional upregulation of the oncogenic c-Myc transcription factor (202). Given the high prevalence of SPOP F133V mutations across patient primary prostate adenocarcinomas, the well-characterized role of BRD4 in promoting oncogenesis, and prior validation of BRD4 inhibition as a strategy to reduce prostate cancer cell growth (209; 210), our strategy to re-induce SPOP F133V-BRD4 interactions to re-enable SPOP-mediated degradation of BRD4 has the potential to be therapeutically impactful by reversing a key mechanism of SPOP mutation-mediated oncogenesis in SPOP mutant prostate tumors.

Through our pilot screen, we have identified two compounds which are able to induce SPOP-BRD4 protein-protein interactions: mitoxantrone and SGI-1027. These compounds are structurally distinct (Figure 3c) and have been characterized to bind to unique protein targets. Mitoxantrone, an anthracenedione compound currently used in clinical treatment of a variety of cancers, is characterized to act as an inhibitor of type II topoisomerases (211). Notably, a combination therapy consisting of mitoxantrone and prednisone, a steroidal anti-inflammatory agent, is currently US FDA-approved for as a second-line, palliative treatment for metastatic, castration-resistant prostate cancer (mCRPC) (212; 213). SGI-1027, a quinoline-based compound that is not currently approved for clinical use, has been characterized to act as a DNA methyltransferase inhibitor (214; 215). In our assays evaluating SPOP-BRD4 PPI induction activity, mitoxantrone and SGI-1027 were able to induce SPOP F133V interaction with BRD4 in a dose-dependent manner with EC_{50} values of ~40 μM (Figure 3.3c). However, these compounds were similarly able to induce SPOP WT interaction with BRD4 with comparable EC_{50} values

(data not shown). Further experimental work will be required to probe how these compounds may bind to SPOP and BRD4, whether these compounds are able to enhance SPOP WT- and SPOP F133V-mediated ubiquitination of BRD4 in *in vitro* and *in vivo* assays, whether these compounds are able to induce SPOP WT and SPOP F133V interactions with other SPOP protein substrates, and to examine whether these compounds may inhibit characteristics of cellular transformation driven by SPOP mutation and/or elevated BRD4 protein levels. Because these compounds have previously characterized protein targets and anti-cancer effects, however, attributing any specific anti-cancer effects of these compounds to induction of SPOP-BRD4 interactions in SPOP mutant prostate tumor models will likely be challenging. Nonetheless, these compounds may represent promising chemical scaffolds that can be further modified to enhance specificity for induction of SPOP-BRD4 interactions.

In conclusion, we have developed and validated a robust, ultra-high-throughput, cell lysate-based TR-FRET assay to screen for small molecule inducers of SPOP F133V-BRD4 interactions. To our knowledge, our study represents the first high-throughput assay developed to screen specifically for SPOP PPI inducers. Larger-scale screens with diverse chemical libraries may yield additional candidate small molecule inducers of mutant SPOP PPIs with potential therapeutic application in reversing SPOP mutant-mediated prostate tumorigenesis. Future small molecule screens by our group will aim to identify small molecules that selectively induce SPOP F133V-BRD4 interactions relative to SPOP WT-BRD4 interactions.

Figure 3.1. TR-FRET assay development for detection of differential SPOP WT-BRD4 and SPOP F133V-BRD4 interactions.

(a) TR-FRET assay principle for detection of differential SPOP-BRD4 interactions and identification of SPOP F133V-BRD4 PPI inducers. Cell lysates are derived from HEK293T cells with co-expression of GST-SPOP and VF-BRD4, and lysates are incubated with a pair of TR-FRET donor and acceptor fluorophores. In the assay configuration depicted, GST-SPOP is labeled with an anti-GST-Tb cryptate conjugate to enable Tb to act as TR-FRET donor fluorophore, and the Venus (V) component of the VF-BRD4 fusion protein acts as a TR-FRET acceptor fluorophore. Interaction between SPOP and BRD4 brings Tb and Venus into proximity, which, upon laser excitation of Tb, enables fluorescence resonance energy transfer (FRET) from Tb to Venus which is detected as TR-FRET signal.

(b) Example of TR-FRET signal titration in a 384-well format through two-fold serial dilutions of stock cell lysates using the assay configuration depicted in (a). HEK293T cell lysates with the following pairs of proteins were generated and incubated with 1:500 anti-GST-Tb cryptate antibody conjugate: GST with VF-BRD4 (negative control, non-interacting pair equivalent to no-protein TR-FRET signal), GST-SPOP WT with BRD4, GST-SPOP F133V with BRD4. Lysates were diluted in TR-FRET buffer to a starting concentration of 250 μg/mL total protein, and two-fold serial dilution was performed in FRET buffer to generate concentration curves. Data represent means ± standard deviation from triplicate samples.

Figure 3.1

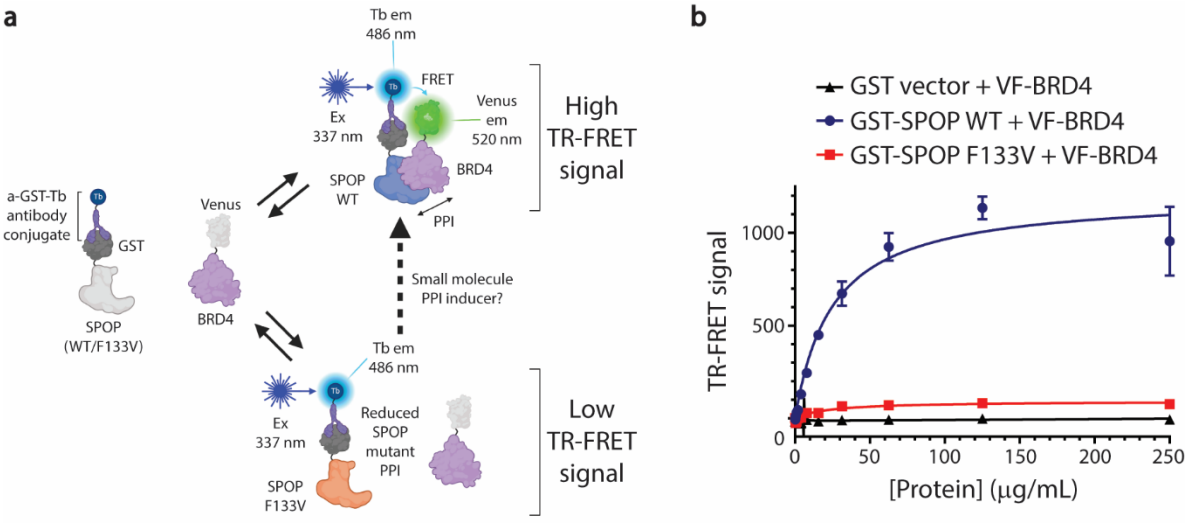
a
Tb em
486 nm
FRET
Ex
337 nm
Venus
em
520 nm
BRD4
SPOP
WT
PPI
High
TR-FRET
signal
a-GST-Tb
antibody
conjugate
GST
SPOP
(WT/F133V)
Venus
BRD4
Small molecule
PPI inducer?
Tb em
486 nm
Ex
337 nm
Reduced
SPOP
mutant
PPI
SPOP
F133V
Low
TR-FRET
signal
b
GST vector + VF-BRD4
GST-SPOP WT + VF-BRD4
GST-SPOP F133V + VF-BRD4
TR-FRET signal
1000
500
0
0
50
100
150
200
250
[Protein] (μg/mL)

Figure 3.2. TR-FRET assay performance parameters in 384-well HTS and 1536-well uHTS formats.

(a) Z' and signal window of the 384-well plate assay configuration at various concentrations of protein lysate. Assay configuration is the same as described for Figure 3.1.

(b) Comparison of TR-FRET signal for differential SPOP WT-BRD4 and SPOP F133V-BRD4 interactions in 384-well and 1536-well plate formats.

(c) Comparison of S/B ratios for SPOP WT-BRD4 and SPOP F133V-BRD4 interactions in 384-well and 1536-well plate formats.

(d) Comparison of assay signal window and Z' for SPOP WT-BRD4 and SPOP F133V-BRD4 in 384-well and 1536-well plate formats.

(e) Analysis of TR-FRET signal stability for different protein pairs over time in 1536-well plate format.

Figure 3.2

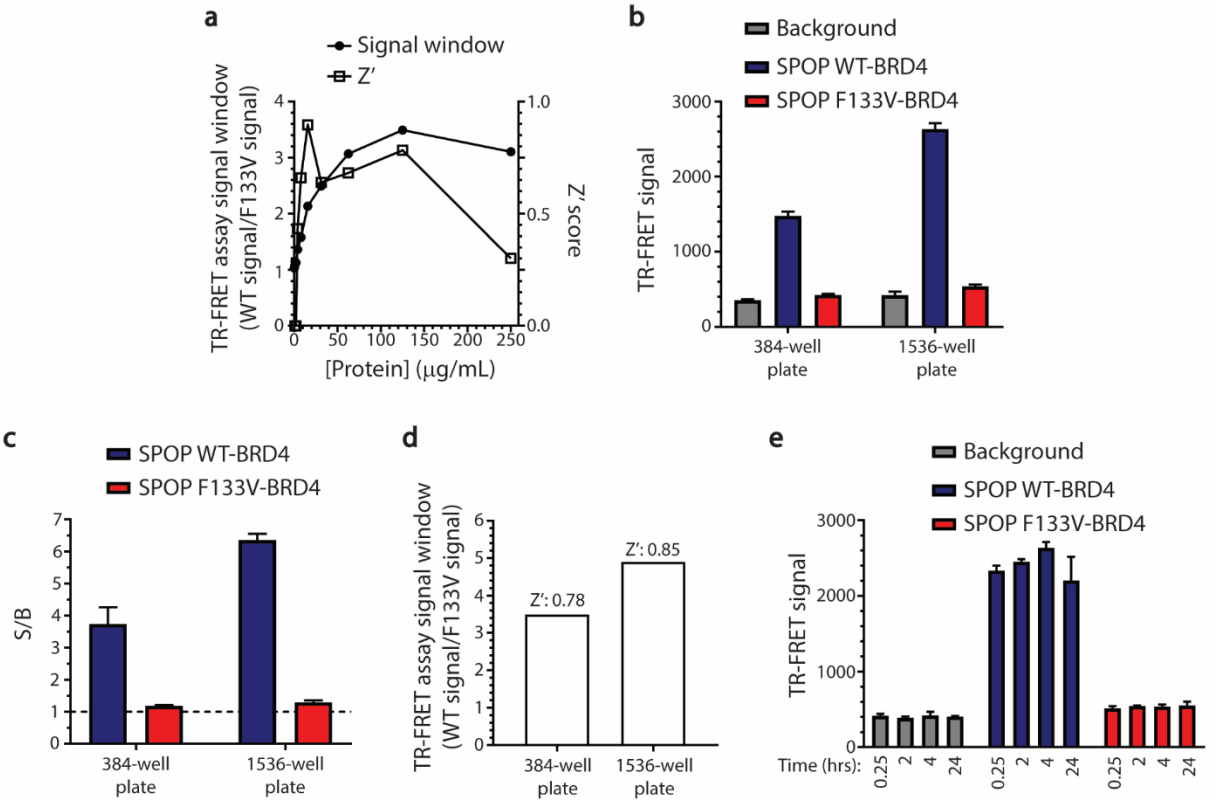
a
Signal window
Z′
TR-FRET assay signal window (WT signal/F133V signal)
Z′ score
[Protein] (μg/mL)
b
Background
SPOP WT-BRD4
SPOP F133V-BRD4
TR-FRET signal
384-well plate
1536-well plate
c
SPOP WT-BRD4
SPOP F133V-BRD4
S/B
384-well plate
1536-well plate
d
TR-FRET assay signal window (WT signal/F133V signal)
Z′: 0.78
Z′: 0.85
384-well plate
1536-well plate
e
Background
SPOP WT-BRD4
SPOP F133V-BRD4
TR-FRET signal
Time (hrs): 0.25 2 4 24 0.25 2 4 24 0.25 2 4 24

Figure 3.3. Pilot screen for SPOP F133V-BRD4 PPI inducers in a 1536-well uHTS format.

(a) Summary of results for pilot screen for SPOP F133V-BRD4 PPI inducers using the LOPAC and EEL small molecule chemical libraries. Small molecules were incubated with HEK293T cell lysate containing co-expressed GST-SPOP F133V and VF-BRD4 for 4 hrs at 25°C at a compound concentration of 20 μM and 2% (v/v) DMSO. Percent induction of SPOP F133V-BRD4 interaction was calculated for each compound relative to SPOP 133V-BRD4 with 2% (v/v) DMSO addition only (red dotted line). Light blue shading indicates TR-FRET signal ≥250% of non-compound control, which was used as the criteria for determining compound hits for further validation.TR-FRET signal for SPOP WT-BRD4 interaction (blue dotted line) was used as a benchmark for SPOP F133V-BRD4 PPI induction by compounds.

(b) Single-dose (20 μM) GST pull down validation of small molecule hits from pilot screen exhibiting ≥250% induction of SPOP F133V-BRD4 interaction.

(c) Dose-response GST pull down validation and PPI induction EC_{50} calculation for two compounds validated in single-dose GST pull down validation.

Figure 3.3

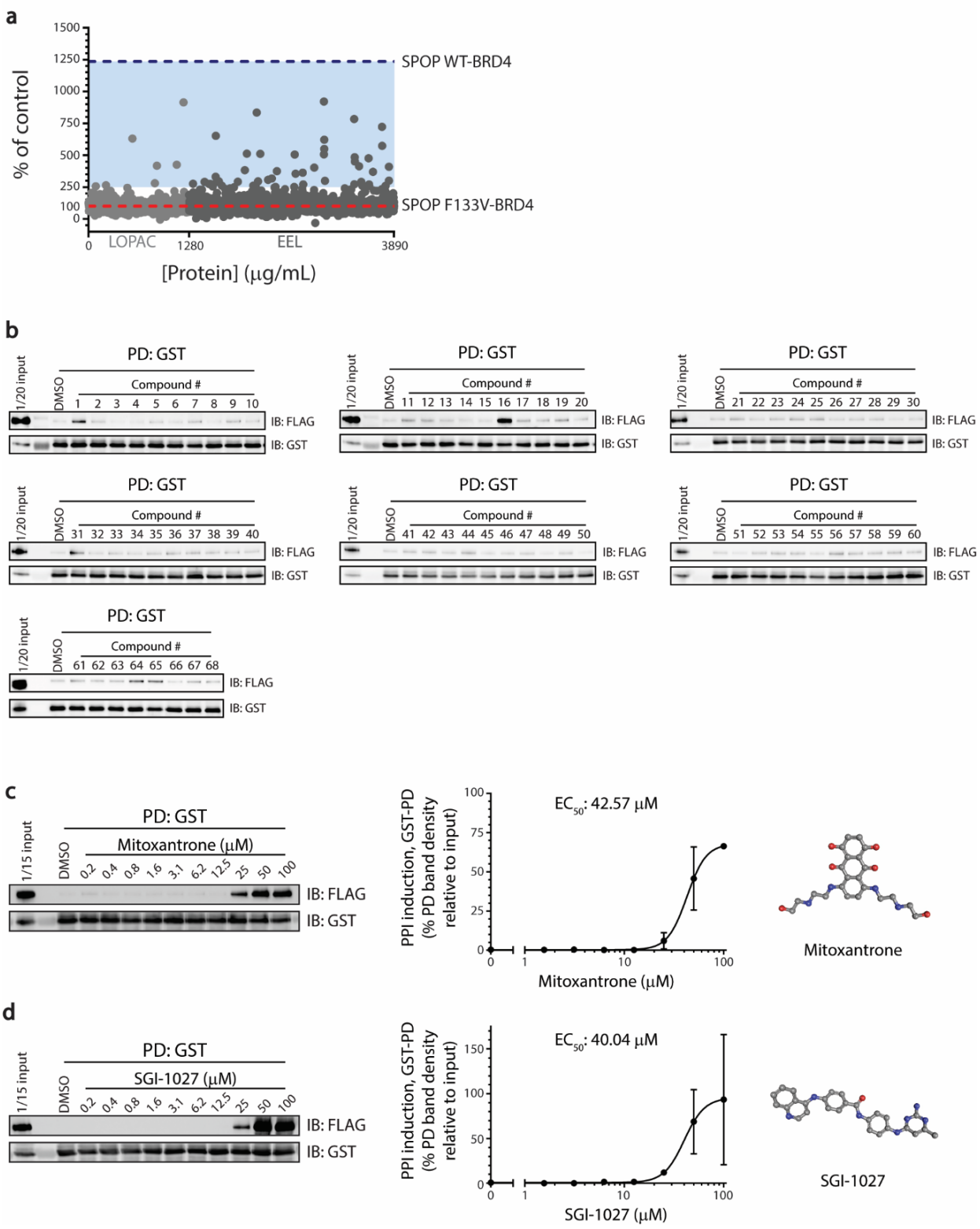
a
% of control
SPOP WT-BRD4
SPOP F133V-BRD4
LOPAC
EEL
[Protein] (μg/mL)
b
PD: GST
1/20 input
DMSO
Compound #
IB: FLAG
IB: GST
c
PD: GST
1/15 input
Mitoxantrone (μM)
PPI induction, GST-PD (% PD band density relative to input)
EC50: 42.57 μM
Mitoxantrone (μM)
Mitoxantrone
d
SGI-1027 (μM)
EC50: 40.04 μM
SGI-1027 (μM)
SGI-1027

Table 3.1. Summary of TR-FRET assay configurations evaluated for 384-well HTS assay development.

Test Condition Number	SPOP Construct	Substrate Construct	TR-FRET Donor	TR-FRET Acceptor	Signal-to-Background Ratio	Assay Window (WT Signal/ F133V Signal)
1	GST-SPOP WT	Venus-FLAG-BRD4	α-GST-Tb	Venus	4.3	3.5
2	GST-SPOP F133V				1.2	
3	GST-SPOP WT			α-FLAG-d2	1.9	1.5
4	GST-SPOP F133V				1.2	
5	GST-SPOP WT		α-FLAG-Tb	α-GST-d2	1.2	1.2
6	GST-SPOP F133V				1.0	

CHAPTER 4:

DISCUSSION AND FUTURE DIRECTIONS

4.1 Identification of novel SPOP-binding proteins: functional implications

SPOP functions as a critical regulator of cellular signaling pathways through its interactions with other proteins. Our knowledge of the extent of cellular pathways that SPOP modulates under both normal physiological and pathophysiological conditions remains limited, however, because we currently have limited knowledge regarding the number and identify of proteins to which SPOP can bind and regulate. The work presented in this dissertation expands the characterized SPOP protein-protein interactome by validating several SPOP protein binding partners which have not been previously characterized. These novel SPOP binding partners include B-raf (*BRAF*), E2F6, MAGEA6, SDHA, MRE11A (MRE11), ELOC (*TCEB1*), OLIG2, E2F2, AXL, prostasin (*PRSS8*), ASCL1, ZNF483, FAM46C (TENT5C), VHL, FOXP1, CBFA2T1 (*RUNX1T1*), synphilin-1 (*SNCAIP*), GATA1, c-Jun (*JUN*), c-Rel (*REL*), cIAP1 (*BIRC2*), Cbl-b (*CBLB*), CUL4B, and ZBTB2. Our identification of SPOP interactions with these proteins nominates new cellular pathways which SPOP may be able to regulate (and, vice versa, pathways that may regulate SPOP) across various cell lineages. These SPOP protein binding partners' associated cellular pathways may furthermore be influenced by dysregulation of SPOP activity through alterations in SPOP protein expression level, *SPOP* gene deletion or mutation, and changes in SPOP subcellular localization. These SPOP binding partners' characterized functions, major associated cellular pathways, known connections to oncogenesis, and frequency and mode of alteration in prostate cancer specifically (Figure 4.1) are briefly discussed here:

B-raf (*BRAF*): BRAF is a kinase that functions as a critical, positive regulator of the RAF-RAS-MEK-ERK (MAPK) pathway to promote several properties associated with cancer "hallmarks," including cell proliferation, migration and survival (216). *BRAF* mutations frequently drive

oncogenesis in melanoma, glioblastoma, colon cancer, and lung cancer. Increased activation of the MAPK pathway is associated with progression of prostate cancer toward a more advanced, hormone-resistant state (217). B-raf has also been characterized to phosphorylate the homeobox transcription factor NANOG, an SPOP substrate (74). B-raf phosphorylation of NANOG inhibits SPOP binding to NANOG, and reduces SPOP-mediated ubiquitination and degradation of NANOG.

E2F6 and E2F2: E2Fs are a family of transcription factors that regulate the transcription of many genes, and most prominently several cell cycle-related genes (218; 219). E2F2 is associated with transcriptional upregulation of target genes that promotes cell proliferation, while E2F6 is associated with transcriptional downregulation of the same target genes to inhibit cell growth.

MAGEA6: The MAGE family of proteins have been characterized to bind to E3 RING ubiquitin ligases to enhance their E3 ubiquitination function and are generally proto-oncogenes (190; 220; 221). Elevated MAGEA6 expression specifically has been associated with poor cancer patient clinical outcomes (222; 223), and has been demonstrated to promote cellular transformation and anchorage-independent cellular growth *in vitro* (190; 221). Given MAGEA6's function as an E3 enhancer, it is possible that MAGEA6 binding to SPOP WT may enhance $CRL3^{SPOP}$ E3 ligase ubiquitination of SPOP substrates; SPOP F133L/V mutation-enhanced interactions with MAGEA6 could further amplify this function. Because MAGEA6 demonstrates high sequence homology with other MAGE family members (224) (which are not currently included our lab's OncoPPi screening library (17)), it is also highly possible that SPOP may be able to interact with several MAGE family members beyond MAGEA6.

SDHA: SDHA encodes a catalytic subunit of succinate dehydrogenase, which functions in the metabolic Krebs cycle that takes place in the mitochondrial matrix (225). Dysregulation of Krebs cycle component enzymes have been associated with several diseases such as cancer.

MRE11A (MRE11): MRE11 forms a complex with proteins RAD50 and NBS1 to sense DNA double strand breaks and facilitate their repair through activation of kinase ATM (another protein which SPOP can bind to) (191; 226). MRE11 plays a role in specifically promoting homology directed repair (HDR) of DNA double strand breaks rather than non-homologous end joining (NHEJ). Inherited, inactivating mutations of MRE11 cause ataxia-telangiectasia-like disorder (ATLD), a syndrome that features defects in DNA damage repair that increase the frequency of cancer development (227). Importantly, downregulation of *SPOP* expression and *SPOP* missense mutation have also both been associated with impaired homology-directed repair of DNA double strand breaks (98; 193). The identification of SPOP-MRE11 interactions by our research group suggests an additional mechanism by which SPOP may play a role in regulation of HDR. Recent work by Watanabe et al also suggests that overexpression of SPOP F133V, but not SPOP WT or SPOP Y87C, uniquely reduces MRE11 protein levels, leading the group to hypothesize that SPOP F133V mutations may exert gain of function effects on MRE11 (193). Our data revealing that SPOP can interact with MRE11, and furthermore that SPOP F133L/V mutations may enhance this PPI, suggests that this phenomenon may potentially be mediated through F133V-induced interactions.

Elongin C (*TCEB1*): Elongin C (ELOC) was first described as a subunit of the SIII transcription elongation factor that enhances RNA polymerase II transcription elongation beyond transcription arrest sites (228). ELOC was later characterized to be an adaptor subunit of CUL2-RING (CRL2) E3 ubiquitin ligases complexes that binds to substrate recruitment proteins, such as

VHL, to enable CRL2 ubiquitination of substrate proteins (42; 43; 229). The gene *TCEB1* that encodes ELOC is frequently amplified in prostate tumors (Figure 4.1).

OLIG2: OLIG2 is a transcription factor expressed primarily in CNS cells that promotes oligodendrocyte differentiation (230). Elevated OLIG2 expression has been associated with gliomagenesis.

AXL: AXL is a member of the TAM family of receptor tyrosine kinases (RTKs) (231). When activated, AXL signals through the Ras-Raf-MEK-ERK (MAPK) and PI3K-Akt cell signaling pathways to promote cell proliferation, migration, and survival. AXL also modulates integrins to regulate actin reorganization. AXL was originally discovered through its ability to induce CML leukemogenesis.

Prostasin (PRSS8): Prostasin is a serine protease whose primary characterized function is as a proteolytic activator of the epithelial sodium channel (ENaC) (232). Prostasin is uniquely expressed at high levels in prostate tissue and seminal fluid. Downregulation of prostasin levels in prostate epithelial cells has been associated with cellular oncogenic transformation (233).

ASCL1: ASCL1 has been characterized as a transcription factor that regulates the transcription of several proto-oncogenes and promotes pulmonary neuroendocrine differentiation (234). High ASCL1 expression has been associated with the ‘classic’ subtype of small cell lung carcinoma.

ZNF483: The activity of ZNF483 is currently not well characterized.

FAM46C (TENT5C): FAM46C has recently been characterized as a poly(A) polymerase that enhances expression of ER-targeted mRNAs (235). Deletions or missense mutations of *TENT5C* are collectively associated with up to 30% of multiple myeloma cases.

VHL: Like SPOP, VHL is a substrate recognition subunit of E3 ubiquitin ligase complexes (236). VHL E3 complexes consist of VHL-elongin B/elongin C-CUL2-RBX1 (referred to

collectively as VCB complexes). VHL functions to recruit HIFα transcription factors, which promote adaptation to cellular hypoxia, for ubiquitin-mediated degradation. Inherited or acquired deletions or mutations of VHL promote loss of HIFα regulation and are strongly associated with the development of ccRCC (49; 237), a subtype of kidney cancer that SPOP WT overexpression and cytoplasmic subcellular localization are also strongly associated with. Our group's identification of both SPOP-VHL and SPOP-ELOC interactions suggest potential SPOP-mediated regulation of HIFα activity through modulation of VCB E3 complexes.

FOXP1: FOXP1 belongs to the FOXP family of transcription factors that regulate transcription of many genes that influence cell growth, proliferation, and differentiation (238). FOXP1 is expressed primary in B lymphocytes and its overexpression is associated with several subtypes of B-cell lymphoma.

CBFA2T1 (*RUNX1T1*): CBFA2T1 is a transcriptional co-repressor that is predominantly expressed in hematopoietic lineage cells (239). The biological roles of CBFA2T1 alone remain poorly characterized, but translocation of the *RUNX1T1* gene with *RUNX1* drives acute myeloid leukemia by inducing dysregulation of RUNX1-mediated gene transcription.

Synphilin-1 (*SNCAIP*): The biological function of synphilin-1 is currently unclear; however, the presence of Lewy body-like protein aggregates containing synphilin-1 in neurons are associated with the development of neurodegenerative diseases such as Lewy body dementia and Parkinson disease (240).

GATA1: GATA1 is a member of the GATA family of transcription factors that promotes hematopoiesis (241). GATA1 deletions and mutations are associated primarily with hematological disorders such as acute megakaryoblastic leukemia and Diamond-Blackfan anemia (congenital erythroid hypoplasia).

c-Jun (*JUN*): c-Jun is a proto-oncogenic transcription factor that regulates the transcription of several genes that promote cell proliferation, survival and apoptosis across virtually all cell lineages (242). c-Jun overexpression and overactivation, which most often occurs through overactivation induced by up-pathway oncogenes, contributes to cellular transformation and tumorigenesis in several cell lineages.

JunD (*JUND*): Like c-Jun, JunD belongs to the JUN transcription factor family (242). JunD has been characterized to generally antagonize the pro-growth and pro-cellular transformation activities of c-Jun, but has also been found to be essential for prostate cancer cell proliferation (243).

c-Rel (*REL*): c-Rel is a subunit of dimeric NF-κB transcription complexes that drive transcription of inflammation-associated genes, such as those that encode cytokines (244). c-Rel overexpression and overactivation has been associated with the development of several types of lymphoid cancer.

cIAP1 (*BIRC2*): cIAP1 is a member of the inhibitor of apoptosis (IAP) family of proteins (245). cIAP1 performs many biological functions, the best characterized of which are its activities as an E3 ubiquitin ligase that downregulates caspase activity and that promotes ubiquitin-mediated modulation of proteins within the NF-κB pathway to alter innate immune responses. cIAP1 has been characterized to act as a tumor suppressor or a proto-oncogene in different cellular contexts: loss of cIAPs has been associated with multiple myeloma, while amplification of *BIRC2* has been associated with development of liver, lung, pancreatic, and brain cancers.

Cbl-b (*CBLB*): Cbl-b functions as a RING E3 ubiquitin ligase that negatively regulates T cell receptor, B cell receptor, CD28 and 40 receptor pathways to modulate innate and adaptive immune responses in T and B lymphocytes, natural killer cells, and macrophages (246).

CUL4B: Analagous to CUL3 function in $CRL3^{SPOP}$ complexes, CUL4B acts as a scaffold protein subunit within DDB-CUL4-RING (CRL4) E3 ubiquitin ligase complexes (247). CRL4B E3 ubiquitin ligases complexes have been characterized to regulate several DNA repair processes. ZBTB2: ZBTB2 is a member of the BTB/POZ zinc-finger protein family. The biological functions of ZBTB2 have not been well characterized to date, though ZBTB2 has been found to bind to methylated DNA and influence DNA methylation patterns and to inhibit p53 activity (248; 249).

4.2 SPOP point variants feature unique protein-protein interactomes that suggest novel mechanisms of SPOP-mediated biology, oncogenesis, and therapeutic vulnerability

The data presented in this dissertation suggest that recurrent, prostate cancer-associated missense mutations in *SPOP* alter SPOP-protein interactions. Indeed, prostate adenocarcinoma-associated missense mutations in SPOP have previously been characterized to drive tumorigenesis by promoting SPOP loss of interaction with oncogenic protein substrates, leading to a reduction in their SPOP-mediated ubiquitination. Our data confirm that recurrent, prostate cancer-associated SPOP missense mutations Y87C, F102C, F133L, and F133V induce loss of interaction with previously characterized SPOP substrates such as BRD4 and SRC-3. Our data also suggest several additional proteins that lose interaction with SPOP as a result of SPOP missense mutation, including MYD88, BRAF, OLIG2, RUNX1T1, and synphilin-1. SPOP missense mutation-induced loss of interaction with these proteins suggests loss of potential SPOP regulation of their associated cellular signaling pathways, which may represent additional mechanisms of SPOP mutation-mediated oncogenesis. Alternatively, these proteins may also

normally serve to modulate SPOP function in different cellular contexts, and SPOP missense mutation-induced loss of interaction may result in loss of key regulatory mechanisms governing SPOP function. For example, post-translational phosphorylation of SPOP by AURKA and LIMK2 has been described to regulate SPOP subcellular localization and protein level. BRAF, a kinase we have newly identified to bind to SPOP, could conceivably also phosphorylate SPOP and modulate SPOP function, and this potential function would be lost upon SPOP missense mutation-induced inhibition of the PPI. Other SPOP binding partners may simply be able to influence SPOP function directly through protein-protein interactions that promote conformational changes in SPOP and/or alter SPOP binding to other proteins. Further work will be required to determine how this identified SPOP missense mutation-induced loss of interaction with these novel SPOP binding partners may influence their associated cell signaling pathways to alter cellular behavior.

A second set of SPOP protein binding partners identified by our group does not demonstrate significant change in interaction affinity with SPOP as a result of prostate adenocarcinoma-associated SPOP missense mutations, including SPOP, CUL3, E2F6, ASCL1 and JUND. As described in Chapter 2, SPOP-SPOP and SPOP-CUL3 interactions have previously been characterized to be mediated through the SPOP BTB domain, an SPOP protein domain whose structure has been observed to be unaltered by the cancer-associated missense mutations that recur in SPOP's substrate recognition MATH domain (72). Because E2F6, ASCL1, and JunD similarly demonstrate no difference in interaction affinity with mutant SPOP relative to wild-type SPOP, it is possible that these three proteins may similarly bind to SPOP through the SPOP BTB domain rather than the SPOP MATH domain. Alternatively, these proteins may interact with SPOP through a region of the SPOP MATH domain outside the

characterized SPOP substrate binding cleft, though this would be a form of SPOP-protein interaction through the MATH domain that has not been previously observed. Finally, while SPOP mutation does not appear to significantly influence SPOP interaction with this group of proteins, alterations in SPOP protein levels (downregulation or upregulation) leading to diminished or enhanced interaction of SPOP with these proteins could represent mechanisms of SPOP WT-associated pathogenesis.

The data presented in this dissertation, along with the data from a large-scale BRET-based protein-protein interaction screen performed by our lab, also reveal that a subset of recurrent SPOP missense mutations, specifically SPOP F133L and F133V, can enhance or induce interaction with several cancer-associated proteins while promoting loss of interaction with others such as SRC-3 and BRD4. For the roughly 600 of cancer-associated proteins our lab has screened against wild-type and mutant SPOP and subsequently validated, this phenomenon appears to be particular to SPOP F133L and F133V mutants and does not generally extend to recurrent Y87C and F102C mutants. Proteins which demonstrate clear induction of interaction with SPOP due to F133L/V mutation include AXL, MRE11A, TCEB1, FOXP1, cIAP1, Cbl-b, CUL4B, GATA1, c-Jun, c-Rel, and ZBTB2. Another set of proteins also appear to exhibit slight induction of interaction with SPOP F133L/V mutants, such as MAGEA6, SDHA, E2F2, PRSS8, ZNF483, FAM46C, and VHL. Collectively, these mutation-induced interactions suggest that SPOP F133L/V mutants gain a unique ability to physically intervene in several cancer-relevant cell signaling pathways. Such SPOP mutation-induced protein-protein interactions are a phenomenon that has not been previously described for recurrent, prostate cancer-associated SPOP missense mutants, though this phenomenon has previously been hypothesized to be possible (111). However, precedent that particular missense mutations in the SPOP MATH

domain may actually enhance SPOP interaction with particular substrates does exist for endometrial cancer-associated SPOP missense mutations: in contrast to prostate cancer-associated mutations, which induce SPOP loss of interaction with substrate BRD4, endometrial cancer-associated missense mutations have been observed to enhance SPOP interaction with, and SPOP-mediated degradation of, oncogenic substrate BRD4 (119; 189). Overall, these mutation-induced protein-protein interactions may represent a *gain of oncogenic function* for SPOP F133L/V mutants beyond their previously associated mutation-induced loss of tumor suppressor activity.

Currently, all prostate cancer-associated SPOP missense mutations are characterized to uniformly induce loss of interaction with SPOP substrates and promote loss of SPOP tumor suppressor activity. Through this work, however, we have identified SPOP mutation-specific networks of SPOP-protein interactions in which distinct SPOP mutants are able to differentially interact with divergent sets of proteins. Further functional characterization of these divergent, SPOP mutation-specific protein-protein interaction networks may uncover additional SPOP mutation-specific mechanisms of oncogenesis and unique therapeutic vulnerabilities in SPOP-mutant prostate tumors that can serve as biomarkers for SPOP-mutant prostate tumor behaviors and treatment responses.

Finally, based on the findings discussed in this dissertation, I propose there may be yet another unique mechanism by which SPOP missense mutations may alter SPOP and cellular function: through SPOP multimerization. SPOP missense mutations occur in primary prostate adenocarcinomas almost exclusively as heterozygous (rather than homozygous) missense mutations in the SPOP MATH domain (110; 111), and these missense mutations do not significantly impact SPOP's ability to homo-oligomerize through the SPOP BTB domain (79).

Furthermore, SPOP missense mutations do not appear to influence SPOP's ability to condense into lower-order membrane-less organelles (i.e., the nuclear speckles for which SPOP is named), although they can inhibit higher order liquid-liquid phase separation induced by SPOP WT interactions with substrates such as DAXX (substrates which also individually phase separate) (79). Because SPOP WT and SPOP F133L/V mutants are capable of binding to distinct sets of proteins, I propose that SPOP WT hetero-oligomerization with SPOP F133L/V, as well as SPOP F133L/V homo-oligomerization, through the SPOP BTB domain may also act as a scaffold to aggregate a diverse set of proteins that may not otherwise experience close proximity in an SPOP WT cellular background. The condensed protein compositions of the membrane-less organelles (nuclear speckles) formed by SPOP WT-SPOP F133L/V hetero-oligomers and SPOP F133L/V homo-oligomers may then enable the aggregated proteins to physically influence one another to perform unique functions. For example, SPOP F133L/V-induced interactions with E3 ligase-associated proteins Cbl-b, cIAP1, CUL4B, VHL, elongin C, and MAGEA6 may enable SPOP to connect into E3 ligase complexes distinct from the well-characterized $CRL3^{SPOP}$ E3 complex that SPOP participates in. The formation of these distinct E3 ligase complexes may then allow for unique patterns of SPOP-mediated ubiquitination for other SPOP WT and/or SPOP F133L/V-binding proteins. SPOP multimers could also potentially serve as hubs for recruitment of various SPOP WT-binding and SPOP F133L/V-binding transcription factors (e.g., E2F2, E2F6, c-Jun, c-Rel, GATA1, SRC-3) or epigenetic readers (e.g., BRD4) to form transcription-promoting protein complexes specific to SPOP-mutant prostate tumor cells.

4.3 Unique structural determinants of SPOP-c-Jun interactions

To gain insight into how recurrent SPOP F133L/V mutations induce interaction with particular proteins, this dissertation work characterized SPOP and c-Jun protein elements that enable SPOP-c-Jun interactions. First, using an expanded panel of SPOP mutants including all reported prostate tumor mutations of the F133 residue (Y87C, F102C, W131C, W131G, F133C, F133L, F133I, F133S, F133V), we detected that SPOP mutation-induced interaction with c-Jun is a phenomenon particular to F133 mutants. SPOP F133I, F133L, and F133V mutations strongly induced interaction with c-Jun (Figure 2.2). F133C mutation also induced interaction with c-Jun to a lesser extent, while F133S mutation did not enhance SPOP interaction with c-Jun. In contrast, SPOP Y87C, F102C, W131C, and W131G mutations reduced interaction with c-Jun relative to SPOP WT. These results suggest that SPOP F133I/L/V mutations, all substitutions which replace an aromatic R group with R groups consisting of aliphatic methyl chains at the F133 position, may represent a distinct subclass of SPOP mutations that are able to induce interactions with a subset of proteins such as c-Jun.

SPOP protein deletion mapping analyses indicate that SPOP F133L mutations induce interaction with c-Jun specifically through the mutated SPOP MATH domain. However, it appears that the mutated F133 residue may not directly participate in SPOP-c-Jun interactions: our data indicate that SPOP MATH domain fragments consisting of SPOP residues 93-138 and either F133 or F133L are able to bind to c-Jun equally well regardless of F133 residue status. The smallest SPOP MATH domain fragment tested, comprised of residues 113-138 with either F133 or F133L, was not detected to interact with c-Jun, indicating a requirement of SPOP residues 93-112 for the interaction. If recurrent F133 SPOP mutants enable interaction with c-Jun through a neighboring SPOP amino acid residue region outside the F133 site, it is possible that F133 mutations may induce a local conformational change in the SPOP MATH domain that

exposes a c-Jun-binding “epitope” common among all SPOP point variants within residue region 93-138. It is also possible that F133 mutations cause complete loss of SPOP MATH domain structural stability, rather than inducing local conformational change, to enable unique access to this 93-138 residue region, though this possibility seems less likely because previous structural studies examining SPOP mutation effects on SPOP MATH domain stability suggest that recurrent SPOP MATH domain mutations preserve overall MATH domain structure (72; 132).

In terms of c-Jun protein elements that enable SPOP-c-Jun interactions, a minimal c-Jun protein fragment consisting of residues 1-82 was determined to be sufficient to enable interaction with SPOP F133L. This region of c-Jun consists of the N-terminal half of the c-Jun transactivation domain (Figure 2.2a), an intrinsically disordered region of c-Jun that undergoes posttranslational modification to regulate c-Jun activity in AP1 transcription factor complexes. Of note, this region of c-Jun does not contain a canonical SPOP binding motif (φ-π-S-S/T-S/T, where φ represents a general non-polar residue and π indicates a general polar residue) (72), which suggests that SPOP variants interact with c-Jun through recognition of a novel motif. However, c-Jun residue region 1-82 does prominently feature major sites of interaction with and regulation by JNKs: JNK1 and JNK2 bind to c-Jun through a c-Jun region characterized as the ‘δ domain’, comprised of c-Jun residues 31-60. JNKs then phosphorylate c-Jun at residues S63 and S73 to induce c-Jun dimerization with JUN, FOS and ATF family proteins to form functional AP1 transcriptional complexes. Interaction of SPOP with c-Jun through this transactivation domain region thus suggests potential SPOP influence on JNK-mediated regulation of c-Jun. Indeed, our data suggest that SPOP F133L may be able to partially compete with JNK1 for binding to c-Jun, which indicates that JNK1 and SPOP may share partially overlapping binding sites on c-Jun (Figure 4.2). However, SPOP overexpression in our system does not seem to

significantly influence JNK phosphorylation of c-Jun at residues S63 and S73 under basal conditions or after anisomycin simulation of JNK1 kinase activity (data not shown). Further experimental exploration of the interplay between SPOP and JNK1 in binding to and modulating c-Jun will be required to determine how this dynamic may influence overall c-Jun function in different contexts.

Of note, c-Jun residue region 1-82 also shares partial N-terminal sequence homology with JUN protein family members JunB and JunD (188). Our protein-protein interaction assays detected SPOP interaction with both c-Jun and JunD, but not with JunB. Our data further indicate that recurrent SPOP F133L/V mutations enhance interaction with c-Jun, but not with JunD. SPOP F133L/V-induced interactions with c-Jun thus appear to be a unique phenomenon among JUN protein family members. c-Jun, JunB, and JunD have also been characterized to have differing abilities to interact with JNKs: c-Jun and JunB, but not JunD, are capable of interacting with JNKs through their N-terminal transactivation domains (250). Thus, although SPOP can compete with JNK1 for binding to c-Jun, it seems that SPOP does not recognize protein motifs identical to those recognized by JNK1, as SPOP was not detected to bind to JNK1-interaction-competent JunB.

4.4 SPOP-mediated stabilization of c-Jun as a potential mechanism of SPOP-mediated oncogenesis

This dissertation presents *in vitro* data demonstrating SPOP-mediated stabilization of c-Jun protein that is enhanced by SPOP F133L mutation. The SPOP F133L MATH domain alone, which mediates SPOP F133L interaction with c-Jun, is not sufficient to promote stabilization of c-Jun. It was subsequently determined that CUL3 expression is necessary for SPOP F133L

stabilization of c-Jun. These data suggest that SPOP-CUL3 complexes, rather than SPOP alone, may be necessary to promote c-Jun protein stabilization. *In vivo* ubiquitination assays also suggested that SPOP F133L is capable of ubiquitinating c-Jun in a CUL3-dependent manner, and that ubiquitin may be conjugated to c-Jun through ubiquitin K63 residues. Collectively, these data suggest a mechanism for SPOP F133L stabilization of c-Jun that is mediated by SPOP-CUL3 K63-linked ubiquitination.

SPOP's biological roles to date have largely been attributed to its function as a substrate recognition subunit of CRL3 E3 ubiquitin ligases complexes, through which SPOP targets substrate proteins featuring one or more SPOP binding motifs for ubiquitination. SPOP-mediated ubiquitination has most often been associated with proteasomal degradation of substrates, although non-degradative functions of SPOP-mediated ubiquitination have also been described for MacroH2A, MyD88, and INF2 (67; 80; 81). No studies to date have examined what types of ubiquitin lysine chain linkages SPOP can promote on substrates, though previous studies have characterized other individual E3 ligases as being capable of catalyzing diverse ubiquitin chain linkages in a substrate-specific manner. Our data provide an indication that SPOP can enable K63-linked ubiquitination of substrates, and suggest a unique, stabilizing role for $CRL3^{SPOP}$ complexes toward c-Jun.

c-Jun, originally identified as the cellular counterpart of avian sarcoma retroviral oncogene v-Jun, was one of the first human proto-oncogenes to be discovered and characterized (251; 252). As a terminal effector of the MKK4/7-JNK cellular signaling pathway, c-Jun is activated via phosphorylation by JNKs to dimerize with other JUN, FOS and ATF protein family members and form activated AP-1 transcription factor complexes. JNK-mediated activation of c-Jun is an early response to mitogenic stimuli, DNA damage and cellular stress, and activated AP-

1/c-Jun complexes subsequently alter transcription of hundreds of genes that collectively promote cell proliferation, migration, survival, and apoptosis. Many cancers exhibit upregulation of c-Jun protein levels as a mechanism to promote oncogenesis, tumor maintenance and tumor metastasis (242), including castration-resistant, metastatic, and recurrent prostate tumors which often feature c-Jun overexpression (196).

In normal cells, c-Jun protein levels are tightly regulated to guard against cellular transformation that would otherwise be promoted by high c-Jun protein levels. Modulation of c-Jun protein levels is achieved through posttranslational modification of c-Jun that influences c-Jun protein stability. These posttranslational modifications include JNK phosphorylation of c-Jun, which stabilizes c-Jun protein levels and activates c-Jun transcriptional activity (253), and degradative ubiquitination of c-Jun mediated by proteins such as ITCH (254), FBXW7 (255; 256), DET1 (257), and BLM (258) that reduce c-Jun protein levels. Given the importance of tight regulation of c-Jun protein stability in maintaining normal cellular behavior and the role of c-Jun overexpression in promoting prostate cancer, our data demonstrating that SPOP F133L mutation enhances c-Jun protein stability may represent a novel mechanism by which SPOP F133L mutation can promote prostate tumorigenesis (Figure 4.2). SPOP F133L stabilization of c-Jun thus suggests a unique gain of oncogenic function for SPOP F133L beyond previous reports of its mutation-induced loss of function. This elevated c-Jun protein expression promoted by SPOP F133L/V furthermore has potential to synergize with other upregulated cell signaling pathways in SPOP F133L/V mutant tumors described by other research groups, such as the AR and PI3K/AKT pathways (85), to uniquely promote cellular characteristics associated with various hallmarks of cancer. Further studies into the specific cellular consequences of SPOP F133L-mediated stabilization of c-Jun will be necessary to establish the roles of SPOP F133L-c-

Jun interactions and their potential synergy with other cancer-associated cell signaling pathways in SPOP-mutant tumorigenesis.

4.5 Small molecule restorers of SPOP protein-protein interactions as a strategy to reverse SPOP mutation-driven oncogenesis

Last, this dissertation also describes the development and validation of an ultra-high-throughput TR-FRET assay to identify small molecule inducers of SPOP F133V-BRD4 interactions. Recurrent, prostate cancer-associated SPOP missense mutations such as SPOP F133V have been characterized to induce loss of interaction with BRD4, an SPOP substrate (118-120). SPOP mutation-induced loss of interaction with BRD4 subsequently causes a reduction in SPOP-mediated ubiquitination and degradation of BRD4, and leads to an abnormal elevation of BRD4 protein levels. As an epigenetic reader protein that binds to acetylated lysine residues, BRD4 then promotes transcriptional elongation and the transcription of proto-oncogenes such as c-Myc (202; 206-208). Strategies to re-induce mutant SPOP-BRD4 interactions and restore SPOP ubiquitin-mediated regulation of BRD4 may thus represent a promising therapeutic strategy to reverse SPOP mutation-driven oncogenesis. Our TR-FRET-based, uHTS pilot screen for SPOP F133V-BRD4 PPI inducers suggests that it is possible to identify small molecule inducers of SPOP F133V-BRD4 interactions. Our pilot screen yielded two compounds, mitoxantrone and SGI-1027, which are capable of inducing SPOP-BRD4 interactions, although the compounds can induce both SPOP F133V and SPOP WT interaction with BRD4. The results of this pilot screen, in which only a few thousand compounds were tested, support the execution of additional screens with larger, more diverse small molecule libraries to pursue identification of small molecules which may be able to selectively restore

SPOP F133V interactions with SPOP protein substrates such as BRD4. With the validation of this method provided by this proof-of-concept pilot screen described herein, this approach could also theoretically be expanded in the future to discover small molecules that target SPOP mutants beyond SPOP F133V and/or that restore interaction with additional SPOP substrates.

4.6 Limitations

As with all research methods and approaches, the experimental methods and approaches employed in this research work have limitations which must be considered during interpretation of this dissertation's research findings. Most prominently, the protein-protein interactions described in this work have largely been identified and characterized through approaches using overexpressed, rather than endogenous, proteins. Experimental approaches using overexpressed proteins enable protein-protein interactions and protein functional effects to be more readily detected, but these protein-protein interactions and protein effects may not accurately reflect protein interactions and behaviors that occur under endogenous protein expression conditions. Future work should seek to confirm that the SPOP-protein interactions and SPOP functional effect under protein overexpression conditions also occur under (near-)endogenous protein expression conditions where possible. Methods that could confirm protein-protein interactions at endogenous levels include endogenous protein co-immunoprecipitation and proximity ligation assay (PLA). Similarly, to confirm the effects of wild-type and mutant SPOP variants on their protein binding partners, cell lines and model organisms with relevant biological backgrounds that feature endogenous expression of SPOP variants should be employed where possible; these model systems could theoretically be engineered through the use of CRISPR approaches.

4.7 Conclusions and future directions

In summary, this dissertation 1) identifies and validates novel protein-protein interaction perturbations induced by recurrent, prostate cancer-associated SPOP missense mutations, 2) describes a novel mechanism of SPOP F133L binding to and stabilization of oncogenic transcription factor c-Jun, and 3) outlines the establishment of a uHTS platform to identify small molecule inducers of SPOP F133V-BRD4 interactions. Overall, this work contributes to our understanding of how SPOP mutations may promote oncogenesis and presents an approach to reverse mutant SPOP's loss of tumor suppressor activity through restoration of SPOP PPIs. Furthermore, this dissertation provides a framework for several future directions additional research work could take:

First, the data in this dissertation demonstrate that distinct prostate cancer-associated missense mutations (i.e., mutations of residues Y87, F102, W131, F133) in SPOP induce unique SPOP PPI perturbations. A subset of serous endometrial cancers is also driven by recurrent *SPOP* missense mutations, but these endometrial cancer-associated SPOP mutations characteristically recur at distinct amino acid residues (e.g., E47, E50, R121, D140) (109). In both prostate and endometrial cancers, these *SPOP* missense mutations that recur in the MATH domain are currently hypothesized to equivalently induce loss of interaction with SPOP substrates, and it remains unclear why prostate cancer-associated *SPOP* mutations occur at different amino acid residues from endometrial cancer-associated *SPOP* mutations. Our approaches revealing differential protein-protein interactions among prostate cancer-associated SPOP missense mutants suggests, by extension, that yet other SPOP missense mutants, such as those characteristic in endometrial cancers, may similarly exhibit unique protein-protein interactions. Our lab's resonance energy transfer-based PPI detection platforms could readily be

expanded to test how these endometrial cancer-associated SPOP missense mutants differentially alter interactions with the roughly 600 cancer-associated proteins in the OncoPPi library. Identification of such differential interactions (both loss of interaction and potential gain of interaction) could provide new hypotheses for why prostate tumorigenesis and endometrial tumorigenesis are driven by distinct subsets of *SPOP* missense mutations, potentially through identification of SPOP protein binding partners that are differentially expressed in prostate and endometrial tissues.

Second, SPOP interactions with these newly identified protein binding partners could be evaluated for function, as this will likely enhance our understanding of SPOP-mediated biology and tumorigenesis in different cellular contexts. Among the new SPOP binding partners we have identified, several may be of particular interest because their known cellular functions are related to observations of SPOP-mediated biology for which no clear molecular mechanisms have been established. In this regard, two potential directions for this future work are especially salient. One direction is related to SPOP function in DNA repair: SPOP F133V missense mutation in prostate cells is associated with impaired homology-directed repair (HDR) and promotion of non-homologous end joining (NHEJ) of DNA double strand breaks (DSB), and furthermore induces cellular transcriptional responses that resemble those caused by *BRCA1* inactivation (98). A recent study also indicated that overexpression of SPOP F133V, but not SPOP WT or SPOP Y87C, resulted in reduced protein levels of H2AX and MRE11 and an increased ratio of γH2AX:H2AX (193). Genomic instability promoted by *SPOP* transcriptional downregulation and SPOP F133V missense mutation furthermore corelates with enhanced sensitivity to ionizing radiation and small molecule inhibitors of DNA repair such as PARP inhibitors (98; 226; 259; 260). Our detection of SPOP interactions with DNA repair-related protein MRE11, and

specifically F133V-mutation enhanced interaction, could provide a direct mechanistic link for these observations. SPOP WT may normally function to regulate MRE11 protein abundance and/or function within MRE11-RAD50-NBS1 (MRN) DNA repair complexes. Because MRN complexes promote HDR of DSBs, SPOP F133V-enhanced binding to, and potentially ubiquitin-mediated degradation of, MRE11 could directly impair HDR in a manner that explains SPOP F133V-mediated genomic instability in these previous studies. Work to characterize the effects of the SPOP-MRE11 interaction on HDR, and specifically to evaluate potential SPOP-mediated ubiquitination and degradation of MRE11, could thus provide a novel mechanism for SPOP regulation of DNA DSB repair.

Another particularly interesting direction for future functional evaluation of SPOP binding partners could be examination of SPOP effects on HIFα pathway-associated proteins in prostate cells, which has not been extensively explored previously. SPOP has previously been characterized to be involved in hypoxia and HIFα-related pathways (though most of these studies have focused on renal cells specifically): *SPOP* transcription is promoted by HIFα transcription factors, SPOP translocates to the cytoplasm from the nucleus under hypoxic conditions (where SPOP WT has been characterized to have a predominantly oncogenic function), and SPOP also binds to and degrades EGLN2, an oxygen-sensitive prolyl hydroxylase that activates HIFα transcriptional activity in response to cellular hypoxia (82; 151). We have detected two novel SPOP protein binding partners, VHL and ELOC, that play critical roles in regulating HIFα-mediated responses to cellular hypoxia. Both VHL and ELOC also demonstrate enhanced interaction with prostate cancer-associated SPOP missense mutants. Functionally, VHL and ELOC are both components of VHL-elongin B/elongin C-CUL2-RBX1 (VCB) E3 ubiquitin ligase complexes that play critical roles in regulating HIFα protein levels through ubiquitin-

mediated degradation. Much like SPOP, VHL functions as a substrate recognition subunit of these VCB complexes, and inherited or acquired deletions or mutations of *VHL* promote development of cancer (particularly ccRCC) through loss of VHL interaction with HIFαs (49; 237). SPOP WT overexpression and cytoplasmic subcellular localization are also strongly associated with ccRCC development through mechanisms that remain unclear. Our group's identification of both SPOP-VHL and SPOP-ELOC interactions suggest potential SPOP-mediated regulation of HIFα activity through direct modulation of VCB E3 complexes. If SPOP plays a role in degrading VHL and/or ELOC through ubiquitination, this could provide an explanation for why SPOP overexpression in renal cells promotes ccRCC development in a manner comparable with VHL mutation or deletion: elevated SPOP WT expression may potentially promote enhanced turnover of VHL and/or ELOC, leading to loss of VCB complex formation, loss of regulation of HIFαs, and uncontrolled HIFα promotion of hallmarks of cancer such as angiogenesis, cellular growth, and metastasis. SPOP prostate cancer mutation-enhanced interactions with VHL and ELOC could similarly promote aberrant VHL/ELOC degradation to enable aberrantly elevated HIFα transcriptional activity, which could also enhance HIFα-mediated cancer hallmarks in SPOP-mutant prostate tumors. Thus, further work to characterize SPOP-VHL and SPOP-ELOC interactions, in both renal and prostate cells, could yield critical insights into how SPOP influences cellular response to hypoxia in a manner that may promote cancer development and progression.

Third, the effects of SPOP F133L-c-Jun interactions on cellular characteristics and behaviors associated with the hallmarks of cancer (3; 4) could be explored to further validate the SPOP F133L-c-Jun interaction as a mechanism of SPOP F133L-mediated oncogenesis in prostate tumors. Chapter 2 of this dissertation presents data that suggest that SPOP variants

promote c-Jun protein stabilization and transcriptional activity. C-Jun overexpression and overactivation has been characterized to promote several cellular capabilities associated with cancer hallmarks, including cell proliferation, migration, tissue invasion and metastasis, angiogenesis, and drug resistance (196; 242). C-Jun overexpression itself is not sufficient to initiate tumor development, however, and has been characterized the require the activation of additional oncogenes, such as Ras and Src, to enable cellular transformation. Prostate cancer-associated SPOP missense mutants, such as Y87C, F102C, F133L, and F133V, have similarly been characterized to enable oncogenic characteristics in immortalized, patient-derived prostate cancer cell lines in combination with other activated oncogenes (115; 116; 118; 121), but they appear to produce no significant changes in prostate gland organization and histology, cell proliferation, and androgen receptor activity in the absence of other cancer-driving gene alterations (e.g., *PTEN* deletion) in mouse models (85). Additionally, although SPOP WT has been characterized to have an overall tumor suppressive function in prostate cells, the nuances of SPOP WT and SPOP missense mutant function in the absence of other cancer-driving genetic alterations remain unclear. Published research work to characterize SPOP's tumor suppressor function in immortalized prostate cell lines has centered largely on genetic approaches to knock down or knock out *SPOP* (83; 118), rather than to ectopically overexpress SPOP WT or SPOP missense mutants (where missense mutants have been characterized to have a dominant-negative effect toward SPOP WT function (116-118)). Because *SPOP* typically experiences heterozygous missense mutation, rather than homozygous mutation, homozygous deletion, or transcriptional downregulation, in prostate tumors, these prior approaches that knockdown or knockout *SPOP* may not accurately capture aspects of SPOP function (and dysfunction) relevant to SPOP-mutant prostate tumor biology. Furthermore, no studies to date have identified significant functional

differences between different prostate cancer-associated SPOP missense mutants. It thus currently remains unclear what specific cellular characteristics of oncogenic transformation may be enabled by SPOP missense mutants in isolation, and whether there are any functional differences between SPOP missense mutants in terms of their effects on cellular behavior. During my dissertation research work, I sought to identify unique characteristics of SPOP F133L/V mutation-induced cellular transformation through ectopic overexpression of SPOP WT, Y87C, F102C, F133L, and F133V in immortalized, patient-derived prostate cancer cell lines (22Rv1, C4-2, DU145, PC-3), with a goal of identifying characteristics that could be linked back to characteristics of elevated c-Jun activity (Appendix). I was unable to detect any characteristics of cellular transformation unique to SPOP F133L/V overexpression under the conditions I tested, although my approaches could likely be further optimized: *SPOP* expression level and length of time could be modified; different prostate cell lines that more closely resemble the normal prostate epithelial cell environment in which SPOP mutations occur (e.g., untransformed, primary prostate epithelial cells) could be tested; and mutant SPOP and c-Jun could be ectopically co-expressed with other activated oncogenes that commonly drive prostate tumorigenesis. Future work will thus be required to determine how SPOP F133L/V-mediated stabilization of c-Jun protein levels may contribute to characteristics of cellular transformation in prostate tumor cells.

Fourth, an expanded uHTS TR-FRET screen with a larger, more diverse collection of small molecules could be performed to further identify small molecule inducers of SPOP-BRD4 (and, more broadly, SPOP-substrate interactions), and to potentially identify selective small molecule inducers of *mutant* SPOP-BRD4 interactions. While the research work described in chapter 3 of this dissertation identified two potential small molecule inducers of SPOP-BRD4

interactions, these small molecules appeared to induce BRD4 interactions with both SPOP WT and SPOP F133V. The goal of future work will be to identify small molecules that can selectively re-induce PPIs for *mutant* SPOP, which represents a tumor-specific molecular target in SPOP-mutant prostate tumors. To identify small molecules that selectively induce missense mutant-SPOP PPIs, it will likely be necessary to identify small molecules that can bind specifically to mutant SPOP itself (and not SPOP WT) and restore SPOP function. Identification of such small molecules is likely challenging but possible, as missense mutations in the SPOP MATH domain, such as F133V, minimally perturb the overall tertiary structure of the MATH domain (72; 189). Small molecule binders to SPOP F133V could thus conceivably act orthosterically at the site of the preserved SPOP substrate binding cleft as a molecular glue (261) that directly participates in and mediates intermolecular interactions between SPOP F133V and BRD4, or could alternatively bind to mutant SPOP allosterically to remotely promote perturbations in the SPOP substrate binding cleft that bolster the interaction interface with BRD4. Because SPOP binds to BET proteins such as BRD4 through recognition of SBCs that are linear, continuous peptide sequences, an alternative approach to identify small molecules that selectively restore SPOP F133V interaction with BRD4 could be to use fluorescence polarization (FP) methodology with the SPOP F133V MATH domain as the receptor and a BRD4 SBC peptide sequence as a fluorophore-tagged tracer. After identification of any such selective small molecule inducers of SPOP F133V-BRD4 interactions through these or other approaches, subsequent work will be required to determine whether these small molecules are able to re-induce SPOP F133V interactions with other SPOP substrates beyond BRD4, whether small molecule restoration of SPOP F133V-BRD4 interactions re-enables SPOP-mediated

ubiquitination and degradation of BRD4, and whether restoration of SPOP F133V-BRD4 interactions effectively inhibits BRD4-driven characteristics of oncogenesis.

Figure 4.1. cBioPortal OncoPrint for genetic alterations in *SPOP* and genes encoding identified SPOP binding partners in prostate adenocarcinoma tumor samples (141; 142). The OncoPrint details the genetic alterations in tumors from a combination of three studies that collectively represent 2,977 prostate adenocarcinoma tumor samples (110; 113; 143). Notably, genetic alterations in genes encoding the SPOP binding partners identified in this dissertation do not exhibit significant mutual exclusivity or co-occurrence with *SPOP* genetic alterations.

Figure 4.1

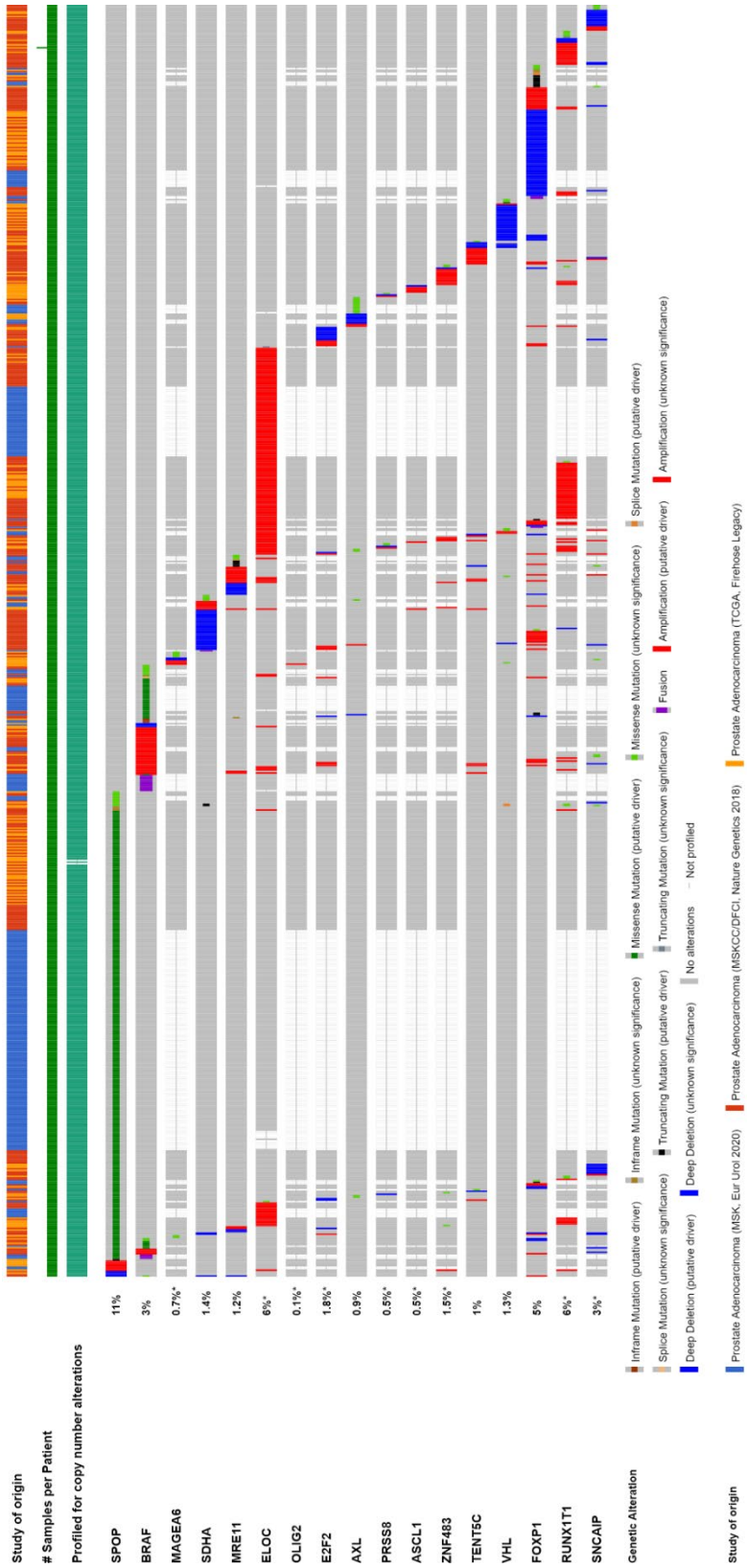
Study of origin
Samples per Patient
Profiled for copy number alterations
SPOP 11%
BRAF 3%
MAGEA6 0.7%*
SDHA 1.4%
MRE11 1.2%
ELOC 6%*
OLIG2 0.1%*
E2F2 1.8%*
AXL 0.9%
PRSS8 0.5%*
ASCL1 0.5%*
ZNF483 1.5%*
TENT5C 1%
VHL 1.3%
FOXP1 5%
RUNX1T1 6%*
SNCAIP 3%*
Genetic Alteration
Inframe Mutation (putative driver)
Inframe Mutation (unknown significance)
Missense Mutation (putative driver)
Missense Mutation (unknown significance)
Splice Mutation (putative driver)
Splice Mutation (unknown significance)
Truncating Mutation (putative driver)
Truncating Mutation (unknown significance)
Fusion
Amplification (putative driver)
Amplification (unknown significance)
Deep Deletion (putative driver)
Deep Deletion (unknown significance)
No alterations
Not profiled
Study of origin
Prostate Adenocarcinoma (MSK, Eur Urol 2020)
Prostate Adenocarcinoma (MSKCC/DFCI, Nature Genetics 2018)
Prostate Adenocarcinoma (TCGA, Firehose Legacy)
Samples per Patient
0
2
Profiled for copy number alterations
Yes
No

Figure 4.2. Evaluation of SPOP F133L effects on c-Jun/JNK1 interaction.

(a) GST pull down assay to examine competition between VF-JNK1 and V5-SPOP F133L for binding to GST-c-Jun. Cell lysates with co-expression of GST-c-Jun with (1) VF-JNK1 alone, (2) V5-SPOP F133L, or (3) VF-JNK1 and V5-SPOP F133L were prepared, and GST-c-Jun protein complexes were captured by glutathione resin to probe presence of VF-JNK1 and/or V5-SPOP F133L. GST-c-Jun, VF-JNK1, and V5-SPOP F133L were detected by blotting with anti-GST, anti-FLAG, and anti-V5 antibodies, respectively (obtained as described in section 2.2). (b) Cell lysates with respective co-expressed proteins were prepared and incubated with Tb-conjugated anti-GST antibodies. TR-FRET was configured with Tb as FRET donor and Venus protein as FRET acceptor. Data represent means ± SD from three independent experiments. Data reflect subtraction of assay background signal, defined as TR-FRET background signal detected in non-interaction PPI control consisting of GST-c-Jun plus Venus-FLAG empty vector (equivalent to background signal from control wells with no GST-/Venus-protein expression).

Figure 4.2

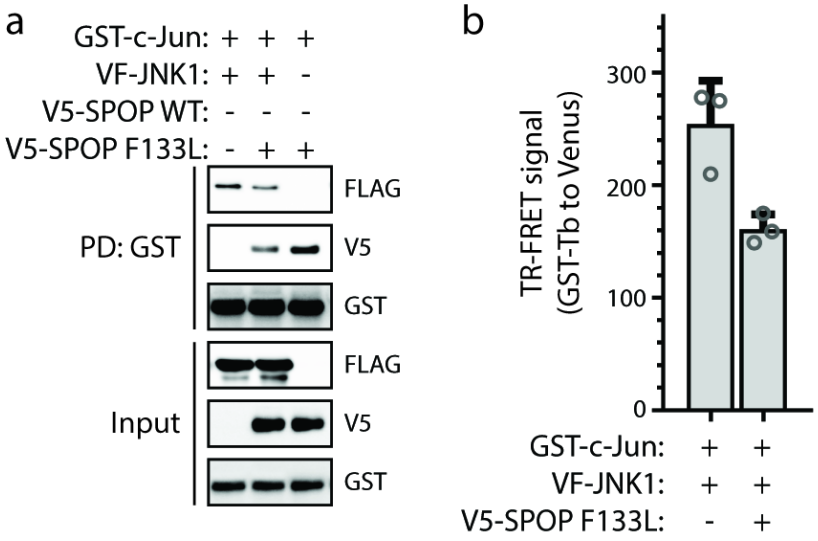
a
GST-c-Jun: + + +
VF-JNK1: + + -
V5-SPOP WT: - - -
V5-SPOP F133L: - + +
PD: GST
FLAG
V5
GST
Input
FLAG
V5
GST
b
TR-FRET signal
(GST-Tb to Venus)
300
200
100
0
GST-c-Jun: + +
VF-JNK1: + +
V5-SPOP F133L: - +

Figure 4.3. Proposed model for SPOP mutation-mediated mechanisms of oncogenesis in prostate adenocarcinoma. SPOP functions as a tumor suppressor in prostate epithelial cells by targeting oncogenic proteins, such as AR, SRC3, and BRD4, for ubiquitin-mediated degradation (left side of figure). SPOP missense mutations induce loss of SPOP interaction with oncogenic substrates, which leads to their aberrant accumulation (middle of figure). High levels of these oncogenic proteins then enable tumor-promoting programs in prostate epithelial cells by upregulating AR and PI3K/Akt cell signaling pathways. The results in this dissertation reveal an additional mechanism by which SPOP may promote oncogenic transformation in prostate epithelial cells: through SPOP F133L/V missense mutation-induced *gain of interaction* with oncogenic transcription factor c-Jun (right side of figure). SPOP F133L/V interacts with c-Jun to promote c-Jun protein stability and c-Jun/AP-1 transcriptional activity. Enhanced c-Jun expression and activation in prostate cancer cells has previously been associated with tumor castration resistance, tumor metastasis, and tumor recurrence (196). Elevated c-Jun protein activity may synergize with AR- and PI3K/Akt-driven oncogenic programs to uniquely promote oncogenesis in SPOP F133L/V mutation-driven prostate tumors.

Figure 4.3

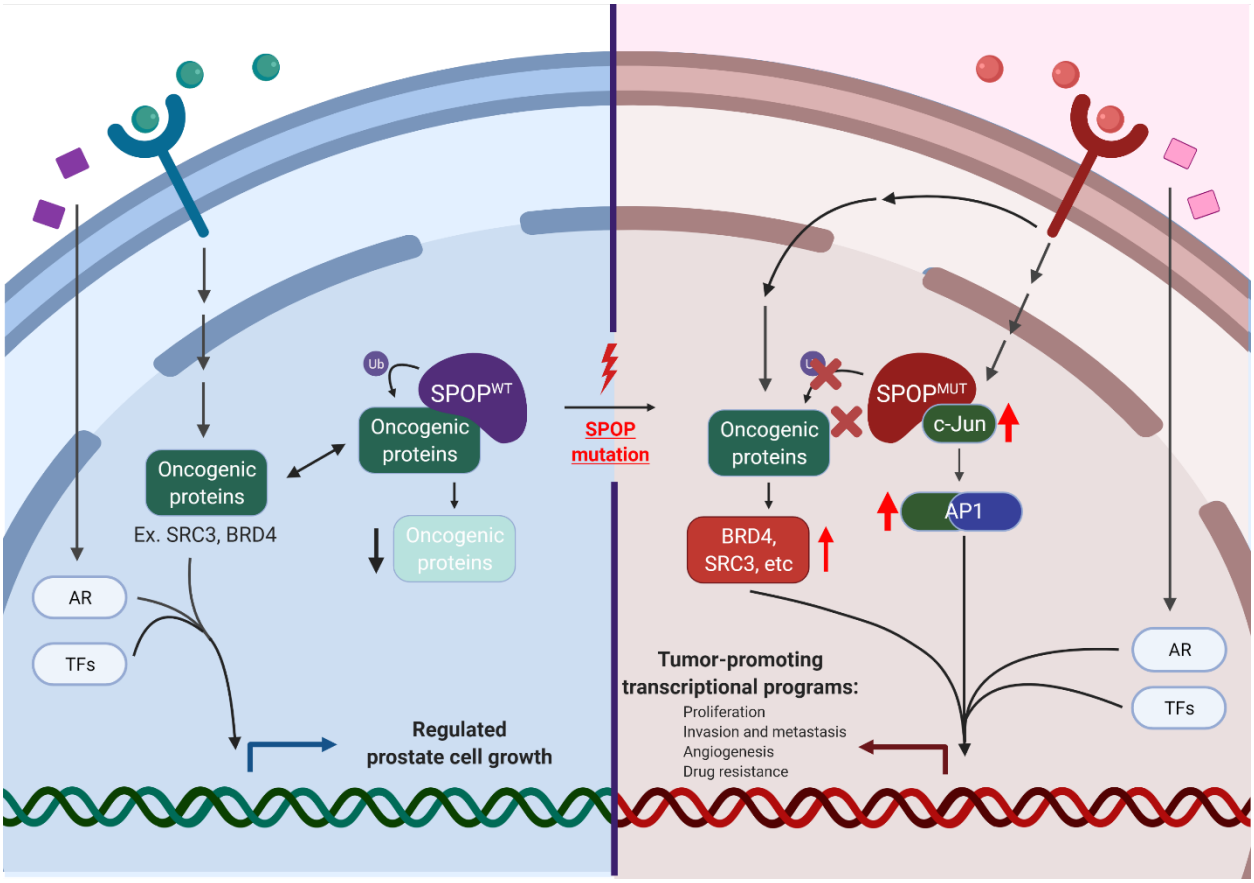
Ub
SPOP^WT
Oncogenic proteins
Oncogenic proteins
Ex. SRC3, BRD4
Oncogenic proteins
AR
TFs
Regulated prostate cell growth
SPOP mutation
Ub
SPOP^MUT
c-Jun
Oncogenic proteins
AP1
BRD4, SRC3, etc
Tumor-promoting transcriptional programs:
Proliferation
Invasion and metastasis
Angiogenesis
Drug resistance
AR
TFs

Figure 4.4. Proposed model for small molecule restoration of mutant SPOP interactions with oncogenic proteins such as BRD4 to reverse SPOP mutation-mediated oncogenesis. SPOP functions through its interactions with other proteins, and SPOP missense mutations abrogate SPOP function by inhibiting SPOP's interactions with other proteins. One potential strategy to restore missense mutant-SPOP function may be to re-induce mutant SPOP's lost interactions with its substrate proteins. The data presented in this dissertation demonstrate that it is feasible to identify small molecule inducers of SPOP F133V-BRD4 interactions. Such small molecule restorers of mutant SPOP protein-protein interactions may a represent novel, selective therapeutic strategy to reverse SPOP mutant-mediated mechanisms of oncogenesis in prostate tumors driven by SPOP mutation.

Figure 4.4

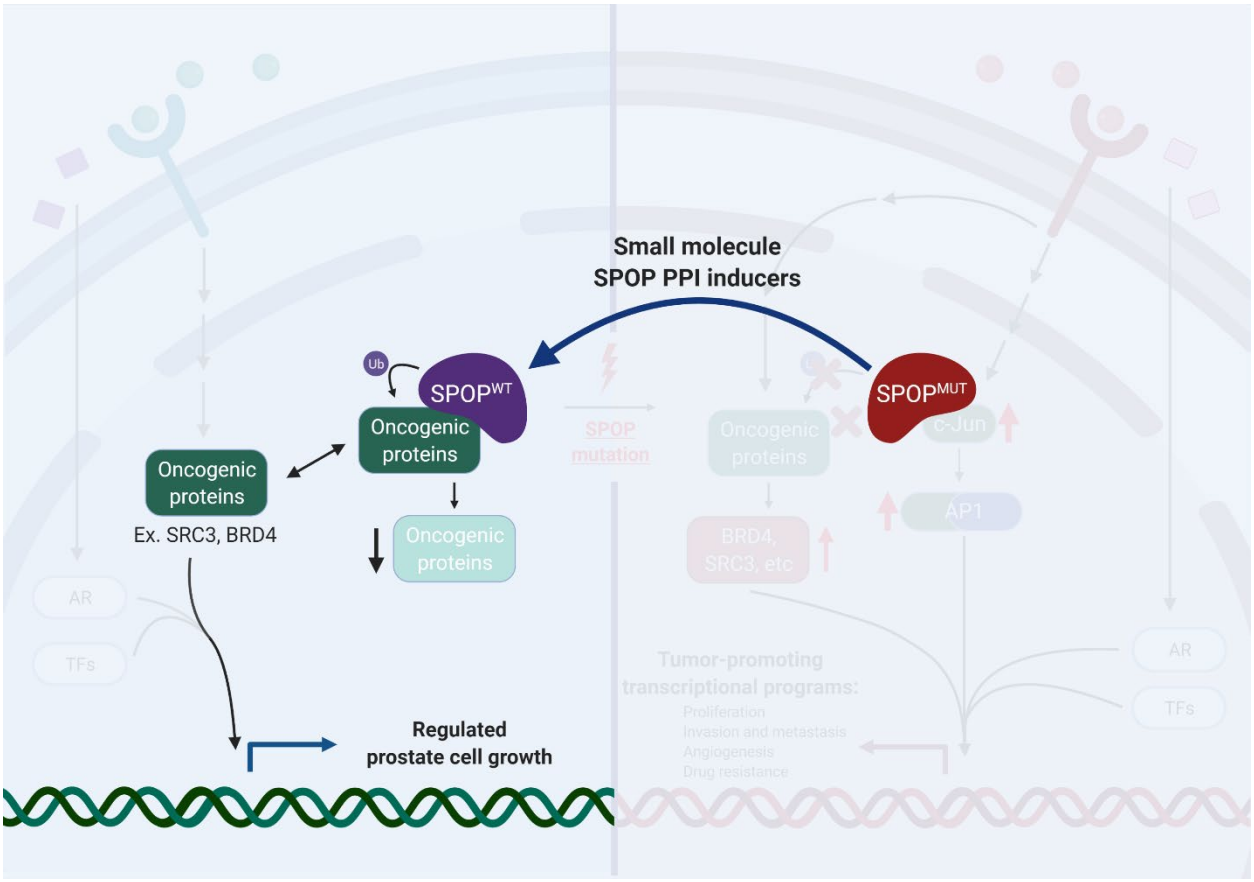
Small molecule
SPOP PPI inducers
Ub
SPOP^WT
Oncogenic proteins
Oncogenic proteins
Ex. SRC3, BRD4
Oncogenic proteins
Regulated prostate cell growth
SPOP^MUT
SPOP mutation
Oncogenic proteins
c-Jun
AP1
BRD4, SRC3, etc
AR
TFs
Tumor-promoting transcriptional programs:
Proliferation
Invasion and metastasis
Angiogenesis
Drug resistance
AR
TFs

REFERENCES

1. Xu JQ, Murphy SL, Kochanek KD, Arias E. 2020. Mortality in the United States, 2018, National Center for Health Statistics, Hyattsville, MD
2. Ruddon RW. 2007. *Cancer Biology*. Oxford University Press
3. Hanahan D, Weinberg RA. 2000. The hallmarks of cancer. *Cell* 100:57-70
4. Hanahan D, Weinberg RA. 2011. Hallmarks of cancer: the next generation. *Cell* 144:646-74
5. Alberts B. 2002. *Molecular biology of the cell*. New York: New York : Garland Science
6. Barabasi AL, Gulbahce N, Loscalzo J. 2011. Network medicine: a network-based approach to human disease. *Nat Rev Genet* 12:56-68
7. Fodde R, Smits R, Clevers H. 2001. APC, signal transduction and genetic instability in colorectal cancer. *Nat Rev Cancer* 1:55-67
8. Cancer Genome Atlas N. 2012. Comprehensive molecular characterization of human colon and rectal cancer. *Nature* 487:330-7
9. Amberger J, Bocchini CA, Scott AF, Hamosh A. 2009. McKusick's Online Mendelian Inheritance in Man (OMIM). *Nucleic Acids Res* 37:D793-6
10. Wachi S, Yoneda K, Wu R. 2005. Interactome-transcriptome analysis reveals the high centrality of genes differentially expressed in lung cancer tissues. *Bioinformatics* 21:4205-8
11. Jonsson PF, Bates PA. 2006. Global topological features of cancer proteins in the human interactome. *Bioinformatics* 22:2291-7
12. Goh KI, Cusick ME, Valle D, Childs B, Vidal M, Barabasi AL. 2007. The human disease network. *Proc Natl Acad Sci U S A* 104:8685-90

13. Oti M, Snel B, Huynen MA, Brunner HG. 2006. Predicting disease genes using protein-protein interactions. *J Med Genet* 43:691-8

14. Ivanov AA, Khuri FR, Fu H. 2013. Targeting protein-protein interactions as an anticancer strategy. *Trends Pharmacol Sci* 34:393-400

15. Huttlin EL, Bruckner RJ, Paulo JA, Cannon JR, Ting L, et al. 2017. Architecture of the human interactome defines protein communities and disease networks. *Nature* 545:505-9

16. Luck K, Kim DK, Lambourne L, Spirohn K, Begg BE, et al. 2020. A reference map of the human binary protein interactome. *Nature* 580:402-8

17. Li Z, Ivanov AA, Su R, Gonzalez-Pecchi V, Qi Q, et al. 2017. The OncoPPi network of cancer-focused protein-protein interactions to inform biological insights and therapeutic strategies. *Nat Commun* 8:14356

18. Taylor IW, Linding R, Warde-Farley D, Liu Y, Pesquita C, et al. 2009. Dynamic modularity in protein interaction networks predicts breast cancer outcome. *Nat Biotechnol* 27:199-204

19. Hein MY, Hubner NC, Poser I, Cox J, Nagaraj N, et al. 2015. A human interactome in three quantitative dimensions organized by stoichiometries and abundances. *Cell* 163:712-23

20. Huttlin EL, Ting L, Bruckner RJ, Gebreab F, Gygi MP, et al. 2015. The BioPlex Network: A Systematic Exploration of the Human Interactome. *Cell* 162:425-40

21. Schulman BA, Harper JW. 2009. Ubiquitin-like protein activation by E1 enzymes: the apex for downstream signalling pathways. *Nat Rev Mol Cell Biol* 10:319-31

22. Ye Y, Rape M. 2009. Building ubiquitin chains: E2 enzymes at work. *Nat Rev Mol Cell Biol* 10:755-64

23. Deshaies RJ, Joazeiro CA. 2009. RING domain E3 ubiquitin ligases. *Annu Rev Biochem* 78:399-434

24. Mattiroli F, Sixma TK. 2014. Lysine-targeting specificity in ubiquitin and ubiquitin-like modification pathways. *Nat Struct Mol Biol* 21:308-16

25. Swatek KN, Komander D. 2016. Ubiquitin modifications. *Cell Res* 26:399-422

26. Yau R, Rape M. 2016. The increasing complexity of the ubiquitin code. *Nat Cell Biol* 18:579-86

27. Chau V, Tobias JW, Bachmair A, Marriott D, Ecker DJ, et al. 1989. A multiubiquitin chain is confined to specific lysine in a targeted short-lived protein. *Science* 243:1576-83

28. Scheffner M, Huibregtse JM, Vierstra RD, Howley PM. 1993. The HPV-16 E6 and E6-AP complex functions as a ubiquitin-protein ligase in the ubiquitination of p53. *Cell* 75:495-505

29. Petroski MD, Deshaies RJ. 2005. Mechanism of lysine 48-linked ubiquitin-chain synthesis by the cullin-RING ubiquitin-ligase complex SCF-Cdc34. *Cell* 123:1107-20

30. Chen B, Mariano J, Tsai YC, Chan AH, Cohen M, Weissman AM. 2006. The activity of a human endoplasmic reticulum-associated degradation E3, gp78, requires its Cue domain, RING finger, and an E2-binding site. *Proc Natl Acad Sci U S A* 103:341-6

31. Deng L, Wang C, Spencer E, Yang L, Braun A, et al. 2000. Activation of the IkappaB kinase complex by TRAF6 requires a dimeric ubiquitin-conjugating enzyme complex and a unique polyubiquitin chain. *Cell* 103:351-61

32. Wang C, Deng L, Hong M, Akkaraju GR, Inoue J, Chen ZJ. 2001. TAK1 is a ubiquitin-dependent kinase of MKK and IKK. *Nature* 412:346-51

33. Xu M, Skaug B, Zeng W, Chen ZJ. 2009. A ubiquitin replacement strategy in human cells reveals distinct mechanisms of IKK activation by TNFalpha and IL-1beta. *Mol Cell* 36:302-14

34. Doil C, Mailand N, Bekker-Jensen S, Menard P, Larsen DH, et al. 2009. RNF168 binds and amplifies ubiquitin conjugates on damaged chromosomes to allow accumulation of repair proteins. *Cell* 136:435-46

35. Stewart GS, Panier S, Townsend K, Al-Hakim AK, Kolas NK, et al. 2009. The RIDDLE syndrome protein mediates a ubiquitin-dependent signaling cascade at sites of DNA damage. *Cell* 136:420-34

36. Song EJ, Werner SL, Neubauer J, Stegmeier F, Aspden J, et al. 2010. The Prp19 complex and the Usp4Sart3 deubiquitinating enzyme control reversible ubiquitination at the spliceosome. *Genes Dev* 24:1434-47

37. Liu P, Gan W, Su S, Hauenstein AV, Fu TM, et al. 2018. K63-linked polyubiquitin chains bind to DNA to facilitate DNA damage repair. *Sci Signal* 11

38. Buetow L, Huang DT. 2016. Structural insights into the catalysis and regulation of E3 ubiquitin ligases. *Nat Rev Mol Cell Biol* 17:626-42

39. Li W, Bengtson MH, Ulbrich A, Matsuda A, Reddy VA, et al. 2008. Genome-wide and functional annotation of human E3 ubiquitin ligases identifies MULAN, a mitochondrial E3 that regulates the organelle's dynamics and signaling. *PLoS One* 3:e1487

40. Kumari N, Jaynes PW, Saei A, Iyengar PV, Richard JLC, Eichhorn PJA. 2017. The roles of ubiquitin modifying enzymes in neoplastic disease. *Biochim Biophys Acta Rev Cancer* 1868:456-83

41. Maxwell PH, Wiesener MS, Chang GW, Clifford SC, Vaux EC, et al. 1999. The tumour suppressor protein VHL targets hypoxia-inducible factors for oxygen-dependent proteolysis. *Nature* 399:271-5

42. Hon WC, Wilson MI, Harlos K, Claridge TD, Schofield CJ, et al. 2002. Structural basis for the recognition of hydroxyproline in HIF-1 alpha by pVHL. *Nature* 417:975-8

43. Min JH, Yang H, Ivan M, Gertler F, Kaelin WG, Jr., Pavletich NP. 2002. Structure of an HIF-1alpha -pVHL complex: hydroxyproline recognition in signaling. *Science* 296:1886-9

44. Chen F, Kishida T, Yao M, Hustad T, Glavac D, et al. 1995. Germline mutations in the von Hippel-Lindau disease tumor suppressor gene: correlations with phenotype. *Hum Mutat* 5:66-75

45. Hoffman MA, Ohh M, Yang H, Klco JM, Ivan M, Kaelin WG, Jr. 2001. von Hippel-Lindau protein mutants linked to type 2C VHL disease preserve the ability to downregulate HIF. *Hum Mol Genet* 10:1019-27

46. Zbar B, Brauch H, Talmadge C, Linehan M. 1987. Loss of alleles of loci on the short arm of chromosome 3 in renal cell carcinoma. *Nature* 327:721-4

47. Iliopoulos O, Kibel A, Gray S, Kaelin WG, Jr. 1995. Tumour suppression by the human von Hippel-Lindau gene product. *Nat Med* 1:822-6

48. Foster K, Prowse A, van den Berg A, Fleming S, Hulsbeek MM, et al. 1994. Somatic mutations of the von Hippel-Lindau disease tumour suppressor gene in non-familial clear cell renal carcinoma. *Hum Mol Genet* 3:2169-73

49. Gnarra JR, Tory K, Weng Y, Schmidt L, Wei MH, et al. 1994. Mutations of the VHL tumour suppressor gene in renal carcinoma. *Nat Genet* 7:85-90

50. Whaley JM, Naglich J, Gelbert L, Hsia YE, Lamiell JM, et al. 1994. Germ-line mutations in the von Hippel-Lindau tumor-suppressor gene are similar to somatic von Hippel-Lindau aberrations in sporadic renal cell carcinoma. *Am J Hum Genet* 55:1092-102

51. Knauth K, Bex C, Jemth P, Buchberger A. 2006. Renal cell carcinoma risk in type 2 von Hippel-Lindau disease correlates with defects in pVHL stability and HIF-1alpha interactions. *Oncogene* 25:370-7

52. Clifford SC, Cockman ME, Smallwood AC, Mole DR, Woodward ER, et al. 2001. Contrasting effects on HIF-1alpha regulation by disease-causing pVHL mutations correlate with patterns of tumourigenesis in von Hippel-Lindau disease. *Hum Mol Genet* 10:1029-38

53. Li L, Zhang L, Zhang X, Yan Q, Minamishima YA, et al. 2007. Hypoxia-inducible factor linked to differential kidney cancer risk seen with type 2A and type 2B VHL mutations. *Mol Cell Biol* 27:5381-92

54. Rankin EB, Rha J, Unger TL, Wu CH, Shutt HP, et al. 2008. Hypoxia-inducible factor-2 regulates vascular tumorigenesis in mice. *Oncogene* 27:5354-8

55. Kondo K, Klco J, Nakamura E, Lechpammer M, Kaelin WG, Jr. 2002. Inhibition of HIF is necessary for tumor suppression by the von Hippel-Lindau protein. *Cancer Cell* 1:237-46

56. Kondo K, Kim WY, Lechpammer M, Kaelin WG, Jr. 2003. Inhibition of HIF2alpha is sufficient to suppress pVHL-defective tumor growth. *PLoS Biol* 1:E83

57. Zimmer M, Doucette D, Siddiqui N, Iliopoulos O. 2004. Inhibition of hypoxia-inducible factor is sufficient for growth suppression of VHL-/- tumors. *Mol Cancer Res* 2:89-95

58. Momand J, Zambetti GP, Olson DC, George D, Levine AJ. 1992. The mdm-2 oncogene product forms a complex with the p53 protein and inhibits p53-mediated transactivation. *Cell* 69:1237-45

59. Oliner JD, Pietenpol JA, Thiagalingam S, Gyuris J, Kinzler KW, Vogelstein B. 1993. Oncoprotein MDM2 conceals the activation domain of tumour suppressor p53. *Nature* 362:857-60

60. Haupt Y, Maya R, Kazaz A, Oren M. 1997. Mdm2 promotes the rapid degradation of p53. *Nature* 387:296-9

61. Honda R, Tanaka H, Yasuda H. 1997. Oncoprotein MDM2 is a ubiquitin ligase E3 for tumor suppressor p53. *FEBS Lett* 420:25-7

62. Kubbutat MH, Jones SN, Vousden KH. 1997. Regulation of p53 stability by Mdm2. *Nature* 387:299-303

63. Oliner JD, Kinzler KW, Meltzer PS, George DL, Vogelstein B. 1992. Amplification of a gene encoding a p53-associated protein in human sarcomas. *Nature* 358:80-3

64. Momand J, Jung D, Wilczynski S, Niland J. 1998. The MDM2 gene amplification database. *Nucleic Acids Res* 26:3453-9

65. Nagai Y, Kojima T, Muro Y, Hachiya T, Nishizawa Y, et al. 1997. Identification of a novel nuclear speckle-type protein, SPOP. *FEBS Lett* 418:23-6

66. Furukawa M, He YJ, Borchers C, Xiong Y. 2003. Targeting of protein ubiquitination by BTB-Cullin 3-Roc1 ubiquitin ligases. *Nat Cell Biol* 5:1001-7

67. Hernandez-Munoz I, Lund AH, van der Stoop P, Boutsma E, Muijrers I, et al. 2005. Stable X chromosome inactivation involves the PRC1 Polycomb complex and requires

histone MACROH2A1 and the CULLIN3/SPOP ubiquitin E3 ligase. *Proc Natl Acad Sci U S A* 102:7635-40

68. Kwon JE, La M, Oh KH, Oh YM, Kim GR, et al. 2006. BTB domain-containing speckle-type POZ protein (SPOP) serves as an adaptor of Daxx for ubiquitination by Cul3-based ubiquitin ligase. *J Biol Chem* 281:12664-72

69. Kent D, Bush EW, Hooper JE. 2006. Roadkill attenuates Hedgehog responses through degradation of Cubitus interruptus. *Development* 133:2001-10

70. Zhang Q, Zhang L, Wang B, Ou CY, Chien CT, Jiang J. 2006. A hedgehog-induced BTB protein modulates hedgehog signaling by degrading Ci/Gli transcription factor. *Dev Cell* 10:719-29

71. Liu J, Ghanim M, Xue L, Brown CD, Iossifov I, et al. 2009. Analysis of Drosophila segmentation network identifies a JNK pathway factor overexpressed in kidney cancer. *Science* 323:1218-22

72. Zhuang M, Calabrese MF, Liu J, Waddell MB, Nourse A, et al. 2009. Structures of SPOP-substrate complexes: insights into molecular architectures of BTB-Cul3 ubiquitin ligases. *Mol Cell* 36:39-50

73. Ostertag MS, Messias AC, Sattler M, Popowicz GM. 2019. The Structure of the SPOP-Pdx1 Interface Reveals Insights into the Phosphorylation-Dependent Binding Regulation. *Structure* 27:327-34 e3

74. Wang X, Jin J, Wan F, Zhao L, Chu H, et al. 2019. AMPK Promotes SPOP-Mediated NANOG Degradation to Regulate Prostate Cancer Cell Stemness. *Dev Cell* 48:345-60 e7

75. Errington WJ, Khan MQ, Bueler SA, Rubinstein JL, Chakrabartty A, Prive GG. 2012. Adaptor protein self-assembly drives the control of a cullin-RING ubiquitin ligase. *Structure* 20:1141-53

76. van Geersdaele LK, Stead MA, Harrison CM, Carr SB, Close HJ, et al. 2013. Structural basis of high-order oligomerization of the cullin-3 adaptor SPOP. *Acta Crystallogr D Biol Crystallogr* 69:1677-84

77. Pierce WK, Grace CR, Lee J, Nourse A, Marzahn MR, et al. 2016. Multiple Weak Linear Motifs Enhance Recruitment and Processivity in SPOP-Mediated Substrate Ubiquitination. *J Mol Biol* 428:1256-71

78. Marzahn MR, Marada S, Lee J, Nourse A, Kenrick S, et al. 2016. Higher-order oligomerization promotes localization of SPOP to liquid nuclear speckles. *EMBO J* 35:1254-75

79. Bouchard JJ, Otero JH, Scott DC, Szulc E, Martin EW, et al. 2018. Cancer Mutations of the Tumor Suppressor SPOP Disrupt the Formation of Active, Phase-Separated Compartments. *Mol Cell* 72:19-36 e8

80. Jin X, Shi Q, Li Q, Zhou L, Wang J, et al. 2020. CRL3-SPOP ubiquitin ligase complex suppresses the growth of diffuse large B-cell lymphoma by negatively regulating the MyD88/NF-kappaB signaling. *Leukemia* 34:1305-14

81. Jin X, Wang J, Gao K, Zhang P, Yao L, et al. 2017. Dysregulation of INF2-mediated mitochondrial fission in SPOP-mutated prostate cancer. *PLoS Genet* 13:e1006748

82. Li G, Ci W, Karmakar S, Chen K, Dhar R, et al. 2014. SPOP promotes tumorigenesis by acting as a key regulatory hub in kidney cancer. *Cancer Cell* 25:455-68

83. Geng C, Kaochar S, Li M, Rajapakshe K, Fiskus W, et al. 2017. SPOP regulates prostate epithelial cell proliferation and promotes ubiquitination and turnover of c-MYC oncoprotein. *Oncogene* 36:4767-77

84. Ju LG, Zhu Y, Long QY, Li XJ, Lin X, et al. 2019. SPOP suppresses prostate cancer through regulation of CYCLIN E1 stability. *Cell Death Differ* 26:1156-68

85. Blattner M, Liu D, Robinson BD, Huang D, Poliakov A, et al. 2017. SPOP Mutation Drives Prostate Tumorigenesis In Vivo through Coordinate Regulation of PI3K/mTOR and AR Signaling. *Cancer Cell* 31:436-51

86. Zhi X, Tao J, Zhang L, Tao R, Ma L, Qin J. 2016. Silencing speckle-type POZ protein by promoter hypermethylation decreases cell apoptosis through upregulating Hedgehog signaling pathway in colorectal cancer. *Cell Death Dis* 7:e2569

87. Pachkov M, Balwierz PJ, Arnold P, Ozonov E, van Nimwegen E. 2013. SwissRegulon, a database of genome-wide annotations of regulatory sites: recent updates. *Nucleic Acids Res* 41:D214-20

88. Huang CJ, Chen HY, Lin WY, Choo KB. 2014. Differential expression of speckled POZ protein, SPOP: putative regulation by miR-145. *J Biosci* 39:401-13

89. Xu J, Wang F, Wang X, He Z, Zhu X. 2018. miRNA-543 promotes cell migration and invasion by targeting SPOP in gastric cancer. *Onco Targets Ther* 11:5075-82

90. Ding M, Lu X, Wang C, Zhao Q, Ge J, et al. 2018. The E2F1-miR-520/372/373-SPOP Axis Modulates Progression of Renal Carcinoma. *Cancer Res* 78:6771-84

91. Zhang J, Bu X, Wang H, Zhu Y, Geng Y, et al. 2018. Cyclin D-CDK4 kinase destabilizes PD-L1 via cullin 3-SPOP to control cancer immune surveillance. *Nature* 553:91-5

92. Johnson EO, Chang KH, de Pablo Y, Ghosh S, Mehta R, et al. 2011. PHLDA1 is a crucial negative regulator and effector of Aurora A kinase in breast cancer. *J Cell Sci* 124:2711-22

93. Nikhil K, Kamra M, Raza A, Haymour HS, Shah KV. 2020. Molecular Interplay between AURKA and SPOP Dictates CRPC Pathogenesis via Androgen Receptor. *Cancers* 12

94. Nikhil K, Haymour HS, Kamra M, Shah K. 2020. Phosphorylation-dependent regulation of SPOP by LIMK2 promotes castration-resistant prostate cancer. *Br J Cancer*

95. Garcia-Flores M, Casanova-Salas I, Rubio-Briones J, Calatrava A, Dominguez-Escrig J, et al. 2014. Clinico-pathological significance of the molecular alterations of the SPOP gene in prostate cancer. *Eur J Cancer* 50:2994-3002

96. Hernandez-Llodra S, Segales L, Safont A, Juanpere N, Lorenzo M, et al. 2019. SPOP and FOXA1 mutations are associated with PSA recurrence in ERG wt tumors, and SPOP downregulation with ERG-rearranged prostate cancer. *Prostate* 79:1156-65

97. Xu J, Wang F, Jiang H, Jiang Y, Chen J, Qin J. 2015. Properties and Clinical Relevance of Speckle-Type POZ Protein in Human Colorectal Cancer. *J Gastrointest Surg* 19:1484-96

98. Boysen G, Barbieri CE, Prandi D, Blattner M, Chae SS, et al. 2015. SPOP mutation leads to genomic instability in prostate cancer. *Elife* 4

99. Kim MS, Je EM, Oh JE, Yoo NJ, Lee SH. 2013. Mutational and expressional analyses of SPOP, a candidate tumor suppressor gene, in prostate, gastric and colorectal cancers. *APMIS* 121:626-33

100. Ding D, Song T, Jun W, Tan Z, Fang J. 2015. Decreased expression of the SPOP gene is associated with poor prognosis in glioma. *Int J Oncol* 46:333-41

101. Jia D, Dong R, Jing Y, Xu D, Wang Q, et al. 2014. Exome sequencing of hepatoblastoma reveals novel mutations and cancer genes in the Wnt pathway and ubiquitin ligase complex. *Hepatology* 60:1686-96

102. Huang Y, Tan N, Jia D, Jing Y, Wang Q, et al. 2015. Speckle-type POZ protein is negatively associated with malignancies and inhibits cell proliferation and migration in liver cancer. *Tumour Biol* 36:9753-61

103. Ji P, Liang S, Li P, Xie C, Li J, et al. 2018. Speckle-type POZ protein suppresses hepatocellular carcinoma cell migration and invasion via ubiquitin-dependent proteolysis of SUMO1/sentrin specific peptidase 7. *Biochem Biophys Res Commun* 502:30-42

104. Li Y, Yu Q, Li R, Luo J, Yuan D, et al. 2019. SPOP Regulates The Biological Mechanism Of Ovarian Cancer Cells Through The Hh Signaling Pathway. *Onco Targets Ther* 12:9239-48

105. Li JJ, Zhang JF, Yao SM, Huang H, Zhang S, et al. 2017. Decreased expression of speckle-type POZ protein for the prediction of poor prognosis in patients with non-small cell lung cancer. *Oncol Lett* 14:2743-8

106. Harb OA, Elfeky MA, El Shafaay BS, Taha HF, Osman G, et al. 2018. SPOP, ZEB-1 and E-cadherin expression in clear cell renal cell carcinoma (cc-RCC): Clinicopathological and prognostic significance. *Pathophysiology* 25:335-45

107. Li C, Ao J, Fu J, Lee DF, Xu J, et al. 2011. Tumor-suppressor role for the SPOP ubiquitin ligase in signal-dependent proteolysis of the oncogenic co-activator SRC-3/AIB1. *Oncogene* 30:4350-64

108. Hu X, Yang Z, Zeng M, Liu YI, Yang X, et al. 2016. Speckle-type POZ (pox virus and zinc finger protein) protein gene deletion in ovarian cancer: Fluorescence in situ hybridization analysis of a tissue microarray. *Oncol Lett* 12:658-62

109. Le Gallo M, O'Hara AJ, Rudd ML, Urick ME, Hansen NF, et al. 2012. Exome sequencing of serous endometrial tumors identifies recurrent somatic mutations in chromatin-remodeling and ubiquitin ligase complex genes. *Nat Genet* 44:1310-5

110. Cancer Genome Atlas Research N. 2015. The Molecular Taxonomy of Primary Prostate Cancer. *Cell* 163:1011-25

111. Barbieri CE, Baca SC, Lawrence MS, Demichelis F, Blattner M, et al. 2012. Exome sequencing identifies recurrent SPOP, FOXA1 and MED12 mutations in prostate cancer. *Nat Genet* 44:685-9

112. Blattner M, Lee DJ, O'Reilly C, Park K, MacDonald TY, et al. 2014. SPOP mutations in prostate cancer across demographically diverse patient cohorts. *Neoplasia* 16:14-20

113. Armenia J, Wankowicz SAM, Liu D, Gao J, Kundra R, et al. 2018. The long tail of oncogenic drivers in prostate cancer. *Nat Genet* 50:645-51

114. An J, Wang C, Deng Y, Yu L, Huang H. 2014. Destruction of full-length androgen receptor by wild-type SPOP, but not prostate-cancer-associated mutants. *Cell Rep* 6:657-69

115. Geng C, Rajapakshe K, Shah SS, Shou J, Eedunuri VK, et al. 2014. Androgen receptor is the key transcriptional mediator of the tumor suppressor SPOP in prostate cancer. *Cancer Res* 74:5631-43

116. Geng C, He B, Xu L, Barbieri CE, Eedunuri VK, et al. 2013. Prostate cancer-associated mutations in speckle-type POZ protein (SPOP) regulate steroid receptor coactivator 3 protein turnover. *Proc Natl Acad Sci U S A* 110:6997-7002

117. Groner AC, Cato L, de Tribolet-Hardy J, Bernasocchi T, Janouskova H, et al. 2016. TRIM24 Is an Oncogenic Transcriptional Activator in Prostate Cancer. *Cancer Cell* 29:846-58

118. Dai X, Gan W, Li X, Wang S, Zhang W, et al. 2017. Prostate cancer-associated SPOP mutations confer resistance to BET inhibitors through stabilization of BRD4. *Nat Med* 23:1063-71

119. Janouskova H, El Tekle G, Bellini E, Udeshi ND, Rinaldi A, et al. 2017. Opposing effects of cancer-type-specific SPOP mutants on BET protein degradation and sensitivity to BET inhibitors. *Nat Med* 23:1046-54

120. Zhang P, Wang D, Zhao Y, Ren S, Gao K, et al. 2017. Intrinsic BET inhibitor resistance in SPOP-mutated prostate cancer is mediated by BET protein stabilization and AKT-mTORC1 activation. *Nat Med* 23:1055-62

121. Theurillat JP, Udeshi ND, Errington WJ, Svinkina T, Baca SC, et al. 2014. Prostate cancer. Ubiquitylome analysis identifies dysregulation of effector substrates in SPOP-mutant prostate cancer. *Science* 346:85-9

122. Liu D, Takhar M, Alshalalfa M, Erho N, Shoag J, et al. 2018. Impact of the SPOP Mutant Subtype on the Interpretation of Clinical Parameters in Prostate Cancer. *JCO Precis Oncol* 2018

123. Shoag J, Liu D, Ma X, Oromendia C, Christos P, et al. 2020. Prognostic value of the SPOP mutant genomic subclass in prostate cancer. *Urol Oncol* 38:418-22

124. Fraser M, Sabelnykova VY, Yamaguchi TN, Heisler LE, Livingstone J, et al. 2017. Genomic hallmarks of localized, non-indolent prostate cancer. *Nature* 541:359-64

125. Robinson D, Van Allen EM, Wu YM, Schultz N, Lonigro RJ, et al. 2015. Integrative clinical genomics of advanced prostate cancer. *Cell* 161:1215-28

126. Attard G, Parker C, Eeles RA, Schroder F, Tomlins SA, et al. 2016. Prostate cancer. *Lancet* 387:70-82

127. Boysen G, Rodrigues DN, Rescigno P, Seed G, Dolling D, et al. 2018. SPOP-Mutated/CHD1-Deleted Lethal Prostate Cancer and Abiraterone Sensitivity. *Clin Cancer Res* 24:5585-93

128. Swami U, Isaacsson Velho P, Nussenzveig R, Chipman J, Sacristan Santos V, et al. 2020. Association of SPOP Mutations with Outcomes in Men with De Novo Metastatic Castration-sensitive Prostate Cancer. *Eur Urol* 78:652-6

129. Bernasocchi T, El Tekle G, Bolis M, Mutti A, Vallerga A, et al. 2021. Dual functions of SPOP and ERG dictate androgen therapy responses in prostate cancer. *Nat Commun* 12:734

130. Shi Q, Zhu Y, Ma J, Chang K, Ding D, et al. 2019. Prostate Cancer-associated SPOP mutations enhance cancer cell survival and docetaxel resistance by upregulating Caprin1-dependent stress granule assembly. *Mol Cancer* 18:170

131. El Bezawy R, Tripari M, Percio S, Cicchetti A, Tortoreto M, et al. 2020. SPOP Deregulation Improves the Radiation Response of Prostate Cancer Models by Impairing DNA Damage Repair. *Cancers (Basel)* 12

132. Guo ZQ, Zheng T, Chen B, Luo C, Ouyang S, et al. 2016. Small-Molecule Targeting of E3 Ligase Adaptor SPOP in Kidney Cancer. *Cancer Cell* 30:474-84

133. Dong Z, Wang Z, Guo ZQ, Gong S, Zhang T, et al. 2020. Structure-Activity Relationship of SPOP Inhibitors against Kidney Cancer. *J Med Chem* 63:4849-66

134. Huai Q, Kim HY, Liu Y, Zhao Y, Mondragon A, et al. 2002. Crystal structure of calcineurin-cyclophilin-cyclosporin shows common but distinct recognition of immunophilin-drug complexes. *Proc Natl Acad Sci U S A* 99:12037-42

135. Stahelin HF. 1996. The history of cyclosporin A (Sandimmune) revisited: another point of view. *Experientia* 52:5-13

136. Choi J, Chen J, Schreiber SL, Clardy J. 1996. Structure of the FKBP12-rapamycin complex interacting with the binding domain of human FRAP. *Science* 273:239-42

137. Li J, Kim SG, Blenis J. 2014. Rapamycin: one drug, many effects. *Cell Metab* 19:373-9

138. Schiff PB, Fant J, Horwitz SB. 1979. Promotion of microtubule assembly in vitro by taxol. *Nature* 277:665-7

139. Schiff PB, Horwitz SB. 1980. Taxol stabilizes microtubules in mouse fibroblast cells. *Proc Natl Acad Sci U S A* 77:1561-5

140. Tang C, Mo X, Niu Q, Wahafu A, Yang X, et al. 2020. Hypomorph Mutation-Directed Small-Molecule Protein-Protein Interaction Inducers to Restore Mutant SMAD4-Suppressed TGF-beta Signaling. *Cell Chem Biol*

141. Cerami E, Gao J, Dogrusoz U, Gross BE, Sumer SO, et al. 2012. The cBio cancer genomics portal: an open platform for exploring multidimensional cancer genomics data. *Cancer Discov* 2:401-4

142. Gao J, Aksoy BA, Dogrusoz U, Dresdner G, Gross B, et al. 2013. Integrative analysis of complex cancer genomics and clinical profiles using the cBioPortal. *Sci Signal* 6:pl1

143. Nguyen B, Mota JM, Nandakumar S, Stopsack KH, Weg E, et al. 2020. Pan-cancer Analysis of CDK12 Alterations Identifies a Subset of Prostate Cancers with Distinct Genomic and Clinical Characteristics. *Eur Urol* 78:671-9

144. Ma J, Chang K, Peng J, Shi Q, Gan H, et al. 2018. SPOP promotes ATF2 ubiquitination and degradation to suppress prostate cancer progression. *J Exp Clin Cancer Res* 37:145

145. Kim B, Nam HJ, Pyo KE, Jang MJ, Kim IS, et al. 2011. Breast cancer metastasis suppressor 1 (BRMS1) is destabilized by the Cul3-SPOP E3 ubiquitin ligase complex. *Biochem Biophys Res Commun* 415:720-6

146. Wu F, Dai X, Gan W, Wan L, Li M, et al. 2017. Prostate cancer-associated mutation in SPOP impairs its ability to target Cdc20 for poly-ubiquitination and degradation. *Cancer Lett* 385:207-14

147. La M, Kim K, Park J, Won J, Lee JH, et al. 2004. Daxx-mediated transcriptional repression of MMP1 gene is reversed by SPOP. *Biochem Biophys Res Commun* 320:760-5

148. Sakaue T, Sakakibara I, Uesugi T, Fujisaki A, Nakashiro KI, et al. 2017. The CUL3-SPOP-DAXX axis is a novel regulator of VEGFR2 expression in vascular endothelial cells. *Sci Rep* 7:42845

149. Zhang P, Gao K, Tang Y, Jin X, An J, et al. 2014. Destruction of DDIT3/CHOP protein by wild-type SPOP but not prostate cancer-associated mutants. *Hum Mutat* 35:1142-51

150. Yuan D, Chen Y, Yang Z, Li G, Wu M, et al. 2020. SPOP attenuates migration and invasion of choriocarcinoma cells by promoting DHX9 degradation. *Am J Cancer Res* 10:2428-45

151. Zhang L, Peng S, Dai X, Gan W, Nie X, et al. 2017. Tumor suppressor SPOP ubiquitinates and degrades EglN2 to compromise growth of prostate cancer cells. *Cancer Lett* 390:11-20

152. Zhang P, Gao K, Jin X, Ma J, Peng J, et al. 2015. Endometrial cancer-associated mutants of SPOP are defective in regulating estrogen receptor-alpha protein turnover. *Cell Death Dis* 6:e1687

153. An J, Ren S, Murphy SJ, Dalangood S, Chang C, et al. 2015. Truncated ERG Oncoproteins from TMPRSS2-ERG Fusions Are Resistant to SPOP-Mediated Proteasome Degradation. *Mol Cell* 59:904-16

154. Gan W, Dai X, Lunardi A, Li Z, Inuzuka H, et al. 2015. SPOP Promotes Ubiquitination and Degradation of the ERG Oncoprotein to Suppress Prostate Cancer Progression. *Mol Cell* 59:917-30

155. Luo J, Chen B, Gao CX, Xie HK, Han CN, Zhou CC. 2018. SPOP promotes FADD degradation and inhibits NF-kappaB activity in non-small cell lung cancer. *Biochem Biophys Res Commun* 504:289-94

156. Tan P, Wang A, Chen H, Du Y, Qian B, et al. 2019. SPOP inhibits mice pancreatic stellate cell activation by promoting FADD degradation in cerulein-induced chronic pancreatitis. *Exp Cell Res* 384:111606

157. Gang X, Xuan L, Zhao X, Lv Y, Li F, et al. 2019. Speckle-type POZ protein suppresses lipid accumulation and prostate cancer growth by stabilizing fatty acid synthase. *Prostate* 79:864-71

158. Chen MH, Wilson CW, Li YJ, Law KK, Lu CS, et al. 2009. Cilium-independent regulation of Gli protein function by Sufu in Hedgehog signaling is evolutionarily conserved. *Genes Dev* 23:1910-28

159. Wen X, Lai CK, Evangelista M, Hongo JA, de Sauvage FJ, Scales SJ. 2010. Kinetics of hedgehog-dependent full-length Gli3 accumulation in primary cilia and subsequent degradation. *Mol Cell Biol* 30:1910-22

160. Zeng C, Wang Y, Lu Q, Chen J, Zhang J, et al. 2014. SPOP suppresses tumorigenesis by regulating Hedgehog/Gli2 signaling pathway in gastric cancer. *J Exp Clin Cancer Res* 33:75

161. Cai H, Liu A. 2016. Spop promotes skeletal development and homeostasis by positively regulating Ihh signaling. *Proc Natl Acad Sci U S A* 113:14751-6

162. Cai H, Liu A. 2017. Spop regulates Gli3 activity and Shh signaling in dorsoventral patterning of the mouse spinal cord. *Dev Biol* 432:72-85

163. Zhang Q, Shi Q, Chen Y, Yue T, Li S, et al. 2009. Multiple Ser/Thr-rich degrons mediate the degradation of Ci/Gli by the Cul3-HIB/SPOP E3 ubiquitin ligase. *Proc Natl Acad Sci U S A* 106:21191-6

164. Liu C, Zhou Z, Yao X, Chen P, Sun M, et al. 2014. Hedgehog signaling downregulates suppressor of fused through the HIB/SPOP-Crn axis in Drosophila. *Cell Res* 24:595-609

165. Coquenlorge S, Yin WC, Yung T, Pan J, Zhang X, et al. 2019. GLI2 Modulated by SUFU and SPOP Induces Intestinal Stem Cell Niche Signals in Development and Tumorigenesis. *Cell Rep* 27:3006-18 e4

166. Zhang N, Sun P, Xu Y, Li H, Liu H, et al. 2021. The GPER1/SPOP axis mediates ubiquitination-dependent degradation of ERalpha to inhibit the growth of breast cancer induced by oestrogen. *Cancer Lett* 498:54-69

167. Tan Y, Ci Y, Dai X, Wu F, Guo J, et al. 2017. Cullin 3SPOP ubiquitin E3 ligase promotes the poly-ubiquitination and degradation of HDAC6. *Oncotarget* 8:47890-901

168. Li K, Wu JL, Qin B, Fan Z, Tang Q, et al. 2020. ILF3 is a substrate of SPOP for regulating serine biosynthesis in colorectal cancer. *Cell Res* 30:163-78

169. Wang L, Lin M, Chu M, Liu Y, Ma J, et al. 2020. SPOP promotes ubiquitination and degradation of LATS1 to enhance kidney cancer progression. *EBioMedicine* 56:102795

170. Takahashi I, Kameoka Y, Hashimoto K. 2002. MacroH2A1.2 binds the nuclear protein Spop. *Biochim Biophys Acta* 1591:63-8

171. Guillamot M, Ouazia D, Dolgalev I, Yeung ST, Kourtis N, et al. 2019. The E3 ubiquitin ligase SPOP controls resolution of systemic inflammation by triggering MYD88 degradation. *Nat Immunol* 20:1196-207

172. Hu YH, Wang Y, Wang F, Dong YM, Jiang WL, et al. 2020. SPOP negatively regulates Toll-like receptor-induced inflammation by disrupting MyD88 self-association. *Cell Mol Immunol*

173. Li Q, Wang F, Wang Q, Zhang N, Zheng J, et al. 2020. SPOP promotes ubiquitination and degradation of MyD88 to suppress the innate immune response. *PLoS Pathog* 16:e1008188

174. Zhang J, Chen M, Zhu Y, Dai X, Dang F, et al. 2019. SPOP Promotes Nanog Destruction to Suppress Stem Cell Traits and Prostate Cancer Progression. *Dev Cell* 48:329-44 e5

175. Tan P, Xu Y, Du Y, Wu L, Guo B, et al. 2019. SPOP suppresses pancreatic cancer progression by promoting the degradation of NANOG. *Cell Death Dis* 10:794

176. Claiborn KC, Sachdeva MM, Cannon CE, Groff DN, Singer JD, Stoffers DA. 2010. Pcif1 modulates Pdx1 protein stability and pancreatic beta cell function and survival in mice. *J Clin Invest* 120:3713-21

177. Gao K, Jin X, Tang Y, Ma J, Peng J, et al. 2015. Tumor suppressor SPOP mediates the proteasomal degradation of progesterone receptors (PRs) in breast cancer cells. *Am J Cancer Res* 5:3210-20

178. Luo J, Bao YC, Ji XX, Chen B, Deng QF, Zhou SW. 2017. SPOP promotes SIRT2 degradation and suppresses non-small cell lung cancer cell growth. *Biochem Biophys Res Commun* 483:880-4

179. He W, Zhang J, Liu B, Liu X, Liu G, et al. 2020. S119N Mutation of the E3 Ubiquitin Ligase SPOP Suppresses SLC7A1 Degradation to Regulate Hepatoblastoma Progression. *Mol Ther Oncolytics* 19:149-62

180. Sun S, Kelekar S, Kliewer SA, Mangelsdorf DJ. 2019. The orphan nuclear receptor SHP regulates ER stress response by inhibiting XBP1s degradation. *Genes Dev* 33:1083-94

181. Jin X, Wang J, Li Q, Zhuang H, Yang J, et al. 2019. SPOP targets oncogenic protein ZBTB3 for destruction to suppress endometrial cancer. *Am J Cancer Res* 9:2797-812

182. Clark A, Burleson M. 2020. SPOP and cancer: a systematic review. *Am J Cancer Res* 10:704-26

183. Cheng J, Guo J, Wang Z, North BJ, Tao K, et al. 2018. Functional analysis of Cullin 3 E3 ligases in tumorigenesis. *Biochim Biophys Acta Rev Cancer* 1869:11-28

184. Yoo SK, Lee S, Kim SJ, Jee HG, Kim BA, et al. 2016. Comprehensive Analysis of the Transcriptional and Mutational Landscape of Follicular and Papillary Thyroid Cancers. *PLoS Genet* 12:e1006239

185. Wang Z, Song Y, Ye M, Dai X, Zhu X, Wei W. 2020. The diverse roles of SPOP in prostate cancer and kidney cancer. *Nat Rev Urol* 17:339-50

186. Bailey MH, Tokheim C, Porta-Pardo E, Sengupta S, Bertrand D, et al. 2018. Comprehensive Characterization of Cancer Driver Genes and Mutations. *Cell* 173:371-85 e18

187. Ransone LJ, Verma IM. 1990. Nuclear proto-oncogenes fos and jun. *Annu Rev Cell Biol* 6:539-57

188. Ryder K, Lanahan A, Perez-Albuerne E, Nathans D. 1989. jun-D: a third member of the jun gene family. *Proc Natl Acad Sci U S A* 86:1500-3

189. Ostertag MS, Hutwelker W, Plettenburg O, Sattler M, Popowicz GM. 2019. Structural Insights into BET Client Recognition of Endometrial and Prostate Cancer-Associated SPOP Mutants. *J Mol Biol* 431:2213-21

190. Doyle JM, Gao J, Wang J, Yang M, Potts PR. 2010. MAGE-RING protein complexes comprise a family of E3 ubiquitin ligases. *Mol Cell* 39:963-74

191. Stracker TH, Petrini JH. 2011. The MRE11 complex: starting from the ends. *Nat Rev Mol Cell Biol* 12:90-103

192. Buis J, Wu Y, Deng Y, Leddon J, Westfield G, et al. 2008. Mre11 nuclease activity has essential roles in DNA repair and genomic stability distinct from ATM activation. *Cell* 135:85-96

193. Watanabe R, Maekawa M, Hieda M, Taguchi T, Miura N, et al. 2020. SPOP is essential for DNA-protein cross-link repair in prostate cancer cells: SPOP-dependent removal of topoisomerase 2A from the topoisomerase 2A-DNA cleavage complex. *Mol Biol Cell* 31:478-90

194. Hannah J, Zhou P. 2015. Distinct and overlapping functions of the cullin E3 ligase scaffolding proteins CUL4A and CUL4B. *Gene* 573:33-45

195. Vogt PK. 2001. Jun, the oncoprotein. *Oncogene* 20:2365-77

196. Ouyang X, Jessen WJ, Al-Ahmadie H, Serio AM, Lin Y, et al. 2008. Activator protein-1 transcription factors are associated with progression and recurrence of prostate cancer. *Cancer Res* 68:2132-44

197. Waldmann I, Walde S, Kehlenbach RH. 2007. Nuclear import of c-Jun is mediated by multiple transport receptors. *J Biol Chem* 282:27685-92

198. Schreck I, Al-Rawi M, Mingot JM, Scholl C, Diefenbacher ME, et al. 2011. c-Jun localizes to the nucleus independent of its phosphorylation by and interaction with JNK and vice versa promotes nuclear accumulation of JNK. *Biochem Biophys Res Commun* 407:735-40

199. Owen DJ, Ornaghi P, Yang JC, Lowe N, Evans PR, et al. 2000. The structural basis for the recognition of acetylated histone H4 by the bromodomain of histone acetyltransferase gcn5p. *EMBO J* 19:6141-9

200. Zeng L, Zhou MM. 2002. Bromodomain: an acetyl-lysine binding domain. *FEBS Lett* 513:124-8

201. Dey A, Nishiyama A, Karpova T, McNally J, Ozato K. 2009. Brd4 marks select genes on mitotic chromatin and directs postmitotic transcription. *Mol Biol Cell* 20:4899-909

202. Delmore JE, Issa GC, Lemieux ME, Rahl PB, Shi J, et al. 2011. BET bromodomain inhibition as a therapeutic strategy to target c-Myc. *Cell* 146:904-17

203. Gadd MS, Testa A, Lucas X, Chan KH, Chen W, et al. 2017. Structural basis of PROTAC cooperative recognition for selective protein degradation. *Nat Chem Biol* 13:514-21

204. Lai AC, Crews CM. 2017. Induced protein degradation: an emerging drug discovery paradigm. *Nat Rev Drug Discov* 16:101-14

205. Scheepstra M, Hekking KFW, van Hijfte L, Folmer RHA. 2019. Bivalent Ligands for Protein Degradation in Drug Discovery. *Comput Struct Biotechnol J* 17:160-76

206. French CA, Ramirez CL, Kolmakova J, Hickman TT, Cameron MJ, et al. 2008. BRD-NUT oncoproteins: a family of closely related nuclear proteins that block epithelial differentiation and maintain the growth of carcinoma cells. *Oncogene* 27:2237-42

207. Zuber J, Shi J, Wang E, Rappaport AR, Herrmann H, et al. 2011. RNAi screen identifies Brd4 as a therapeutic target in acute myeloid leukaemia. *Nature* 478:524-8

208. Ott CJ, Kopp N, Bird L, Paranal RM, Qi J, et al. 2012. BET bromodomain inhibition targets both c-Myc and IL7R in high-risk acute lymphoblastic leukemia. *Blood* 120:2843-52

209. Faivre EJ, McDaniel KF, Albert DH, Mantena SR, Plotnik JP, et al. 2020. Selective inhibition of the BD2 bromodomain of BET proteins in prostate cancer. *Nature* 578:306-10

210. Urbanucci A, Barfeld SJ, Kytola V, Itkonen HM, Coleman IM, et al. 2017. Androgen Receptor Deregulation Drives Bromodomain-Mediated Chromatin Alterations in Prostate Cancer. *Cell Rep* 19:2045-59

211. Faulds D, Balfour JA, Chrisp P, Langtry HD. 1991. Mitoxantrone. A review of its pharmacodynamic and pharmacokinetic properties, and therapeutic potential in the chemotherapy of cancer. *Drugs* 41:400-49

212. Tannock IF, Osoba D, Stockler MR, Ernst DS, Neville AJ, et al. 1996. Chemotherapy with mitoxantrone plus prednisone or prednisone alone for symptomatic hormone-resistant prostate cancer: a Canadian randomized trial with palliative end points. *J Clin Oncol* 14:1756-64

213. Kantoff PW, Halabi S, Conaway M, Picus J, Kirshner J, et al. 1999. Hydrocortisone with or without mitoxantrone in men with hormone-refractory prostate cancer: results of the cancer and leukemia group B 9182 study. *J Clin Oncol* 17:2506-13

214. Datta J, Ghoshal K, Denny WA, Gamage SA, Brooke DG, et al. 2009. A new class of quinoline-based DNA hypomethylating agents reactivates tumor suppressor genes by blocking DNA methyltransferase 1 activity and inducing its degradation. *Cancer Res* 69:4277-85

215. Gros C, Fleury L, Nahoum V, Faux C, Valente S, et al. 2015. New insights on the mechanism of quinoline-based DNA Methyltransferase inhibitors. *J Biol Chem* 290:6293-302

216. Holderfield M, Deuker MM, McCormick F, McMahon M. 2014. Targeting RAF kinases for cancer therapy: BRAF-mutated melanoma and beyond. *Nat Rev Cancer* 14:455-67

217. Gioeli D, Mandell JW, Petroni GR, Frierson HF, Jr., Weber MJ. 1999. Activation of mitogen-activated protein kinase associated with prostate cancer progression. *Cancer Res* 59:279-84

218. Trimarchi JM, Lees JA. 2002. Sibling rivalry in the E2F family. *Nat Rev Mol Cell Biol* 3:11-20

219. Chen HZ, Tsai SY, Leone G. 2009. Emerging roles of E2Fs in cancer: an exit from cell cycle control. *Nat Rev Cancer* 9:785-97

220. Hao YH, Doyle JM, Ramanathan S, Gomez TS, Jia D, et al. 2013. Regulation of WASH-dependent actin polymerization and protein trafficking by ubiquitination. *Cell* 152:1051-64

221. Pineda CT, Ramanathan S, Fon Tacer K, Weon JL, Potts MB, et al. 2015. Degradation of AMPK by a cancer-specific ubiquitin ligase. *Cell* 160:715-28

222. Jeon CH, Kim IH, Chae HD. 2014. Prognostic value of genetic detection using CEA and MAGE in peritoneal washes with gastric carcinoma after curative resection: result of a 3-year follow-up. *Medicine (Baltimore)* 93:e83

223. Ayyoub M, Scarlata CM, Hamai A, Pignon P, Valmori D. 2014. Expression of MAGE-A3/6 in primary breast cancer is associated with hormone receptor negative status, high histologic grade, and poor survival. *J Immunother* 37:73-6

224. Barker PA, Salehi A. 2002. The MAGE proteins: emerging roles in cell cycle progression, apoptosis, and neurogenetic disease. *J Neurosci Res* 67:705-12

225. Ryan DG, Murphy MP, Frezza C, Prag HA, Chouchani ET, et al. 2019. Coupling Krebs cycle metabolites to signalling in immunity and cancer. *Nat Metab* 1:16-33

226. Zhang D, Wang H, Sun M, Yang J, Zhang W, et al. 2014. Speckle-type POZ protein, SPOP, is involved in the DNA damage response. *Carcinogenesis* 35:1691-7

227. Stewart GS, Maser RS, Stankovic T, Bressan DA, Kaplan MI, et al. 1999. The DNA double-strand break repair gene hMRE11 is mutated in individuals with an ataxia-telangiectasia-like disorder. *Cell* 99:577-87

228. Conaway JW, Conaway RC. 1999. Transcription elongation and human disease. *Annu Rev Biochem* 68:301-19

229. Liu X, Zurlo G, Zhang Q. 2020. The Roles of Cullin-2 E3 Ubiquitin Ligase Complex in Cancer. *Adv Exp Med Biol* 1217:173-86

230. Meijer DH, Kane MF, Mehta S, Liu H, Harrington E, et al. 2012. Separated at birth? The functional and molecular divergence of OLIG1 and OLIG2. *Nat Rev Neurosci* 13:819-31

231. Antony J, Huang RY. 2017. AXL-Driven EMT State as a Targetable Conduit in Cancer. *Cancer Res* 77:3725-32

232. Aggarwal S, Dabla PK, Arora S. 2013. Prostasin: An Epithelial Sodium Channel Regulator. *J Biomark* 2013:179864

233. Lopez-Otin C, Matrisian LM. 2007. Emerging roles of proteases in tumour suppression. *Nat Rev Cancer* 7:800-8

234. Sabari JK, Lok BH, Laird JH, Poirier JT, Rudin CM. 2017. Unravelling the biology of SCLC: implications for therapy. *Nat Rev Clin Oncol* 14:549-61

235. Mroczek S, Chlebowska J, Kulinski TM, Gewartowska O, Gruchota J, et al. 2017. The non-canonical poly(A) polymerase FAM46C acts as an onco-suppressor in multiple myeloma. *Nat Commun* 8:619

236. Gossage L, Eisen T, Maher ER. 2015. VHL, the story of a tumour suppressor gene. *Nat Rev Cancer* 15:55-64

237. Latif F, Tory K, Gnarra J, Yao M, Duh FM, et al. 1993. Identification of the von Hippel-Lindau disease tumor suppressor gene. *Science* 260:1317-20

238. Kim JH, Hwang J, Jung JH, Lee HJ, Lee DY, Kim SH. 2019. Molecular networks of FOXP family: dual biologic functions, interplay with other molecules and clinical implications in cancer progression. *Mol Cancer* 18:180

239. Swart LE, Heidenreich O. 2021. The RUNX1/RUNX1T1 network: translating insights into therapeutic options. *Exp Hematol* 94:1-10

240. Kruger R. 2004. The role of synphilin-1 in synaptic function and protein degradation. *Cell Tissue Res* 318:195-9

241. Fujiwara T. 2017. GATA Transcription Factors: Basic Principles and Related Human Disorders. *Tohoku J Exp Med* 242:83-91

242. Lopez-Bergami P, Lau E, Ronai Z. 2010. Emerging roles of ATF2 and the dynamic AP1 network in cancer. *Nat Rev Cancer* 10:65-76

243. Elliott B, Millena AC, Matyunina L, Zhang M, Zou J, et al. 2019. Essential role of JunD in cell proliferation is mediated via MYC signaling in prostate cancer cells. *Cancer Lett* 448:155-67

244. Hunter JE, Leslie J, Perkins ND. 2016. c-Rel and its many roles in cancer: an old story with new twists. *Br J Cancer* 114:1-6

245. Gyrd-Hansen M, Meier P. 2010. IAPs: from caspase inhibitors to modulators of NF-kappaB, inflammation and cancer. *Nat Rev Cancer* 10:561-74

246. Tang R, Langdon WY, Zhang J. 2019. Regulation of immune responses by E3 ubiquitin ligase Cbl-b. *Cell Immunol* 340:103878

247. Jackson S, Xiong Y. 2009. CRL4s: the CUL4-RING E3 ubiquitin ligases. *Trends Biochem Sci* 34:562-70

248. Jeon BN, Choi WI, Yu MY, Yoon AR, Kim MH, et al. 2009. ZBTB2, a novel master regulator of the p53 pathway. *J Biol Chem* 284:17935-46

249. Karemaker ID, Vermeulen M. 2018. ZBTB2 reads unmethylated CpG island promoters and regulates embryonic stem cell differentiation. *EMBO Rep* 19

250. Kallunki T, Deng T, Hibi M, Karin M. 1996. c-Jun can recruit JNK to phosphorylate dimerization partners via specific docking interactions. *Cell* 87:929-39

251. Maki Y, Bos TJ, Davis C, Starbuck M, Vogt PK. 1987. Avian sarcoma virus 17 carries the jun oncogene. *Proc Natl Acad Sci U S A* 84:2848-52

252. Varmus HE. 1987. Oncogenes and transcriptional control. *Science* 238:1337-9

253. Musti AM, Treier M, Bohmann D. 1997. Reduced ubiquitin-dependent degradation of c-Jun after phosphorylation by MAP kinases. *Science* 275:400-2

254. Gao M, Labuda T, Xia Y, Gallagher E, Fang D, et al. 2004. Jun turnover is controlled through JNK-dependent phosphorylation of the E3 ligase Itch. *Science* 306:271-5

255. Nateri AS, Riera-Sans L, Da Costa C, Behrens A. 2004. The ubiquitin ligase SCFFbw7 antagonizes apoptotic JNK signaling. *Science* 303:1374-8

256. Wei W, Jin J, Schlisio S, Harper JW, Kaelin WG, Jr. 2005. The v-Jun point mutation allows c-Jun to escape GSK3-dependent recognition and destruction by the Fbw7 ubiquitin ligase. *Cancer Cell* 8:25-33

257. Wertz IE, O'Rourke KM, Zhang Z, Dornan D, Arnott D, et al. 2004. Human De-etiolated-1 regulates c-Jun by assembling a CUL4A ubiquitin ligase. *Science* 303:1371-4

258. Priyadarshini R, Hussain M, Attri P, Kaur E, Tripathi V, et al. 2018. BLM Potentiates c-Jun Degradation and Alters Its Function as an Oncogenic Transcription Factor. *Cell Rep* 24:947-61 e7

259. Dong Y, Zhang D, Cai M, Luo Z, Zhu Y, et al. 2019. SPOP regulates the DNA damage response and lung adenocarcinoma cell response to radiation. *Am J Cancer Res* 9:1469-83

260. Zhu Y, Wen J, Huang G, Mittlesteadt J, Wen X, Lu X. 2021. CHD1 and SPOP synergistically protect prostate epithelial cells from DNA damage. *Prostate* 81:81-8

261. Schreiber SL. 2019. A Chemical Biology View of Bioactive Small Molecules and a Binder-Based Approach to Connect Biology to Precision Medicines. *Isr J Chem* 59:52-9

Figure references and acknowledgements:

Figures 1.1, 1.2a, 3.1a, 4.3, 4.4 were generated using Biorender.com. Figure 1.2c derived from PDB structure 3hqi (72). Figures 1.2b, 4.1 generated using cBioPortal (141; 142).

APPENDIX

Patient-derived prostate cancer cell line models for cellular characteristics of oncogenic transformation driven by SPOP variant expression

Introduction

To assess the potential biological functions of the SPOP F133L/V mutation-induced PPIs described in this dissertation, including the SPOP F133L-c-Jun PPI, we sought to develop cell-based assays to detect and monitor unique SPOP F133L/V mutation-induced characteristics of cellular transformation.

Process and Results

I developed prostate cell lines with tetracycline-inducible (Tet-on) *SPOP* expression from patient-derived parental prostate cancer cell lines 22Rv1, C4-2, DU145 and PC3 (Figure A3) using pInducer20-SPOP lentivirus. I also used the pHAGE-IRES-eGFP lentivirus vector to develop SPOP-IRES-eGFP lentivirus to generate populations of prostate cancer cells with stable overexpression of SPOP. These cell line tools were used in assays to assess SPOP-induced cellular characteristics of oncogenic transformation, in which we tested cellular proliferation (Figure A1), migration (Figure A2), colony formation (not shown), growth in soft agar (not shown), apoptosis (not shown), and drug resistance (not shown). Under the conditions tested in these 22Rv1, C4-2, DU145 and PC3 cell line backgrounds with stable overexpression of SPOP WT or SPOP mutants, no significant changes in cellular behaviors were observed within a period of 5-7 days (e.g., proliferation in Figure A1). Beyond 7 days, stable overexpression of SPOP, Y87C, SPOP F133L and SPOP F133V was observed to induce cell death; stable overexpression of SPOP WT had minimal effect on cell growth across cell lines; and stable overexpression of

SPOP F102C had a pro-colony formation and pro-wound closure effect (Figure A2; PC3 cell line).

Conclusions

Under the conditions tested (featuring various combinations of cell line backgrounds, SPOP variant expression levels, and length of SPOP variant expression time), overexpression of SPOP F133L/V variants was not observed to provoke significant changes in cellular behavior within 5-7 days, although overexpression of these mutants was observed to induce cell death in periods >7 days and/or when cell line sub-culturing was performed. Work to characterize SPOP F133L/V-induced changes in cellular behavior will continue with further optimization of conditions.

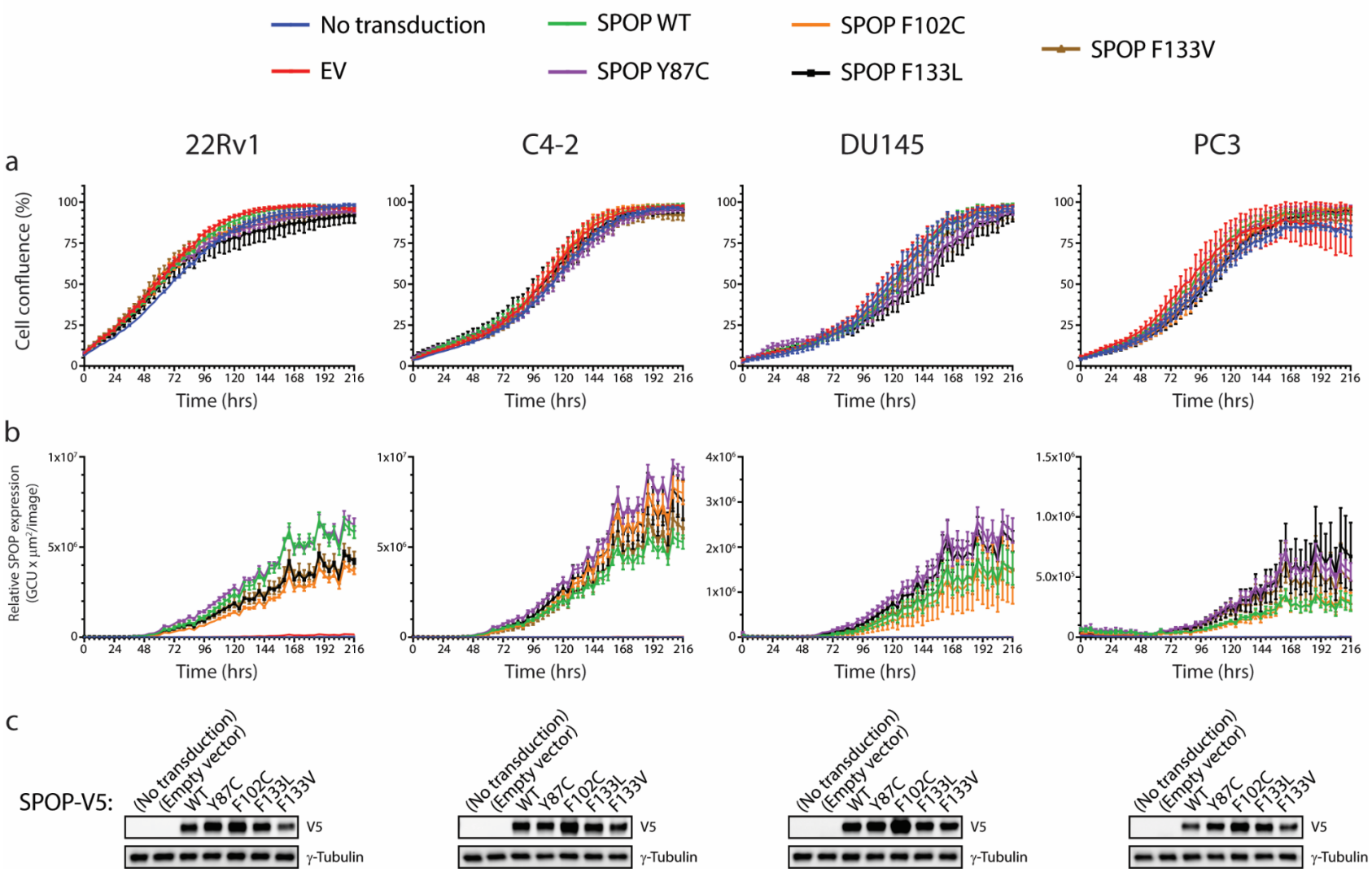
No transduction
EV
SPOP WT
SPOP Y87C
SPOP F102C
SPOP F133L
SPOP F133V
a
22Rv1
C4-2
DU145
PC3
Cell confluence (%)
Time (hrs)
b
Relative SPOP expression (GCU x µm²/image)
c
SPOP-V5:
(No transduction)
(Empty vector)
WT
Y87C
F102C
F133L
F133V
V5
γ-Tubulin

Figure A1. Cell proliferation assays with lenti-PHAGE SPOP-V5-IRES-eGFP transduction in 22RV1, C4-2, DU145 and PC3 patient-derived prostate cancer cell lines.

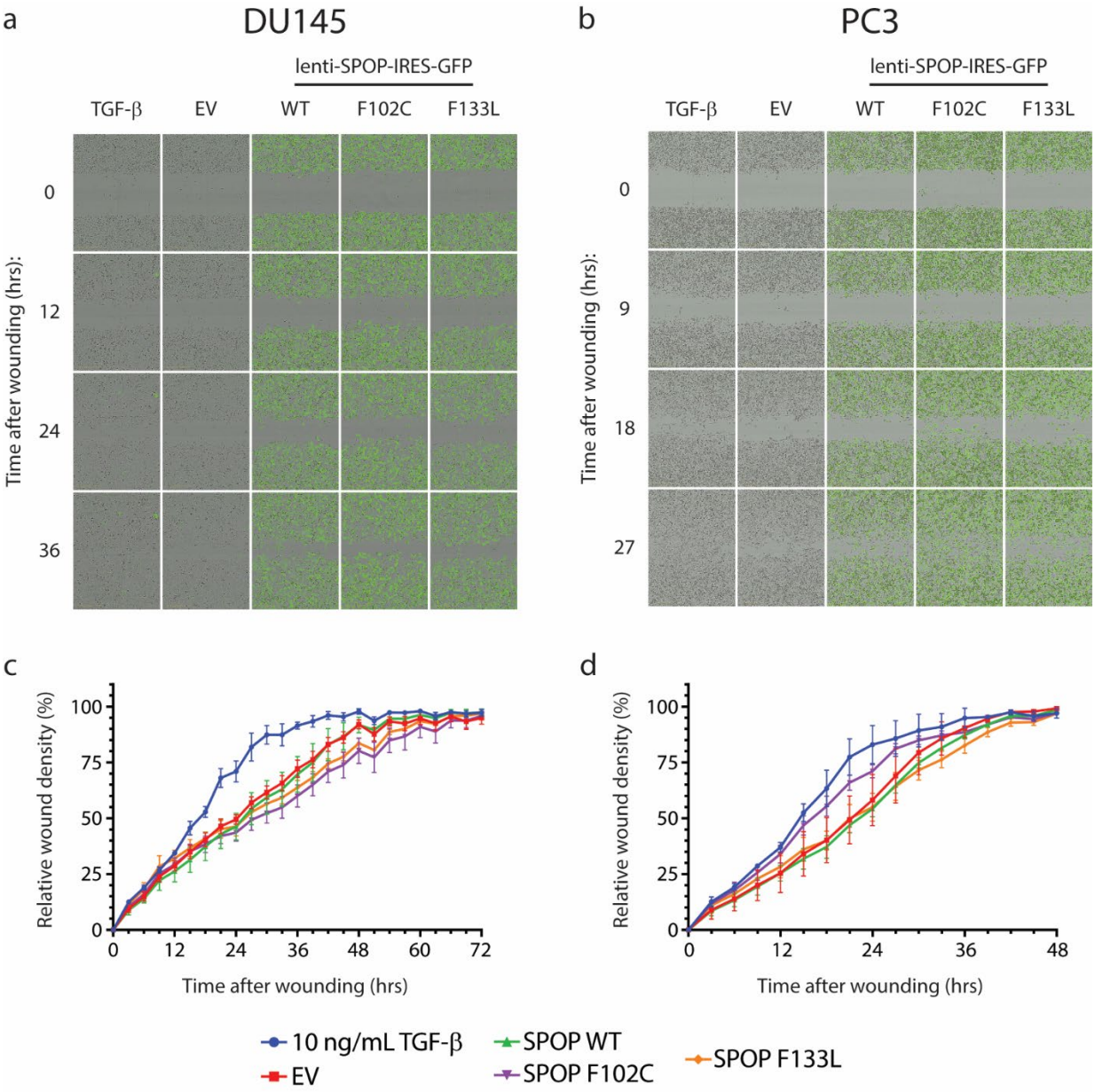
a
DU145
lenti-SPOP-IRES-GFP
TGF-β
EV
WT
F102C
F133L
Time after wounding (hrs):
0
12
24
36
b
PC3
lenti-SPOP-IRES-GFP
TGF-β
EV
WT
F102C
F133L
Time after wounding (hrs):
0
9
18
27
c
Relative wound density (%)
100
75
50
25
0
0
12
24
36
48
60
72
Time after wounding (hrs)
d
Relative wound density (%)
100
75
50
25
0
0
12
24
36
48
Time after wounding (hrs)
10 ng/mL TGF-β
EV
SPOP WT
SPOP F102C
SPOP F133L

Figure A2. Wound scratch migration assays with lenti-PHAGE SPOP-V5-IRES-eGFP transduction in DU145 and PC3 patient-derived prostate cancer cell lines.

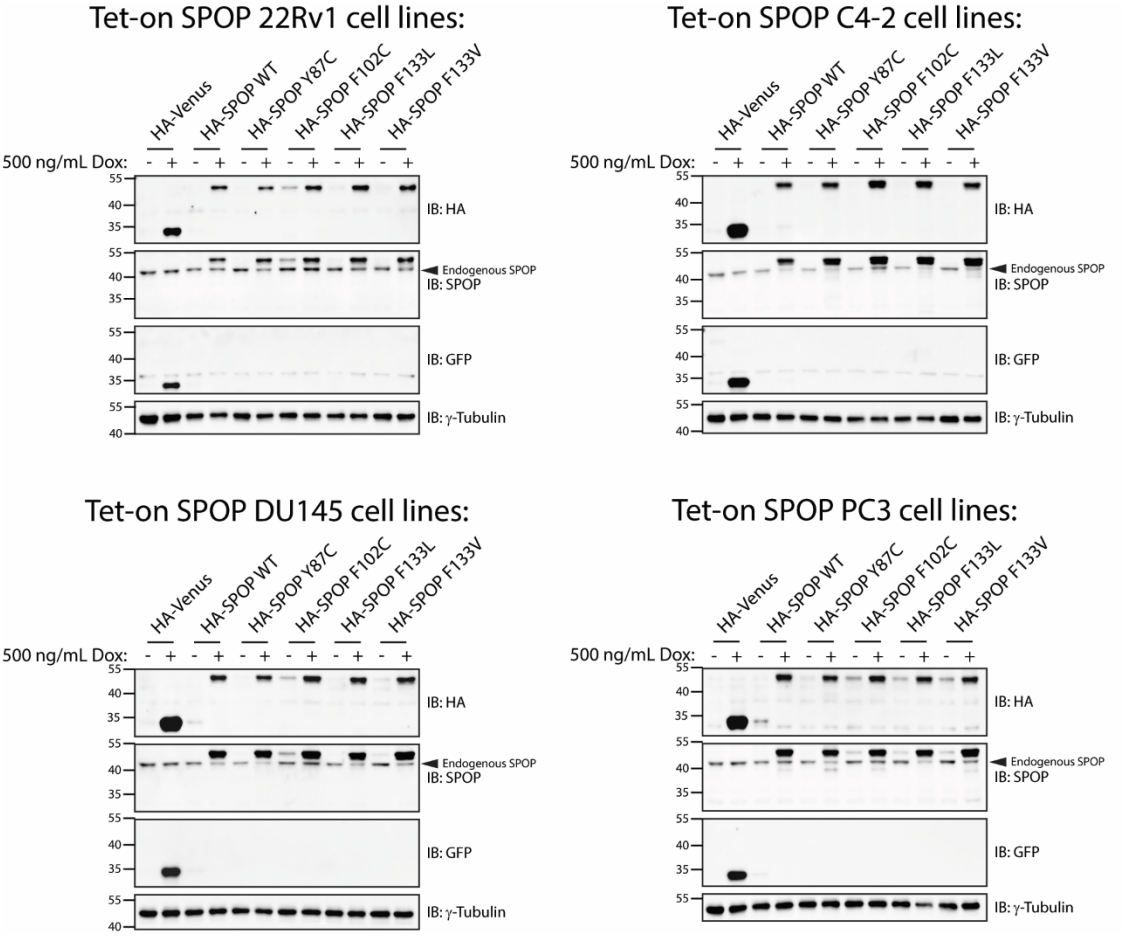
Tet-on SPOP 22Rv1 cell lines:
HA-Venus
HA-SPOP WT
HA-SPOP Y87C
HA-SPOP F102C
HA-SPOP F133L
HA-SPOP F133V
500 ng/mL Dox:
IB: HA
Endogenous SPOP
IB: SPOP
IB: GFP
IB: γ-Tubulin
Tet-on SPOP C4-2 cell lines:
Tet-on SPOP DU145 cell lines:
Tet-on SPOP PC3 cell lines:

Figure A3 Tet-on SPOP cell line development in 22Rv1, C4-2, DU145, and PC3 patient-derived prostate cancer cell lines.